MEASUREMENTS OF THE CROSS-SECTIONS WITH FAST NEUTRONS

S. SHAMSUL HASAN

1970

A THESIS SUBMITTED TO

THE ALIGARH MUSLIM UNIVERSITY ALIGARH

IN

PARTIAL FULFILMENT OF THE REQUIREMENTS

FOR

THE DEGREE OF DOCTOR OF PHILOSOPHY

IN PHYSICS

Certified that the work contained in this thesis is the original work of Mr. S. SHAMSUL HASAN, done under my supervision.

M.L. Sehgal 29.9.70
(M.L. SEHGAL)

Department of Physics
Aligarh Muslim University
ALIGARH, (U.P.), INDIA.

A C K N O W L E D G E M E N T

I wish to express my sincere gratitudes to Dr. M.L. Sehgal for his guidance and discussion throughout the course of this work. I am also thankful to Prof. Rais Ahmed for his kind interest.

I extend my thanks to Drs. Rajeshwari Prasad, A.K. Chaubey and Israr Ahmed for their helpful discussions.

The help given by workshop personnel , during the operation of the neutron generator is also appreciated.

I am thankful to Dr. A.S. Divatia for providing experimental facilities in the Van-de-Graaff, Laboratory at BARC Trombay.

Financial support of CSIR in the form of Senior Research Fellowship is thankfully acknowledged.

S. Shamsul Hasan

(S. SHAMSUL HASAN)

C_O_N_T_E_N_T_S

****

CHAPTER - I

I N T R O D U C T I O N

The problem of establishing the mechanism of nuclear interactions is as old as nuclear physics itself. The two theoretical approaches[1] to this problem are :

a) model treatment

b) many-body methods in nuclear physics.

Model treatment is simpler, since in this approach the actual state of affairs of the nuclear many-body system is replaced by a mathematically solvable model. Many-body methods are more rigorous, where the continuous states of collision problem are treated in analogous way to the bound states of the nucleons in the nucleus. Model treatment being easier, has been most frequently applied to the nuclear phenomena. Though it is felt that many-body approach is more exact and probably a complete theory of nuclear interactions would follow the lines of nuclear many-body approach.

The earliest attempts[3] to explain the nuclear phenomena, e.g. size of the reaction cross-section (then generally predicted to be of the order of nuclear dimensions[2]) were based on a simple potential well model. This model assumes that the passage of incident particle through the target nucleus does not disturb the state of the target nucleus appreciably. Potential well model predicts[2] only two types of reactions,

elastic scattering and radiative capture. Elastic scattering dominates the scene, since neutron travels through the nuclear potential for a time much smaller than the electromagnetic transition time and hence radiative capture becomes more improbable. Another feature of the potential well model is the presence of maxima in the cross-sections at widely spaced energies. On the contrary, it was observed[4-9] experimentally, that neutron cross-sections show large variations in size within the energy interval of few electron volts and at these resonances capture dominates.

In 1936 Bohr[10] introduced the idea of the compound nucleus model: an antithesis of the single particle model. It assumes that all the nucleons forming target nucleus or incident upon it interact strongly. As a consequence of strong interaction, the incident particle and the nucleus coalesce, forming a compound state in which all or very many nucleons participate collectively. The observed sharp resonances are the energy values of the quantum states of the compound system. These states are quasi stationary. The Heisenberg uncertainty relation can be used to correlate the life time of the compound state and the width of the resonance. From the width of the observed resonances lifetime of the compound states turns out to be of the order of 10^{-15} sec, a time comparable with electromagnetic transition time.

Though Bohr's compound nucleus theory successfully explained the presence of sharp and closely spaced resonance in the cross-section and the dominance of radiative capture over elastic scattering, there was no mathematical frame work in quantum mechanics to give quantitative description of it. Breit Wigner[11] treatment of the nuclear reactions based on time dependent perturbation theory, resulted in an expression for the cross-section similar to the one obtained in optical dispersion. Breit Wigner's formula could successfully explain the nuclear reaction cross-sections taking place through the individual compound nuclear levels.

With the increasing energy, compound nuclear levels become more and more closer and ultimately start over-lapping. Description in terms of individual levels becomes impracticable. Bohr generalised his theory for the intermediate and high energy region by making the following assumptions:

a) devide the nuclear reaction into two steps, the formation of the compound nucleus and its subsequent decay

b) decay is independent of the mode of formation.

Reaction cross-section can be calculated[12] in terms of compound nucleus formation cross-section, and inverse cross-section corresponding to a certain mode of decay. This method of calculating cross-section is referred to as "statistical model." The excited compound system is considered to be a heated system and its subsequent decay as evaporation of the particles.[13-14] Independence of the mode of formation and the mode of decay is a

reasonable assumption[2] at higher energies, where the number of overlapping states is very large. Relative phases involved act with respect to decay as if they were random. However, in the intermediate energy region statistical model gives an average cross-section over many resonances within a certain energy interval and so independence hypothesis turns out to be a good approximation. Ghoshal[15] has shown experimentally the validity of independence hypothesis for the compound nuclear reactions.

The two assumptions of the Bohr, namely: a) formation of the compound nucleus as soon as incident particle reaches target nucleus surfaces, b) independence hypothesis, have been challenged by some experimental facts. Experimentally observed fact, that in certain reactions, emitted particles show directional memory with respect to the direction of incident particle, and few other, are contrary to the independence hypothesis. Three-dimensional plot of the experimental total cross-sections[16-18] against energy (E) and atomic mass number (A) exhibits maxima and minima at values of E & A which cannot be explained on compound nucleus model, on the other hand it rather suggests the use of potential well model.

A due compromise between compound nucleus model and the single particle model was achieved by Fashbach, Porter and Weisskopf[19]. In doing so, a complex nuclear potential field $(- V_o(r) - i V_1 (r))$ was taken. The target nucleus in this

model behaves like a moderate absorber in contrast to its behaviour like a strong absorber in compound nucleus model. In this model an incident particle need not form compound nucleus right at the instant of its entry into the nuclear surface. It can move a certain distance within the nucleus before it coalescesto form a compound nucleus. The wave form can be represented by[20].

$$\exp i[(k_0+iK)x - \omega t] = e^{-Kx} \exp i(k_0 x - \omega t)$$

This expression represents a wave penetrating the medium and steadily decreasing in amplitude. This model is referred to as "Cloudy Crystal Ball model" or "Optical model". Optical model approach opens up the possibility of an other class of reactions namely "direct" reactions. In these reactions[21] incident particle may interpenetrate target nucleus without forming compound nucleus, and scatter with or without bringing about a change in the internal structure. Existence of direct reactions has been revealed in many experiments[22-24]. It is believed that direct reaction contribute a little to the total cross-section, except in particular circumstances their contribution exceeds the compound nucleus process.[21]

A rigorous theory of nuclear reactions (not dependent upon any model or any mathematical approximation) was put forth by Kapur and Peierls[25,26] in 1938. This theory and its subsequent versions by Breit[27] and Wigner with coworkers,[28,29] provided a very satisfactory framework for discussing nuclear reactions.

Present situation with regard to the establishment of reaction mechansim is quite unsatisfactory. It is observed that no reaction mechanism can explain the experimental results satisfactorily over a wide range of energy or over a wide range of the periodic table, even for a single specific reaction. However, large discrepancies in the experimental result reported by different group of workers also put a limit to the establishment of the reaction mechanism. From this point of view precise measurements and attempt to unify experimental data are necessary for a more accurate knowledge of the reaction mechanism.

Of the various possible channels to study the nuclear reaction mechanism, studies of the size of nuclear reaction cross-sections have been most extensively used. Ever since the existance of neutron[30] was established, it has been regarded as one of the most useful particle to probe into nuclear reactions. Neutron has no charge and can easily penetrate nucleus without encountering any coulomb barrier. At present a bulk of neutron cross-section data (total, partial and differential cross-sections is available. The applicability of the different reaction mechanisms have been tested by comparing the experimental results with the theoretical predictions. Systematic regularities in reaction cross-sections have been studied to give insight into the nuclear structure i.e. shell effects, pairing effects etc. Apart from its use in the understanding of the reaction mechanism, nuclear reaction cross-section studies are also useful in the reactor design and the stellar nucleosynthesis theories.[31,32]

Present work is an addition to the neutron reaction cross-section studies. (n,γ), (n,α), (n,p) and (n.2n) cross-sections have been measured. Details of neutron sources (used in the present measurements); measurement techniques and the associated errors are given in Chapter II. Whereas the details of the individual measurements, choice of standard reactions etc. are discussed chapterwise (Chap.III to VI).

Neutron radiative capture cross-sections are measured at 24 keV neutron energy using an antimony beryllium photo-neutron source.[33] The results of these measurements are compared with the prediction of statistical theory. Statistical theory gives an average cross-section over compound nucleus levels within the energy spread of incident neutrons. Margolis[34] formalism for (n,γ) cross-section based on statistical theory have been used. A generally observed fact[35-37] that statistical model approach is much dependent on parameters, brings in certain uncertainties in the comparison of the statistical theory predictions with the experimental results. An earlier observed trend[36] in the variation of parameter $\xi = D/2\pi\Gamma_\gamma$ (where D is level spacing and Γ_γ radiation width) with τ is reconfirmed. (For details see Chap. III).

At 14.8 MeV neutron energy few (n,γ) measurements were performed. Neutrons at this energy were produced by the bombardment of 120 keV deuteron beam on tritium (diffused in

a thin zirconium layer). Results of present (n, γ) cross-section measurements at 14.8 MeV and those of earlier measurements[38-41] in this energy region were used to test direct and semi-direct capture theory as proposed by various workers[42-47], for neutron radiative capture at higher energies. Lane and Lynn[43] have developed formalism for direct capture. Their approach to deduce direct capture formalism was that the rigorous theory of nuclear reactions proposed by Peierls and Kapur[25] must be capable of describing all types of reactions. Neglect of mechanism other than compound nucleus one is achieved on the assumption that formal compound system states, far away from the energy where compound nucleus is formed, can be ignored. A break down in this assumption must give the direct reaction cross-section. Enhancement over direct capture due to "semidirect" or "collective" capture is taken into account by the use of Browns[45] enhancement factor. 14.8 MeV neutron capture cross-section data is also used to investigate shell effects. Details of these studies are given in Chap. IV.

Apart from (n, γ) cross-sections a few (n,2n), (n,p) and (n, α) cross-sections were also measured. A large number of workers[48-51,64-70] have measured neutron cross-sections in the 14 MeV energy region. The experimental results have been compared with the theoretical predictions.[48-54] A general conclusion arrived at is that statistical theory can well explain the size of (n,2n) cross-sections. In (n,p) reactions

quite a significant part is contributed by direct reaction mechanism.[53] Systematic regualrites have been studied in(n,2n) (n,p) and (n,α) cross-sections.[52,55-62] Shell effects in (n,2n) (n,p) and (n,α) cross-section were predicted by many workers[55,57,62] but in the recent years their existence have been doubted by few workers.[60,61] However, it is observed that discrepancies in the experimental results are in some cases quite large, when reported by two or more groups of workers. It is worth while to repeat some of the measurements with more precision. It appears that in some cases large statistical errors in counting may cause large uncertainties in the results. Large statistical counting errors may be either due to the small percentage abundance of a particular isotope in the natural element or due to the production of many activities in the irradiated sample. In such cases use of enriched isotopes is advisable. Present measurements of 14.8 MeV neutron cross-sections [other than (n,γ)] have been performed using some enriched isotopes. Experimental results of (n,2n) and (n,p) cross-sections are compared with the statistical theory predictions.[60,63] Details of these measurements are given in chapter entitled "14.8 MeV Neutron Cross-section Measurements."

In nuclear reaction studies level density plays an important role. Level density can be determined only for some given nuclear model. Bethe[71] introduced the idea of applying statistical mechanism at excitation energies where the density of the levels is reasonably high. Treatment of neutron and protons as non-interacting Fermions gives the equation of state as[12]

$$E = at^2$$

where E is the excitation energy, t is thermodynamic temperature and "a" is a constant generally referred to as level density parameter. The form of level density may be given as[12)]

$$\rho(E) \propto \exp 2\sqrt{(aE)}$$

The treatment based on Fermi gas model has many shortcomings. It does not include the effect of collective degrees of freedom, particle correlations (which are responsible for pairing interaction etc.) and shell effects. Various refinements have been proposed in the form of level density. Lang and LeCouteur[72)] proposed a more correct form for the equation of state as:

$$E = at^2 - t$$

which leads to an expression of level density as :

$$\rho(E) \propto (E+t)^{-2} \exp 2\sqrt{(aE)}$$

A careful study of the shell effects by Newton[73)] gave

$$\rho(E) = A^{-5/3} (2\bar{J}_n+1)^{-\frac{1}{2}} (2\bar{J}_p+1)^{-\frac{1}{2}} (2E + 3t)^{-2} \exp \left(\frac{2E}{t} - 8.75 \right)$$

and

$$E = 0.076 (\bar{J}_n + \bar{J}_p + 1) A^{2/3} t^2$$

where $\bar{J}_n$, $\bar{J}_p$ are suitable averages of single particle angular momenta and vary with nuclide numbers. They are tabulated in Ref. 73).

The angular momentum dependent level density, derived through statistical approach, may be given as:[71,74]

$$\rho(E,J) = \rho(E,0)\ (2J + 1)\ \exp\{-(J + \tfrac{1}{2})^2/2\sigma_{sp}^2\}$$

where $\rho(E,J)$ is the density of levels with angular momentum J and at an excitation energy E; $\rho(E,0)$ is the density of levels with angular momentum 0 at the same excitation energy "σ_{sp}" is termed as spin cutoff parameter and characterises spin distribution of levels. Theoretically σ_{sp}^2 can be written as:

$$\sigma_{sp}^2 = c.t$$

where $c\hbar^2$ is moment of inertia of the nucleus. In the "Fermi gas model" treatment $c\hbar^2$ corresponds to rigid body moment of inertia and σ_{sp}^2 can be written as:

$$\sigma_{sp}^2 = \frac{I_{rig}}{\hbar^2} \cdot t$$

and

$$I_{rig} = 2/5\ mAR^2$$

where R is radius and (m.A) is mass of the nucleus.

In the case of departure from Fermi gas model i.e. at low excitation energy where residual interactions are quite significant, one can write for σ_{sp}^2 the following equation:[75]

$$\sigma_{sp}^2 = (I_{rig.}/\hbar^2)\ .t.\ A(E)$$

where A(E) may be a certain function of excitation energy E. Since enough experimental evidences are not available to

predict variation of moment of inertia with the energy; exact behaviour of σ_{sp} with the energy is not known

For reasonably higher excitation energy one can write[76]

$$\sigma_{sp}^2 = \frac{I}{\hbar^2} \cdot \left(\frac{E}{a}\right)^{\frac{1}{2}}$$

A generally noted fact is that at lower excitation energy nuclear moment of inertia (I) is smaller than $I_{rig.}$ due to the particle correlation etc. Empirically it is predicted that at low excitation energies,[20]

$$I = 0.6 \times I_{rig.}$$

σ_{sp} is an important parameter from the point of view of angular momentum distribution in the excited nuclear levels. Many attempts[73,77-80] have been made to study σ_{sp}. Huizenga and Vandenbosch[81,82] suggested a method to calculate σ_{sp} with the isomeric cross-section ratios. A large number of workers[83-90] have measured isomeric ratios for different nuclear reactions and at various energies. From these experimental results they have calculated σ_{sp}. Presently for ^{103}Rh (n, γ) $^{104,m,g}Rh$ reaction, isomeric cross-section ratios are measured at many energies. Following Huizenga method σ_{sp} is calculated at these energies, to study its energy dependence. Isomeric cross-section ratios measured at 14.8 MeV for (n,2n) reactions are also used to calculate σ_{sp}. These "σ_{sp}" are compared with $(\sigma_{sp})_{rig}$ i.e. value of σ_{sp} corresponding to rigid body moment of inertia. Details are given in Chap.VI.

R E F E R E N C E S :

1. N. Cindro, Revs. Mod. Phys., 38 (1966) 391
2. F.L. Friedman and V.F. Weisskopf, Niels Bohr and the Development of Physics, Pergman Press, 1955
3. Bethe, Phys. Rev. 47 (1935) 747
4. Bjerge and Westcott, Proc. Roy. Soc. A150 (1935) 709
5. Moon and Tilman, Nature 135 (1935) 904
6. Szilard, Nature 136 (1935) 849 and 950
7. Fermi and Amaldi, Ric. Sci. A6 (1935) 544
8. Frisch et al., Nature 137 (1936) 149
9. Preiswerk and Halban, Nature 138 (1936) 163
10. N. Bohr, Nature 137 (1936) 344
11. G. Beit and E.P. Wigner, Phys. Rev. 49 (1936) 519 & 642
12. Blatt and Weisskopf, Theoretical Nuclear Physics, John Wiley & Sons, (1952)
13. Weisskopf, Phys. Rev. 52 (1937) 295
14. Frenkel, Sov. Phys. 9 (1936) 533
15. Ghoshal, Phys. Rev. 80 (1950) 939
16. Barschall, Phys. Rev. 86 (1952) 431
17. Okazaki et al., Phys. Rev. 93 (1954) 461
18. Cook and Bonner, Phys. Rev. 94 (1954) 651
19. Feshbach, Porter and Weisskopf, Phys.Rev.90(1953) 166; 96 (1954) 448
20. M.A. Preston, Phys.of the Nucleus, Addison-Wesley Publishing Company (1962)
21. A.M. Lane and R.G. Thomos, Revs.Mod. Phys. 30 (1958) 257
22. S.T. Butler, Phys. Rev. 80 (1950) 1095

23. Austern et al, Phys. Rev. 92 (1953) 350

24. Hayakawa et al., Progr. Theoret. Phys. 13 (1955) 415

25. P.L. Kapur and R.E. Peierls, Proc. Roy. Soc. (London) A166 (1938) 277

26. R.E. Peierls, Proc. Cambridge Phil.Soc. 44 (1947) 242

27. G. Breit, Phys. Rev. 58 (1940) 506, 69 (1946) 472

28. E.P. Wigner, Phys. Rev. 70 (1946) 15 and 606

29. E.P. Wigner, and L. Eisenbud, Phys. Rev. 72 (1947) 29

30. J. Chadwick, Proc. Roy. Soc. A136 (1932) 692

31. E.M. Burbidge et al, Revs. Mod. Phys. 29 (1957) 547

32. G. Gamow, Revs. Mod. Phys. 21 (1949) 367

33. A. Wattenberg, Phys. Rev. 71 (1947) 497

34. B. Margolis, Phys. Rev. 88 (1952) 327

35. J.A. Miskel et al., Phys. Rev. 128 (1962) 2717

36. A.K. Chaubey and M.L. Sehgal, Phys.Rev. 152 (1965) 1055

37. D.C. Stupegia et al., Journ. Nucl.Energy, 22 (1968) 267

38. J.L. Perkin et al., Proc. Phys.Soc. (London) 72A (1958) 505

39. R.G. Wille and R.W. Fink, Phys. Rev. 118 (1960) 242

40. J. Ciskei et al., Nucl. Phys. A95 (1965) 229

41. H.O. Menlove et al., Phys. Rev. 163 (1967) 1299

42. B.L. Cohen, Phys. Rev. 100 (1955) 206

43. A.M. Lane and J.E. Lynn, Proc.Conf.Peaceful Use of the Atomic Energy (GENEVA) (1958) p/4

44. A.M. Lane and J.E. Lynn, Nucl. Phys. 11 (1959) 646

45. G.E. Brown, Nucl. Phys. 57 (1964) 339

46. C.F. Clement et al., Nucl. Phys. 66 (1965) 273 & 293

47. G. Longo and F. Saporetti, Nucl. Phys. A127 (1969) 503

48. S. Lulic et al, Nucl. Phys. A119 (1968) 517

49. E. Kondaiah et al, Nucl. Phys. A120 (1968) 337

50. P. Cuzzorcria et al. Nucl. Phys. A103 (1967) 616

51. P. Cuzzoria et al., Nuovo Cim. 52B (1967) 476

52. D.G. Gardner, Nucl. Phys. 29 (1962) 373

53. G. Brown and H. Muirhead, Phil.Mag. 2 (1957) 473

54. D.G. Gardner and Y.W. Yu, Nucl. Phys. 60 (1964) 49

55. M. Bormann, Nucl. Phys. 65 (1965) 257

56. V.N. Levkovskii, JETP (USSR) 33 (1957) 1520

57. A. Chatterjee, Nucl. Phys. 47 (1963) 511

58. A. Chatterjee, Nucl. Phys.49 (1963) 687

59. A. Chatterjee, Nucl. Phys.60 (1964) 273

60. D.G. Gardner and Rosenblum, Nucl. Phys. A96 (1967) 121

61. P. Hill, Nucl. Phys. A107 (1968) 49

62. D.L. Allen, Nucl. Phys. 24 (1961) 274

63. S. Pearlstein, Nucl. Data A3 (1967) 327

64. H. Liskien and A. Paulsen, EUR-119e Vol. 1(1966)

65. E.B. Paul and R.L. Clark, Can. J. Phys. 31 (1953) 267

66. J. Brozokso et al., Nucl. Phys. 74 (1965) 438

67. P. Strohal et al., Nucl. Phys. 30 (1962) 49

68. M. Bormann et al., Z. Naturforsch A15 (1960) 200

69. R. Prasad (Ph.D. Thesis submitted to AMU, Aligarh (1967)

70. J. Csikai et al., Atomic Energy Rev. 7 (1969) 93

71. H.A. Bethe, Revs. Mod. Phys. 9 (1937) 69

72. J.M.B. Lang and K.J. Le Couteur, Proc. Phys. Soc. A67 (1954) 586

73. T.D. Newton, Cand. J. Phys. 34 (1956) 804

74. C. Bloch, Phys. Rev. 93 (1954) 1094

75. D.W. Lang, Nucl. Phys. 42 (1963) 353

76. T. Ericson, Advance in Phys. 9 (1960) 425

77. T. Eriscon, Nucl. Phys. 11 (1959) 481

78. A.C. Dougals and N. Macdonald, Nucl. Phys. 13 (1959) 382

79. A.G.W. Cameron, Can. J. Phys. 36 (1958) 1040

80. C.T. Hibdon, Phys. Rev. 114 (1959) 179

81. J.R. Huizenga and R. Vandenbosch, Phys. Rev. 120 (1960) 1305

82. R. Vandenbosch and J.R. Huizenga, Phys. Rev. 120 (1960) 1313

83. S.K. Mangal and P.S. Gill, Nucl. Phys. 36 (1962) 542

84. S.K. Mangal and P.S. Gill, Nucl. Phys. 41 (1963) 372

85. M.L. Sehgal, Phys. Rev. 128 (1962) 761

86. H.S. Hans et al., Nucl. Phys. 20 (1960) 183

87. S.K. Mangal and C.S. Khurana, Nucl. Phys. 69 (1965) 158

88. A.K. Chaubey and M.L. Sehgal, Nucl. Phys. A117 (1968) 545

89. R. Prasad and D.C. Sarkar, Nucl. Phys. A94 (1967) 476

90. C.T. Bishop, ANL-6405 (1961)

*****

CHAPTER - II

EXPERIMENTAL DETAILS

2.1 Neutron Production and Irradiation Procedure:

Nuclear reactions, which give neutrons as reaction product, may be used for the production of neutrons. Practical utility of certain nuclear reaction from the point of view of neutron production is determined by the following facts:

a) Yield of the neutrons for a given flux of the bombarding particles must be high. High neutron yield is evidently accompanied by the high value of the cross-section.

b) There must be certain source to provide high flux of monoenergetic bombarding particles, at an energy above the threshold of the nuclear reaction yielding neutrons.

c) The spread in the energy of the emitted neutrons must be small.

Generally (α,n) and (γ,n) reactions are used for the production of neutrons, using α-particles and γ-rays from their respective naturally occuring radioactive emitters. The use of these types of sources is limited to the production of neutrons at isolated energies. Another possibility is the use of accelerated charged particles like proton, deuteron, triton and α-particle etc., obtained from charged particle accelerators. Bombardment of these accelerated charged particles on suitable targets yields neutrons. The latter type of neutron sources have twofold advantages over the former ones:

a) Relatively high flux of neutrons can be obtained.

b) Neutrons can be obtained at different energies in a certain energy interval by varying the energy of the bombarding particles.

A. 24 - keV neutrons.

The fact that threshold for (γ,n) reaction in deuterium and beryllium nuclei are 2.18 MeV and 1.63 MeV respectively, makes these two convenient target nuclei for the production of neutrons using γ-rays from γ-emitters. In our measurements we have used an antimony-beryllium photo-neutron source, which was obtained from BHABHA ATOMIC RESEARCH CENTRE, TROMBAY, BOMBAY-85. In this source 1.692 MeV γ-rays of ^{124}Sb are used to initiate (γ,n) reaction in beryllium. The halflife of the Sb-Be photo-neutron source is the same as that of ^{124}Sb i.e. 60 days.

Wattenberg et al.[1] have made an extensive study of (γ,n) sources, and have given an expression for the energy of emitted neutrons in a certain (γ,n) reaction. The energy of the emitted neutrons in antimony-beryllium photo-neutron source has been measured by various workers[1-6] and the accepted value is 24 keV. However, in Sb-Be photo-neutron source, there is always a contamination due to a second neutron group[7] of energy 380 keV. This neutron group comes as a result of (γ,n) reaction due to 2.044 MeV γ-rays of ^{124}Sb. The intensity of 2.044 MeV γ-rays in ^{124}Sb is very small and so the percentage of 380 keV neutrons is as small as 4.4%.

Sb - Be PHOTONEUTRON SOURCE.

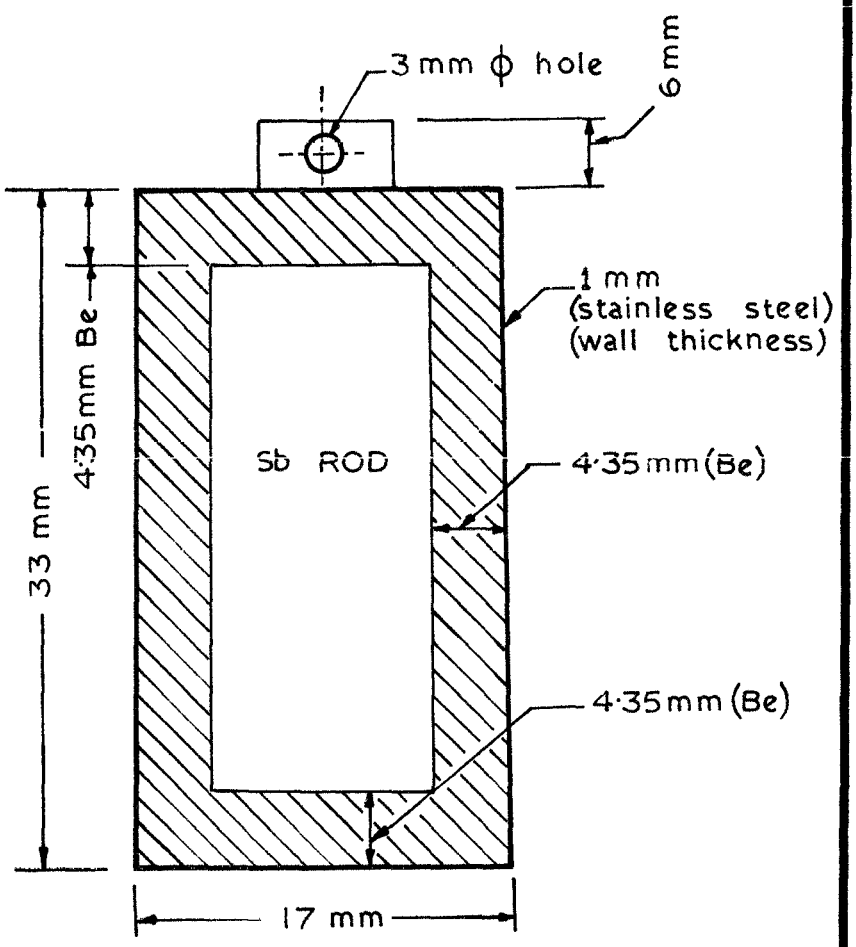

FIG. 1

The spread in the energy of emitted neutrons is partly due to the inherent angle between the direction of emitted neutron and the bombarding particle, and partly due to the inelastic scattering of the neutrons within the source itself. The spread in the energy of the neutron in the present photoneutron source is approximately 3 keV[8]. Fig.1 shows the constructional details of Sb-Be photo-neutron source. The neutron flux at the place of irradiation of the sample was $\sim 10^7$ neutrons/sec. The presence of scattered neutrons at the place of irradiation would introduce serious error in the measurements. So special care was taken to minimize the presence of these neutrons at the place of irradiation.

Irradiations were carried out in a room at remote location. An aluminium stand was used to keep the source and the sample assembly (target samples sandwitched between the standard samples) during irradiation. Remote location of irradiation and absence of any scattering material near the place of irradiation could successfully minimize the scattered neutrons. Measurement of cross-section with sample wrapped in cadmium foil and without being wrapped in cadmium foil, did not show any difference in the value of cross-section.

B. 14.8 - MeV Neutron.

The exoergic reaction $^{3}_{1}H$ (d,n) $^{4}_{2}He$ was used for the production of 14.8 MeV neutrons. 130 keV deuteron beam from the Cockcroft-Walton Accelerator designed in our laboratory[9] was made to fall on a thin tritium target to initiate the reaction:

$$^{3}_{1}H + ^{2}_{1}D \longrightarrow ^{4}_{2}He + ^{1}_{o}n + 17.58 \text{ MeV} \quad \ldots\ldots \quad (1)$$

Studies[10,11] of $^{3}_{1}H$ (d,n) $^{4}_{2}He$ reaction have shown that this reaction has a resonance around 130 keV deuteron bombarding energy, and the cross-section at resonance is 5 barns. Arnold et al.[11] found that at 130 keV bombarding energy the intensity of the emitted neutrons is maximum at zero degree with respect to the incident deuteron beam in laboratory system.

Neutron, being the lighter reaction product in $^{3}_{1}H$(d,n) $^{4}_{2}He$ reaction, takes away most of the available energy. Fowler et al[12] have tabulated the energy of the neutrons at different bombarding energies and at different laboratory angles. At 130 keV bombarding energy of the deuteron, 14.8 MeV neutron are produced in the forward direction at zero degree with respect to the direction of deuteron beam. For the geometry of our irradiations the upper limit for the energy spread[13] was $\pm$ 0.5 MeV.

A ZnS (lucite) crystal mounted on Du-Mond 6292 photo-multiplier tube was used as the neutron monitor. It was kept at 90° to the direction of the deuteron beam, and at a place 50 cms. away from the target.

The sample assembly was irradiated in the 0° forward direction with respect to the deuteron beam, by keeping it at the outer side of 0.28 cm. thick brass backing to whose other side tritium target was fixed.

The inelastic scattering of neutrons with the walls of the room or any heavy scatterer may give rise to slow neutrons. The presence of these slow neutrons at the place of irradiation may cause errors in the measurements. In our experiment the nearest wall from the place of irradiation was at a distance of more than 1.5 meter and so slow neutron background was reasonably small. There was no hydrogenous material near the place of irradiation and so the thermal neutron flux was almost negligible. Perkin et al.[14] have used the same irradiation geometry in his experiment as ours, and have put an upper limit for the ratio of thermal to 14.8 MeV neutrons as 2×10^{-7}. A contamination may also be there due to a second group of 2.8 MeV neutrons. This group of neutrons may be due to the reaction

$$ {}^{2}_{1}H + {}^{2}_{1}H \longrightarrow {}^{3}_{2}He + {}^{1}_{o}n. $$

However, the cross-section for the ${}^{2}_{1}H$ (d,n) ${}^{3}_{2}He$ reaction at 130 keV bombarding energy is as low as 15 mb., which is much smaller than 5 barn, the cross-section for the ${}^{3}_{1}H$(d,n) ${}^{4}_{2}He$ reaction. Hence the ratio of the 2.8 MeV neutron flux to 14.8MeV neutrons is less than 1/300.

C. 2-3 MeV- Neutrons.

Neutrons in the energy range 2-3 MeV were produced by the endothermic reaction ${}^{3}_{1}H$(p,n) ${}^{3}_{2}He$ i.e.

$$ {}^{1}_{1}H + {}^{3}_{1}H \longrightarrow {}^{3}_{2}He + {}^{1}_{o}n - 0.764 \text{ MeV} \quad ..... \quad (2) $$

Accelerated proton beam was obtained from the Van-de-Graff accelerator, B.A.R.C., Trombay, Bombay. The energy of the emitted neutrons at various proton energies and at different laboratory angles was taken from the table of Fowler et al[12]. The different proton beam energies and the corresponding emitted neutron energies, used in our experiment are given below.

Proton Energy	Neutron Energy
2.8 MeV	2.0 ± .2 MeV
3.4 MeV	2.6 ± .25 MeV
3.6 MeV	2.8 ± .28 MeV

The irradiation was carried out at 0^{o} laboratory angle to the direction of proton beam. The spread in the neutron energy is obtained by estimating the solid angle subtended by the sample at the point where neutrons were produced.

2.2 Measurement Techniques:

There are two techniques generally used for the cross-section measurements:

a. Prompt particle measurement technique.

b. Activation technique.

Another technique which is exclusively used for (n,γ) cross-section measurements is the spherical shell transmission technique. Spherical shell transmission measurements do not require absolute detection efficiencies. This technique has few disadvantages, for example, it can be used with homogeneous

neutron sources, and requires large samples. Moreover, in spherical shell transmission experiments corrections for self shielding effects are some time difficult.

The pre-requisite for prompt particle measurements is the knowledge of emitted prompt particle spectrum alongwith the corresponding detection efficiencies. Prompt particle measurements as well as spherical shell transmission measurements both require separated isotopes.

In activation technique cross-section is determined by following the induced activities in the sample. The activities are produced as a consequence of the neutron reaction with the target isotopes. Activation technique measures the cross-section for the formation of specific product and has high sensitivity. However, the use of activation technique is limited to those product nuclei which have convenient halflives and established decay schemes. The formalism for the activation measurements is outlined below.

Let a sample be irradiated by a neutron beam with flux Φ The number of target nuclei, which yield a certain radioactive reaction product (P) on being irradiated with neutrons be N_o. Then the equation which governs the growth of P type activity during irradiation may be given as follows:

$$\frac{dP}{dt} = \sigma_\gamma \Phi N_o - P\lambda \qquad \ldots\ldots\ldots \qquad (3)$$

Where σ_γ is the reaction cross-section and λ is the decay constant of the P type nuclei. Let the irradiation be carried out for time t_e. The activity of P type nuclei at the instant when irradiation was stopped may be given as

$$P_o \lambda = \sigma_\gamma \Phi N_o (1 - e^{-\lambda t_e}) \quad \ldots\ldots\ldots \quad (4)$$

The disintegration rate of the P type nuclei at any instant 't' from the stop of irradiation is given by

$$\frac{dP}{dt} = P_o \lambda e^{-\lambda . t} \quad \ldots\ldots\ldots \quad (5)$$

Let C_t be the disintegration rate recorded by a certain counting device at time 't' from the stop of irradiation then one can write

$$\frac{dP}{dt} = \frac{C_t}{G_e \cdot \epsilon} = P_o \lambda e^{-\lambda . t} \quad \ldots\ldots\ldots \quad (6)$$

Where G_e is the geometrical efficiency of the counting device and ϵ is the detection efficiency of the detector. From equation (4) and (6) one can write for the reaction cross-section,

$$\sigma_\gamma = \frac{C_t e^{\lambda . t}}{\Phi G_e \epsilon N_o (1 - e^{-\lambda t_e})} \quad \ldots\ldots\ldots \quad (7)$$

In actual practice the induced activity in the sample is counted till it reaches the background counts. A graph is plotted between the log of the counting rate and time 't' measured from the stop of the irradiation. The graph will be a straight line and will show the halflife corresponding to the product nuclei.

By extrapolating the graph to zero time we get the counting rate at the instant of stop of irradiation. i.e. $C_{t=0}$. Hence one can write the following expression for σ_γ using equation (7)

$$\sigma_\gamma = \frac{C_{t=0}}{\Phi G_e \epsilon N_0 (1 - e^{-\lambda t_e})} \quad \ldots\ldots\ldots \quad (8)$$

In some cases it is possible that there may be two or more radioactive reaction products in the irradiated sample, either due to more than one reaction channels for the interaction of neutrons with the same isotope or due to interaction of neutrons with other stable isotopes in the natural element. In such cases the activities can be separated provided the half-lives are not very close to each other. By subtracting the activities one after another from the composite decay curve, one can get separate lines each showing a certain specific activity.

2.3 Composite Activity of the Isomeric and Ground State Reaction Products:

In some cases it is possible that the reaction products have two isomers, one in the ground state and the other in the excited state (generally known as the isomeric state). If the isomeric state decays directly to the ground state by isomeric transition then the formalism used for the determination of cross-section is different from the one discussed earlier. In these cases the number of product nuclei in the isomeric state (M_o) and in the ground state (G_o), immediately after irradiation time 't_e' is given by[15]

$$M_o = (1/\lambda_m)\ \Phi\ N_o\ \sigma_m\ (1 - e^{-\lambda_m t_e}) \qquad \ldots\ldots\ldots \quad (9)$$

and

$$G_o = (1/\lambda_g)\ \Phi\ N_o\ (\sigma_m + \sigma_g)(1 - e^{-\lambda_g t_e})$$

$$+ (1/\lambda_g - \lambda_m)\ \Phi\ N_o\ \sigma_m\ (e^{-\lambda_g t_e} - e^{-\lambda_m t_e}) \qquad \ldots\ldots\ldots \quad (10)$$

where λ_g and λ_m are the decay constants for the ground and the isomeric state of the product nuclei respectively; σ_m and σ_g are the cross-sections for the isomeric and ground states; Φ is the neutron flux and N_o is the number of nuclei responsible for the activity under consideration.

After a time 't' from the stop of irradiation the activities of the isomeric and ground states are governed by the following equations respectively.

$$\frac{dM}{dt} = M\lambda_m = M_o \lambda_m e^{-\lambda_m t}$$

$$= N_o \Phi\ \sigma_m\ (1 - e^{-\lambda_m t_e})\ e^{-\lambda_m t} \qquad \ldots\ldots\ldots \quad (11)$$

and

$$\frac{dG}{dt} = N_o \Phi\ \sigma_m\ (\lambda_g/\lambda_g - \lambda_m)\ (1 - e^{-\lambda_m t_e})\ e^{-\lambda_m t}$$

$$+ N_o \Phi\ [(\sigma_m + \sigma_g) - \sigma_m (\lambda_g/\lambda_g - \lambda_m)](1 - e^{-\lambda_g t_e})\ e^{-\lambda_g t} \ldots\ldots\ldots \quad (12)$$

Or one can write for ground state activity

$$\frac{dG}{dt} = A_m e^{-\lambda_m t} + A_g e^{-\lambda_g t} \qquad \ldots\ldots\ldots \quad (13)$$

where

$$A_m = \Phi N_o \sigma_m (\lambda_g/\lambda_g - \lambda_m)(1 - e^{-\lambda_m t_e}) \qquad \ldots\ldots\ldots \quad (14a)$$

and

$$A_g = \Phi N_o [\sigma_g - \sigma_m (\lambda_m/\lambda_g - \lambda_m)](1 - e^{-\lambda_g t_e}) \ldots\ldots\ldots \quad (14b)$$

COMPOSITE DECAY OF THE GROUND STATE
(I.T. 100% ; $\lambda g > \lambda m$)

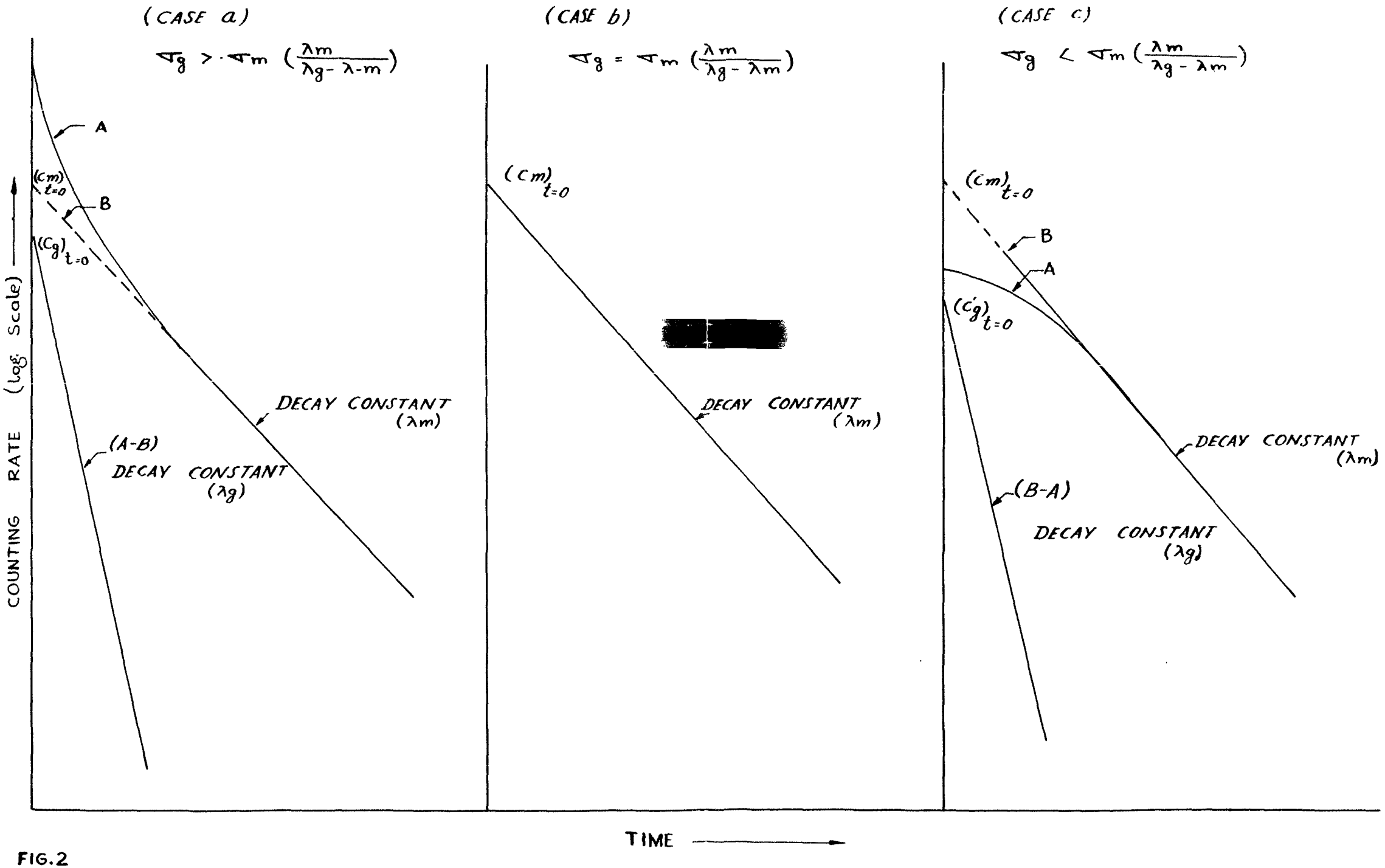

FIG.2

From equation (13) it appears that ground state activity behaves in a similar way as the admixture of two activities with decay constants λ_g and λ_m. If λ_g and λ_m are not very close to each other, one must be able to separate the activities with these two decay constants. The case of our interest is the one in which the isomeric state is longer lived than the ground state i.e. $\lambda_g > \lambda_m$. In these cases cross-sections for both the states can be determined by counting the ground state activity alone, and the following formalism is used.

When $\lambda_g > \lambda_m$, quantity $\{\lambda_g/(\lambda_g - \lambda_m)\}$ is positive and greater than one, and hence A_m must have positive sign. The sign of A_g depends upon the ratio (σ_m / σ_g). There are three possibilities

a) When $\sigma_g > \sigma_m (\lambda_m / \lambda_g - \lambda_m)$. In this case A_g is positive and hence the decay curve would be similar to the one as shown in Fig. 2a. In this case activities may be separated as usual. The cross-section of the two states can be calculated using the following set of equation

$$\frac{(C_m)_{t=0}}{\epsilon_g . G_e} = A_m = \Phi N_0 \sigma_m (\lambda_g / \lambda_g - \lambda_m)(1 - e^{-\lambda_m t_e}) \quad \ldots\ldots\ldots \quad (15a)$$

$$\frac{(C_g)_{t=0}}{\epsilon_g . G_e} = A_g = \Phi N_0 [\sigma_g - \sigma_m (\lambda_m / \lambda_g - \lambda_m)](1 - e^{-\lambda_g t_e}) \quad \ldots\ldots\ldots \quad (15b)$$

where $(C_m)_{t=0}$ and $(C_g)_{t=0}$ are the zero time counting rate of the two separated activities with decay constant λ_m and λ_g.

ϵ_g is the detection efficiency for the particles emitted from the decay of the ground state and Ge is the geometrical efficiency of the counting device.

b) When $\tau_g = \tau_m (\lambda_m/\lambda_g - \lambda_m)$. It is interesting to note that in such a case A_g is zero and there won't be any activity with decay constant λ_g (see Fig.2b). In this case τ_m can be calculated using equation(15a) and τ_g can be calculated by using the relation

$$\tau_g = \tau_m (\lambda_m/\lambda_g - \lambda_m) \quad \ldots\ldots\ldots \quad (16)$$

c) When $\tau_g < \tau_m (\lambda_m/\lambda_g - \lambda_m)$. In this case A_g has a negative sign and one can write for the ground state activity.

$$\frac{dG}{dt} = A_m e^{-\lambda_m t} - A'_g e^{-\lambda_g t_e} \quad \ldots\ldots\ldots \quad (17a)$$

where

$$A'_g = -A_g = [\tau_m (\lambda_m/\lambda_g - \lambda_m) - \tau_g] \quad \ldots\ldots\ldots \quad (17b)$$

In such a case the decay curve would have a shape as shown in Fig.2c. The tail of the decay curve corresponds to the activity with decay constant λ_m. This activity is extrapolated back to zero time. The subtraction of the composite decay curve from the activity with decay constant λ_m gives us the other activity with decay constant λ_g. Let the zero time counting rate of this activity be $(C'_g)_{t=0}$. Then one can write

$$\frac{(C'_g)_{t=0}}{\epsilon_g . Ge} = A'_g = -A_g$$

$$= N_0 \Phi [\tau_m (\lambda_m/\lambda_g - \lambda_m)](1 - e^{-\lambda_g t_e}) \quad \ldots\ldots\ldots \quad (18)$$

Using equations (15a) and (18) one can determine the cross-sections σ_m and σ_g .

2.4 Sample Preparation:

The substances to be studied were taken in the powder form or in the form of the foils. Samples were made by uniformly spreading powdered substances (or the thin foils) within thin perspex ring to have a fixed geometry. The ring and the powdered material was sandwiched between the two thin cellulose tapes. The thickness of the samples, their area of cross-section and the amount of the substance are the things to be chosen carefully in each individual measurement. Larger amount of substances are good for improving the counting statistics, but are limited by the sample thickness (for a certain fixed area of the sample). For thicker sample self absorption of the emitted particles in the sample is larger. Particularly for β-particles the self absorption effects are quite serious. The large sample area may also reduce the sample thickness, but it has got its own limitations. Large sample area can not be used in cases where the neutron source is a point source, because larger sample area is accompanied by the larger solid angle subtended by the sample at the point source, and hence larger neutron energy spread. Larger smaple area may also be inconvenient from the geometry consideration of the counting device. For a certain measurement, a compromise has to be made between these three things. For

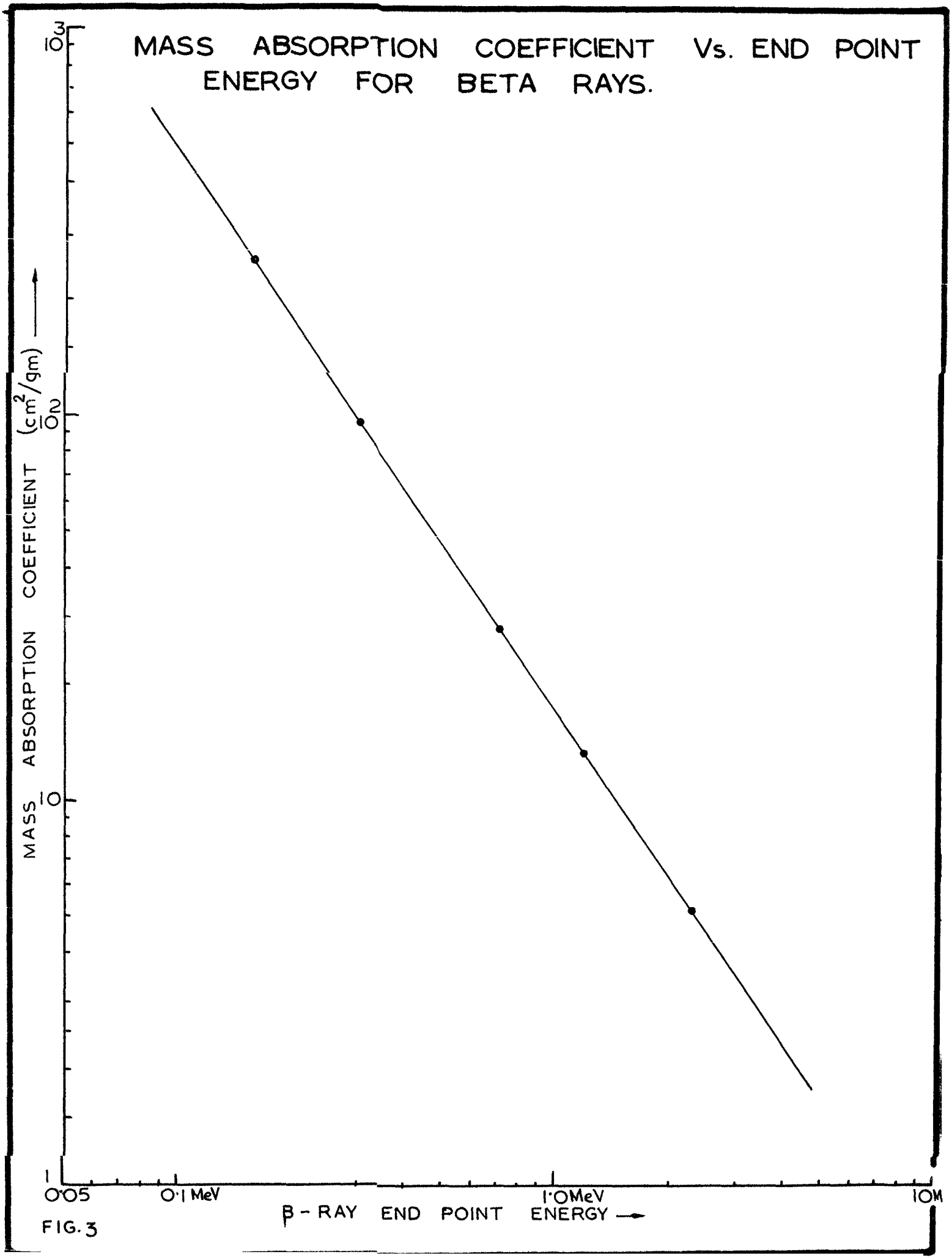
MASS ABSORPTION COEFFICIENT Vs. END POINT ENERGY FOR BETA RAYS.
MASS ABSORPTION COEFFICIENT (cm²/gm)
10³
10²
10
1
0·05
0·1 MeV
1·0MeV
10M
β - RAY END POINT ENERGY

FIG. 3

24-keV measurements area of the sample was taken to be 2.834 Cm^2. For other measurements a smaller area (1.266 cm^2) of the sample was chosen. For β-counting generally lighter sample were taken compared to those used for γ-counting.

2.5 β-Counting Technique:

An end window beta-counter of 2.5 mg/cm^2 window thickness, shielded with 10 cm of lead from all sides was used for β-counting. A stand was designed in such a way that one could always count a sample in the close vicinity of the window of the counter keeping the same fixed geometry. The expression used for the efficiency of the β-particles may be given as:

$$\epsilon = (1/100)(ae^{-\mu_1 t} + be^{-\mu_2 t} + \ldots\ldots\ldots) \quad \ldots\ldots\ldots \quad (19)$$

where a, b, c, ... are the branching ratios of the various β-rays emitted; μ_1, μ_2, μ_3 .... are their corresponding mass absorption coefficients and t is the average thickness (gm/cm^2) which a β-particle has to traverse before entering the counter. A graph was plotted between end point β-energies and their mass absorption coefficients using standard β-sources, which is shown in Fig.3. From this graph mass absorption coefficients for the various β-rays involved in our measurements were determined.

2.6 γ-Counting Technique :

A cylindrical sodium iodide (thallium activated)crystal was used for γ-ray detection. The height and the diameter of

the crystal were 3.8 cms. each. The crystal was canned in an aluminum container of wall thickness 0.1 cm. One of the two flat surfaces of the crystal was polished and optically coupled to a Du-Mond 6292-photo-multiplier tube. Pulses from the photo-multiplier tube were fed to the input of the non-overload linear amplifier through a cathod follower. Output pulses from the amplifier were analysed by a single channel analyser for their various pulse heights. Finally the analysed pulses were counted using a scaler. The sample activity was counted by placing the sample on the top of the flat surface of the crystal.

Spectra were plotted for the γ-rays of known energy using standard γ-ray sources i.e. ^{133}Ba (0.32 MeV), ^{137}Cs(0.663 MeV), ^{22}Na (1.28 MeV & 511 keV) and ^{60}Co (1.17 MeV and 1.32 MeV). From these γ-ray spectra a graph was plotted between γ-ray energy and the height of the photo-peak. Another graph was plotted between the inverse of the square root of energy and the resolution of the photopeak.

In our measurements photopeak intensity of a certain γ-ray emitted from the irradiated sample was plotted against time. The height of the photopeak and the width of the channel necessary to include just the photo-peak out of the total γ-ray spectrum was determined with the help of the two aforesaid graphs. The photo-peak intensity needs to be corrected for the contribution of the back scattered peak or the compton peak, which may be there due to certain higher energy γ-rays, if they are present.

The expression used for calculation of the cross-section may be given as follows:

$$\sigma_\gamma = \frac{(1+\alpha_T)(C_{t=o})}{\phi . N_o G_e \quad D(E)\, e^{-\mu T}\, (1-e^{-\lambda t_e})\, P(E)} \qquad \ldots\ldots \quad (20)$$

where $C_{t=o}$ denotes photo-peak counts at the time t=o, after correcting for the back scattering and compton scattering contribution due to other γ-rays; N_o, ϕ and Ge are the number of target nuclei, neutron flux and geometrical efficiency of the counter respectively; $e^{-\mu T}$ is the correction factor for the absorption of γ-rays in the sample itself and aluminum cane etc, which can be calculated in a similar way as in the case of β-rays; $(1 - e^{-\lambda t_e})$ is the saturation correction for the induced activity; D(E) is the detection efficiency of the crystal which depends upon the size of the crystal as well as the γ-ray energy (E). For the detection efficiency one can write

$$D(E) = (1 - e^{-\mu d}) \qquad \ldots\ldots \quad (21)$$

where 'd' is the average distance inside the crystal which a γ-ray has to traverse before leaving the crystal and μ is the absorption coefficient for the γ-ray in NaI (Tl) crystal. The average distance 'd' was determined by taking the mean of the various pathlengths drawn at 5^o intervals in the same plane through the centre of NaI crystal; P(E) is the photo-peak efficiency. For a gamma ray of given energy, photo-peak efficiency

is defined as the ratio of the photo-peak area to the total area of the γ-ray spectrum. A graph between gamma ray energy and photo-peak efficiency[13] was plotted, and was used to find out the photo-peak efficiency at the γ-ray energies involved in our measurements; $(1 + \alpha_T)$ is the correction for the internal conversion of the γ-rays, where α_T is total conversion coefficient.

2.7 Errors in the Measurements :

The utility of a certain measurement lies in the thorough study of the various sources of error and a careful estimation of these errors. The various sources of error in our measurements are described in the following paragraphs.

1. Non reproducibility of identical geometries of the irradiation and counting system, for the unknown target samples and the standard samples, may introduce certain errors in the measurements. However, fixed sample holders could minimize this error satisfactorily. An estimate of about 2% error was made for the non-reproducibility of the geometry.

2. The inaccurate measurement of irradiation time and the time that lapses between the stop of irradiation and the start of counting can introduce errors. An upper limit for this error can be put as 1% in our measurements.

3. The lack of proper information about the decay scheme of the product nuclei may also introduce certain errors.

In the present measurements latest available data is used to minimize this error.

4. The statistical error in the counting rate is also quite significant in case of small activities induced in the sample. In an admixture of more than one activity, the counting error in the separated activities become large. Proper choice of irradiation time and repeated measurements in some cases can help in minimizing these errors.

5. Errors may be there in the measurements due to γ-detection of β-counter and vice versa. Some times γ-rays accompanying β-rays, when enter the β-counter eject a photo-electron from the cathode of β-counter and hence γ-rays are also detected. We have used a beta counter of small cathode which had a gamma ray detection efficiency less than one percent. In some cases β-rays accompanying γ-rays may enter the NaI (TI) crystal and thus they are detected. It is possible only when β-ray energy is high. These β-rays can be absorbed in a certain absorber and a correction is applied for the attenuation of γ-rays due to this absorber.

6. The error may be introduced in the estimation of total number of target nuclei. This error was minimized to the extent of negligible, by using a weighing balance with 0.0002 gram precision and using the substances whose compositions were known up to .01% precision.

7. In case of using neutrons from accelerated particle sources, errors may be introduced due to fluctuations in the beam current. The runs with larger beam current fluctuation were discarded.

8. The error due to the erratic behaviour of the electronic equipment was minimized by stablizing the equipment before the start of experiment.

The errors due to presence of slow neutrons are discussed in section 2.1.

REFERENCES :

1. A. Wattenberg, Phys. Rev. 71 (1947) 497
2. D. Hughes and C. Eggler, Phys. Rev. 72 (1947) 902
3. A.O. Hanson, Phys. Rev. 75 (1947) 1794
4. Roberts et al., Phys. Rev. 80 (1950) 6
5. R. Clup and B. Hamermesh, Phys. Rev. 93 (1954) 1025
6. H.W. Schmitt, Nuc. Phys. 20 (1960) 220
7. Gibbons et al., Phys. Rev. 114 (1959) 1319
8. A.K. Chaubey (Ph.D. thesis submitted to A.M.U. Aligarh, 1967)
9. C.S. Khurana (Ph.D. thesis submitted to A.M.U. Aligarh, 1960)
10. J.P. Conner et al., Phys. Rev. 88, (1952) 468
11. W.R. Arnold et al., Phys. Rev. 93, (1954) 483
12. J.L. Fowler and J.E. Brolley, JR., Revs.Mod.Phys. 28, (1956) 103
13. R.P. Mathur, (Ph.D. thesis submitted to A.M.U.Aligarh, 1967)
14. J.L. Perkin et al., Proc.Phys. Soc. 72 (1958) 505
15. J. Bacso et al., Nucl. Phys. 67 (1965) 443

****

CHAPTER - III

24 - KEV NEUTRON CAPTURE CROSS-SECTION

3.1 Introduction :

Detailed studies of thermal and slow neutron capture cross-sections have proved very useful in the design of nuclear reactors. Capture cross-section studies especially in the keV region have two-fold interest:

(a) in the studies of nuclear reaction theories.

(b) in the Stellar Nucleosynthesis theory.

Theories of Stellar nucleosynthesis[1-5] of heavy elements predict correlations between the abundances of various elements and the neutron capture cross-section in the energy range 10 to 100 keV. Macklin and Gibbons[5] have measured (n, γ) cross-sections for 'Sr' and 'Te' isotopes in the energy range 30-220keV. They found that their cross-section values are in agreement with the prediction of "Stellar Nucleosynthesis theory". Measurements of the neutron capture cross-section in the keV region furnish valuable information about the nuclear structure, such as the dependence of level spacing on excitation energy. Neutron cross-section also give information about the shell effects and the pairing effects in the nuclei. The studies of the (n, γ) cross-sections over a wide range of energy can give some idea about different reaction mechanisms applicable at various neutron energies.

A number of neutron capture cross-section studies have been performed in the keV region, both at isolated[7-23] energies using photo-neutron sources[6], as well as using accelerated particle sources.[25-44] There are mainly three methods of measuring neutron capture cross-sections:

a) By the study of induced activity.[7-19; 24-39]

b) By the study of capture γ-rays.[40-44]

c) By Spherical shell transmission method.[20-23]

Details of these methods are given in the second chapter alongwith the merits and demerits of each technique.

Present work of capture cross-section measurements at 24 keV, using Sb-Be photoneutron source have got the following motivations:

a) To complete (n,γ) activation cross-sections data at 24 keV.

b) To check the applicability of statistical theory at 24 keV.

c) To see whether capture cross-section measurements can give some information about the resonance parameters e.g. radiation width $\overline{\Gamma_\gamma}$ and level spacing D etc.

3.2 Experimental Results :

All the (n,γ) cross-sections at 24 keV have been measured relative to that of ^{127}I. The reasons for choosing ^{127}I (n,γ) ^{128}I reaction as a standard are the following:

a) Cross-section for this reaction at 24 keV has been measured very precisely by absolute β-counting technique[11] and its accepted value is 0.82 barn.

b) ^{128}I has a moderate halflife (25 min), which is comparable to the halflives of most of the (n,γ) reaction products of the isotopes studied in the present case.

c) The decay scheme of ^{128}I is relatively simple and well established. Moreover ^{127}I is also monoisotopic.

^{127}I was taken in the form of Potassium Iodide which when irradiated by 24 keV neutrons gives admixture of two activities ^{128}I (25 min) and ^{42}K (12.5 hrs). Activity of ^{42}K is obtained as a result of (n,γ) reaction product of ^{41}K. As the two activities have halflives which differ by a factor of 30, they can be easily separated without causing any sizable statistical counting error.

The natural abundances of the isotopes studied and the decay schemes of the reaction products formed by (n,γ) reactions were taken from Nuclear Data Sheets.[45] The activities of the reaction products were followed up to the back-ground level. In cases where the statistical counting errors were large, decay lines were drawn which correspond to the precise known halflives as given in the literature.[45] For such cases the errors introduced in the measurements of the cross-sections will be large.

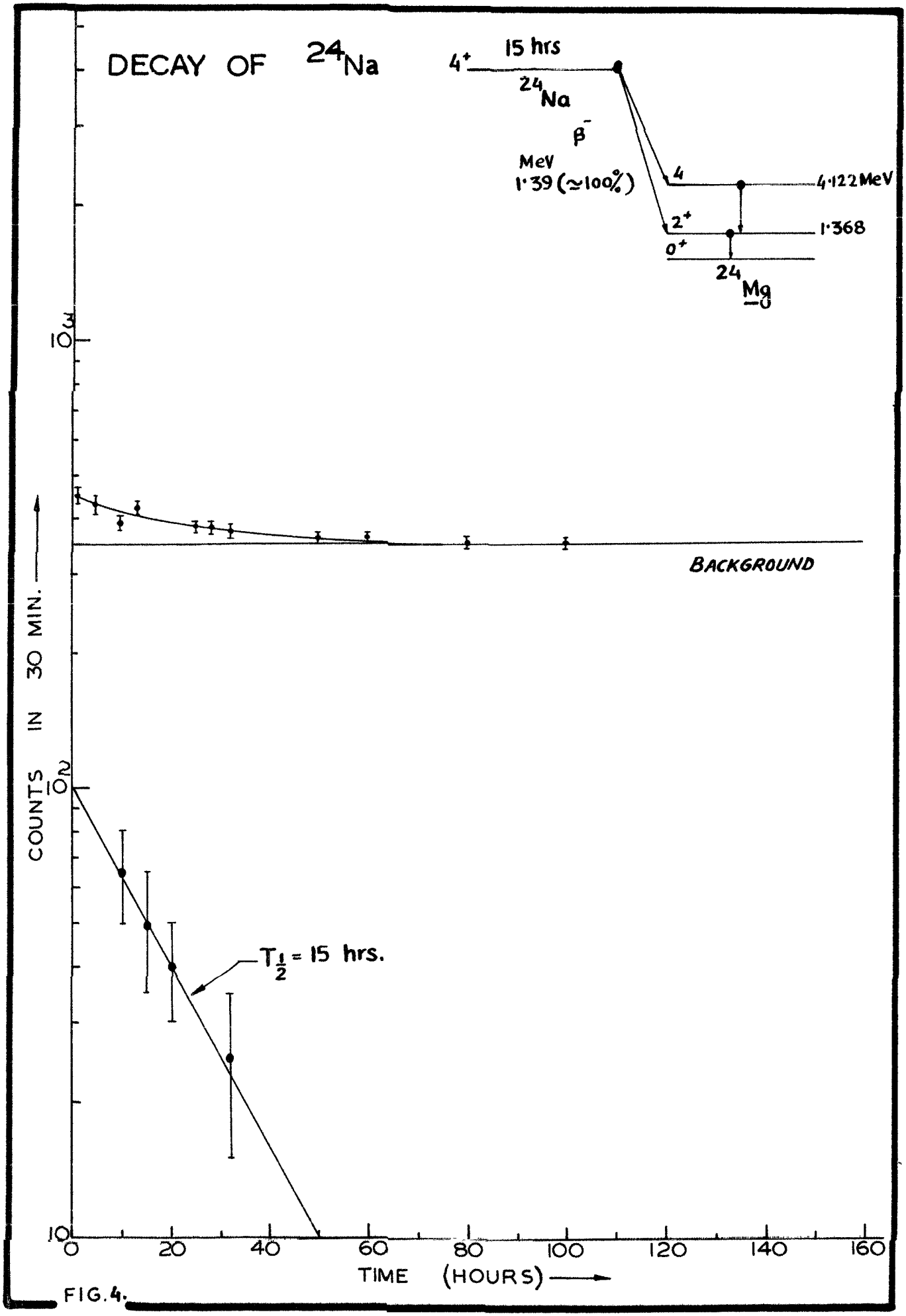
DECAY OF ^{24}Na
4^+
15 hrs
^{24}Na
β^-
MeV
1·39 (≃100%)
4
4·122 MeV
2^+
1·368
0^+
^{24}Mg
BACKGROUND
COUNTS IN 30 MIN.
10^3
10^2
10
$T_{\frac{1}{2}}$ = 15 hrs.
0
20
40
60
80
100
120
140
160
TIME (HOURS)

FIG. 4.

All the chemicals used in our (n,γ) measurements were obtained from M/s Johson Mathey & Co. Ltd., London and were 99.99% pure.

The details of various measurements are described separately for each target nucleus. The decay curves for the induced activities are also given along with the necessary details. In cases where background level is not shown in the decay curves, the curves are plotted after subctracting the back-ground counting rate. While calculating the cross-sections the decay curves were extrapolated back to zero time to find the counting rate at the stop of irradiation. For the sake of understanding the mode of calculations $^{23}Na(n,\gamma)\ ^{24}Na$ reaction is described in more details. All the (n,γ) cross-sections at 24 keV are measured by counting the β-activities induced in the samples.

$^{23}Na\ (n,\gamma)\ ^{24}Na$ - Reaction

The target was taken in the form of Na_2Co_3 and its mass was 0.2182 gms. The sample was sandwiched between two standard samples and then irradiated for 28.5 hrs. Induced activity was followed up to 100 hrs. After subtracting the background, one gets 15 hrs. activity as shown in Fig.4. The outline of the calculations are as follows:

Number of ^{23}Na nuclei in the sample (N_o) = 2.478×10^{21}

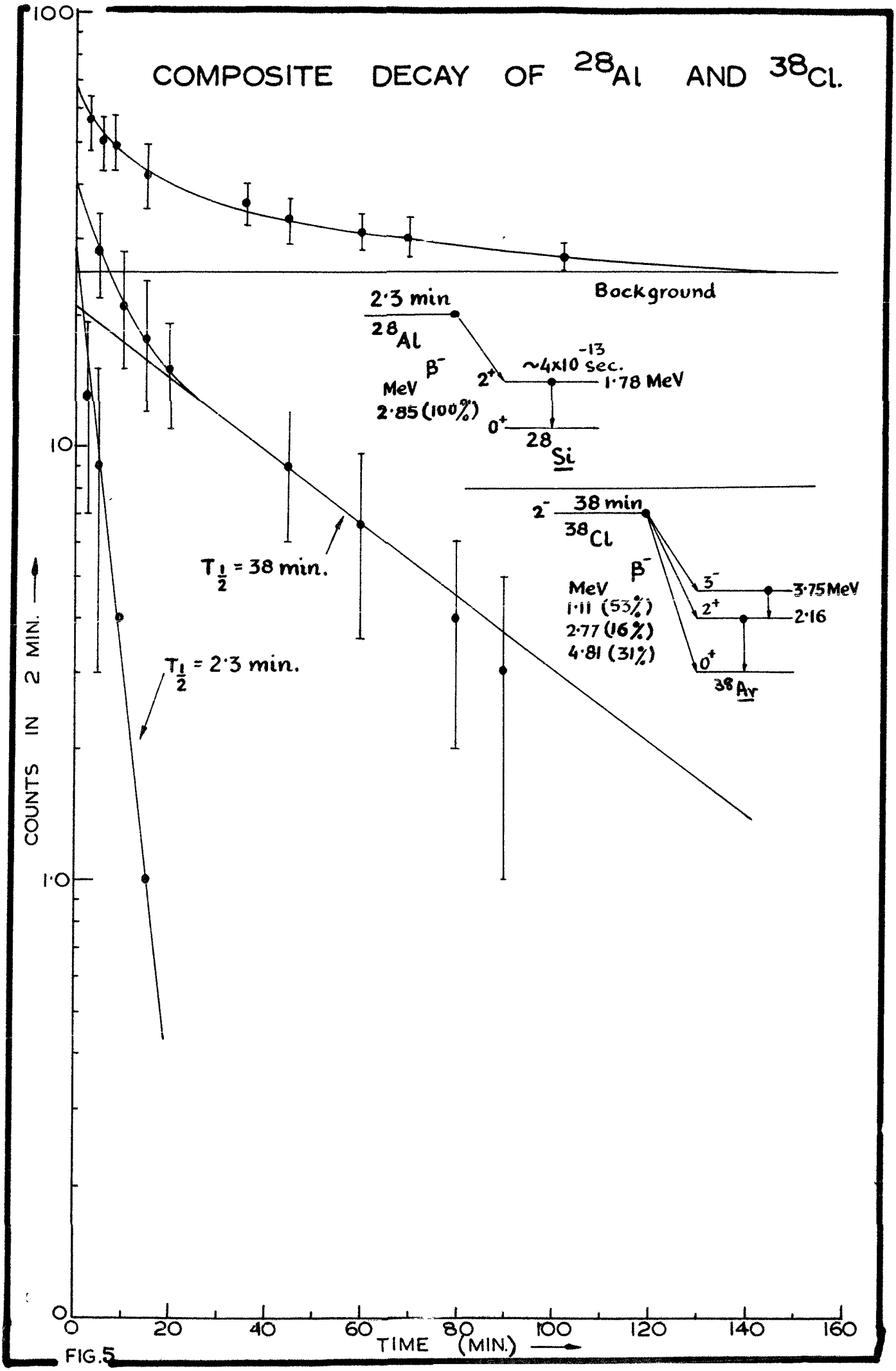
COMPOSITE DECAY OF ^{28}Al AND ^{38}Cl.
100
10
1·0
0
COUNTS IN 2 MIN.
Background
2·3 min
^{28}Al
β⁻
MeV
2·85 (100%)
2⁺
~4x10⁻¹³ sec.
1·78 MeV
0⁺
^{28}Si
2⁻
38 min
^{38}Cl
β⁻
MeV
1·11 (53%)
2·77 (16%)
4·81 (31%)
3⁻
2⁺
0⁺
3·75 MeV
2·16
^{38}Ar
$T_{\frac{1}{2}}$ = 38 min.
$T_{\frac{1}{2}}$ = 2·3 min.
0
20
40
60
80
100
120
140
160
TIME (MIN.)

FIG.5

Average neutron flux obtained from induced activities in KI sample placed on the two sides of actual Na_2Co_3 sample may be given as :

$$\Phi . \text{ Ge} = 0.304 \times 10^5 \quad \text{n/sec.}$$

Detection efficiency of end-window counter (ϵ) = 0.609

saturation correction for the ^{24}Na activity $(1-e^{-\lambda te})$ = 0.731

Counting rate at zero time $(C_{t=o})$ = 100 counts/30 min.

Cross-section for the reaction ^{23}Na (n,γ) ^{24}Na may be given as

$$\sigma = \frac{100/1800}{(2.478 \times 10^{21})\ (0.609)\ (0.731)\ (0.304 \times 10^5)}$$

$$= 1.65 \times 10^{-27} \quad \text{cm}^2$$

Total error in σ = 30%

and so σ = 1.65 $\pm$ 0.48 mb.

^{27}Al (n,γ) ^{28}Al, ^{37}Cl (n,γ) ^{38}Cl - Reactions

1.4056 grams $AlCl_3$ was used to make the target sample. The higher energies of β -rays emitted from the reaction products has made possible the use of thicker sample. Irradiation time in these measurements was 5 hrs. and 22 min. The two resolved halflives are shown in the decay curve of Fig.5. 2.3 min. halflife corresponds to ^{28}Al activity and 38 min. halflife corresponds to ^{38}Cl activity

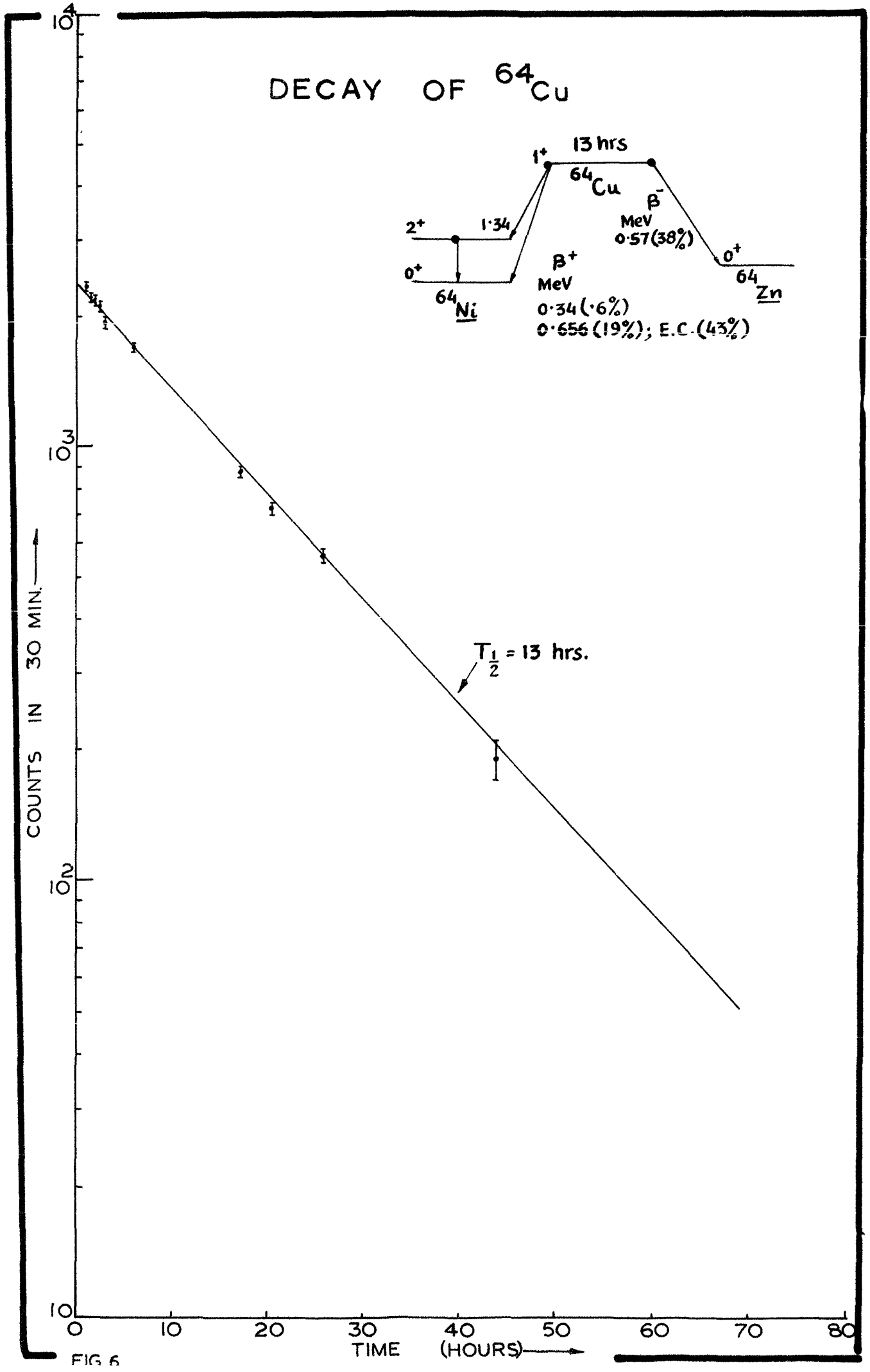
DECAY OF ^{64}Cu
13 hrs
1^+
^{64}Cu
β^-
MeV
0·57(38%)
2^+
1·34
0^+
β^+
MeV
0·34(·6%)
0·656(19%); E.C.(43%)
^{64}Ni
0^+
^{64}Zn
$T_{\frac{1}{2}}$ = 13 hrs.
COUNTS IN 30 MIN.
10^4
10^3
10^2
10
0
10
20
30
40
50
60
70
80
TIME (HOURS)

FIG 6

$^{27}Al(n,\gamma)\ ^{28}Al$ -

Φ Ge = 0.304×10^5 n/sec

N_o = 6.339×10^{21}

$(1-e^{-\lambda t})$ = 1.00

ϵ = 0.373

$C_{t=o}$ = 29 counts/2 min.

σ = 3.36 ± 1 mb.

$^{37}Cl(n,\gamma)\ ^{38}Cl$ -

Φ Ge = 0.304×10^5 n/sec.

N_o = 4.652×10^{21}

$(1-e^{-\lambda te})$ = 1.000

ϵ = 0.396

$C_{t=o}$ = 21 counts/2 min.

σ = 3.12 ± 1 mb.

$^{63}Cu(n,\gamma)\ ^{64}Cu$ - Reaction

0.1562 grams of metallic copper sponge was used for the preparation of the sample. The natural abundance of ^{63}Cu isotope in elemental copper is 69.1%. The sample assembly was irradiated for 25 hours. The decay of ^{64}Cu activity is plotted after subtracting the background counting rate as shown in Fig.6.

Φ Ge = 1.111×10^5 n/sec

N_o = 1.032×10^{21}

$(1-e^{-\lambda te})$ = 0.736

ϵ = 0.150

$C_{t=o}$ = 2400 counts/30 min.

σ = 110 ± 10 mb.

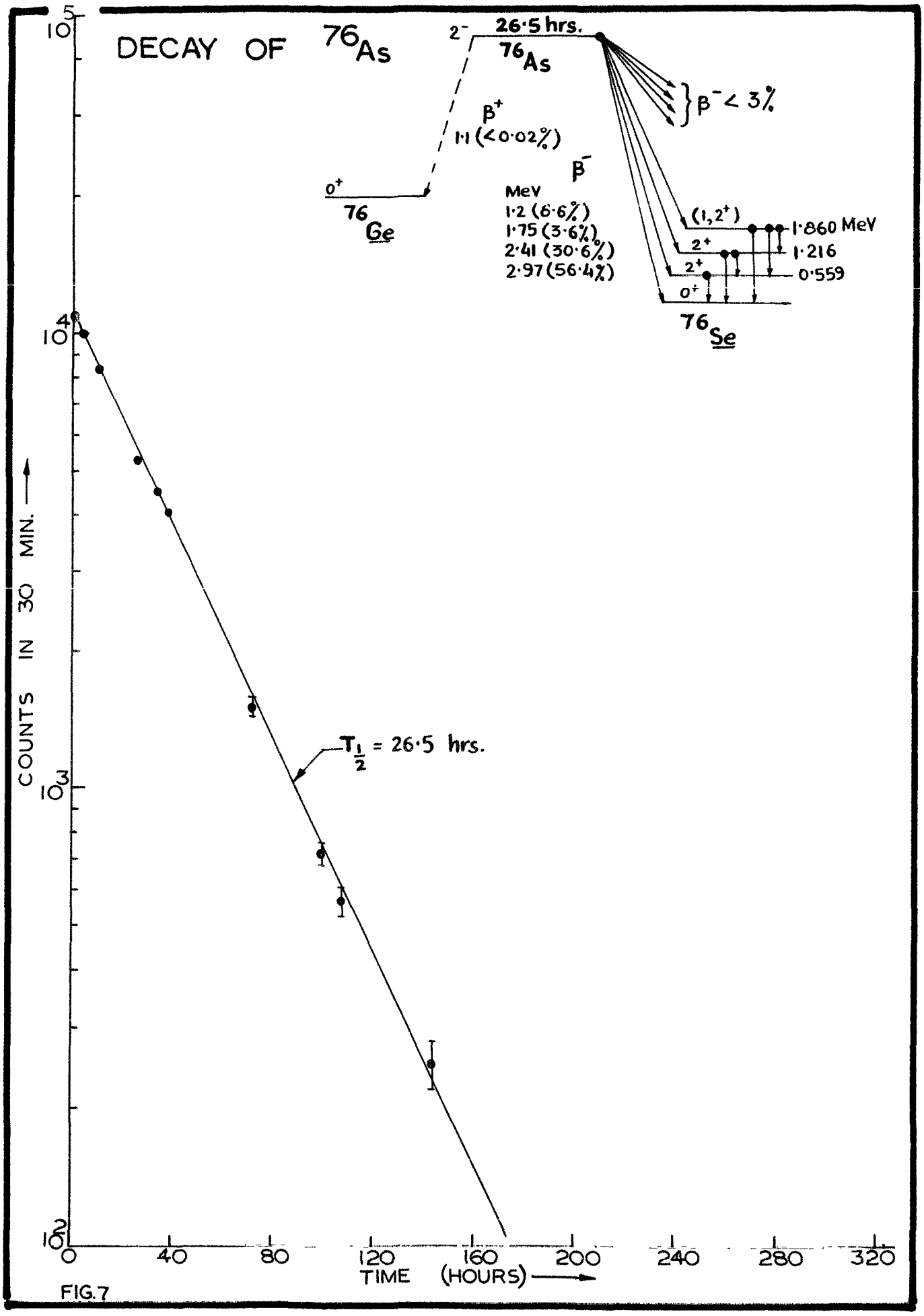
DECAY OF ^{76}As
2^-
26·5 hrs.
^{76}As
β^+
1·1 (<0·02%)
0^+
^{76}Ge
β^-
MeV
1·2 (6·6%)
1·75 (3·6%)
2·41 (30·6%)
2·97 (56·4%)
$\beta^- < 3\%$
$(1, 2^+)$
2^+
2^+
0^+
1·860 MeV
1·216
0·559
^{76}Se
$T_{\frac{1}{2}}$ = 26·5 hrs.
COUNTS IN 30 MIN.
10^5
10^4
10^3
10^2
0
40
80
120
160
200
240
280
320
TIME (HOURS)

FIG. 7

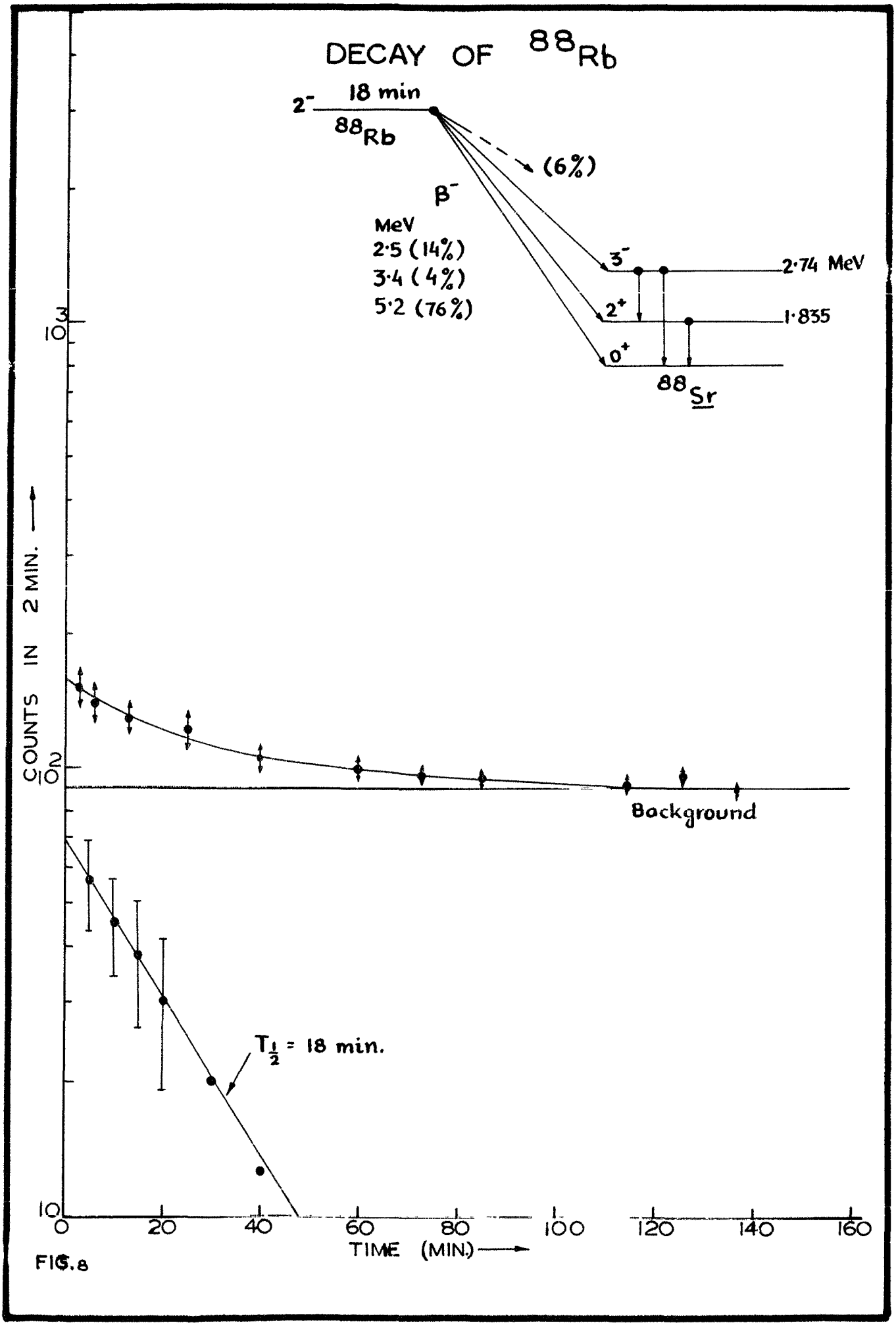
DECAY OF ^{88}Rb
2⁻ 18 min
^{88}Rb
(6%)
β⁻
MeV
2·5 (14%)
3·4 (4%)
5·2 (76%)
3⁻
2⁺
0⁺
2·74 MeV
1·835
^{88}Sr
COUNTS IN 2 MIN. →
10^3
10^2
10
Background
$T_{\frac{1}{2}}$ = 18 min.
0
20
40
60
80
100
120
140
160
TIME (MIN.) →

FIG. 8

$^{75}As(n,\gamma)\ ^{76}As$ - Reaction

0.0802 grams of metallic Arsenic sponge was used for the preparation of the target sample. Arsenic is monoisotopic. The sample assembly was irradiated for 46 hrs. The decay curve after subtracting the background gives 26.5 hrs. halflife as shown in Fig.7.

$\Phi.Ge$ =	0.502×10^5	n/sec.
N_o =	6.443×10^{20}	
$(1-e^{-\lambda t_e})$ =	0.699	
ϵ =	0.874	
$C_{t=o}$ =	11000	counts/30 min
σ =	310 ± 20	mb.

$^{87}Rb(n,\gamma)\ ^{88}Rb$ - Reaction

0.2770 grams of RbCl was used in the preparation of the sample. The sample assembly was irradiated for 39 min.duration. The decay curve on subtracting the background gives 18 min. halflife as shown in Fig.8.

$\Phi.Ge$ =	0.932×10^5	n/sec
N_o =	3.731×10^{20}	
$(1-e^{-\lambda t_e})$ =	0.777	
ϵ =	0.832	
$C_{t=o}$ =	70	counts/ 2 min.
σ =	25 ± 5	mb.

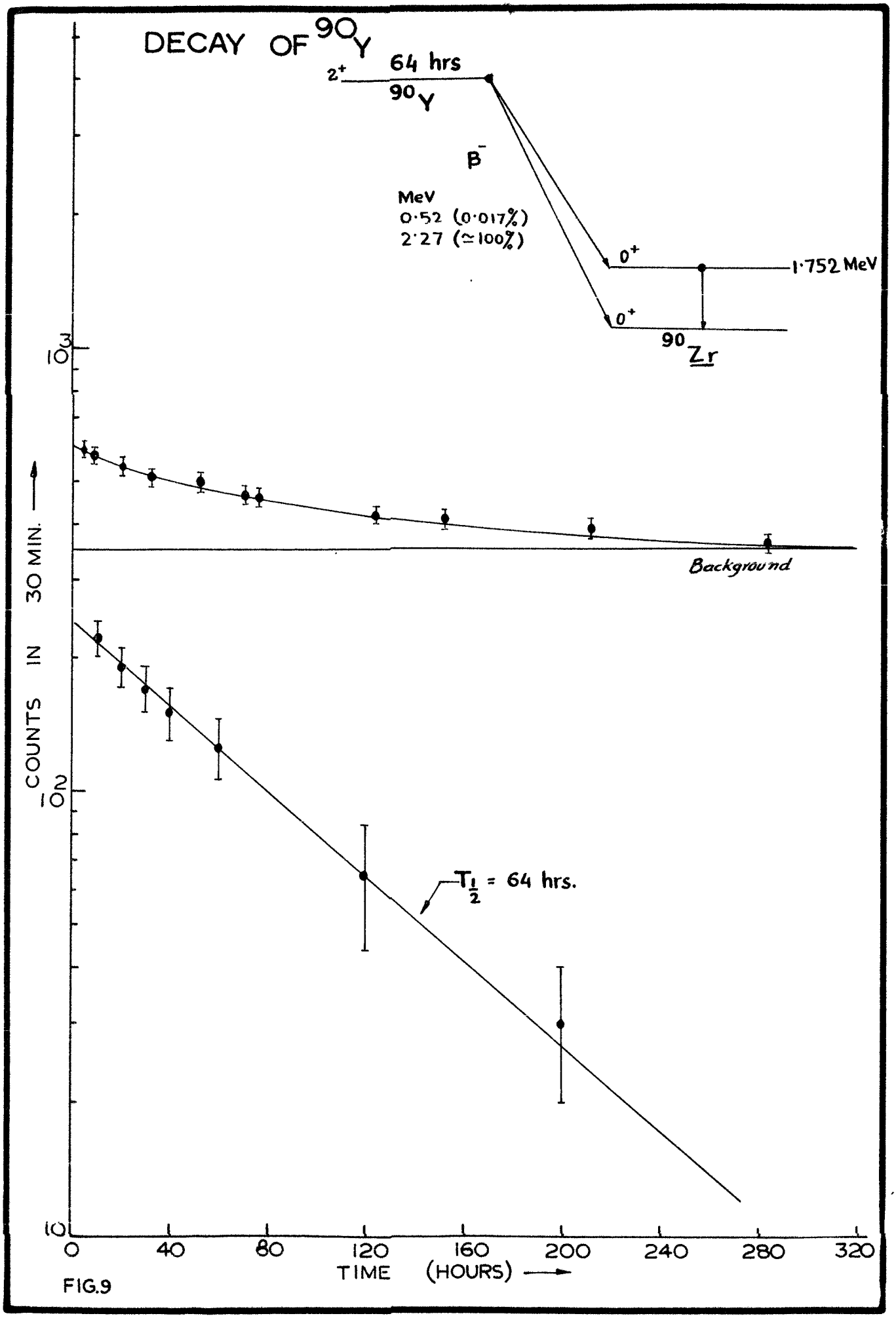
DECAY OF ^{90}Y
2^+
64 hrs
^{90}Y
β^-
MeV
0·52 (0·017%)
2·27 (≃100%)
0^+
1·752 MeV
0^+
^{90}Zr
10^3
COUNTS IN 30 MIN. ⟶
Background
10^2
$T_{\frac{1}{2}}$ = 64 hrs.
10
0
40
80
120
160
200
240
280
320
TIME (HOURS) ⟶

FIG.9

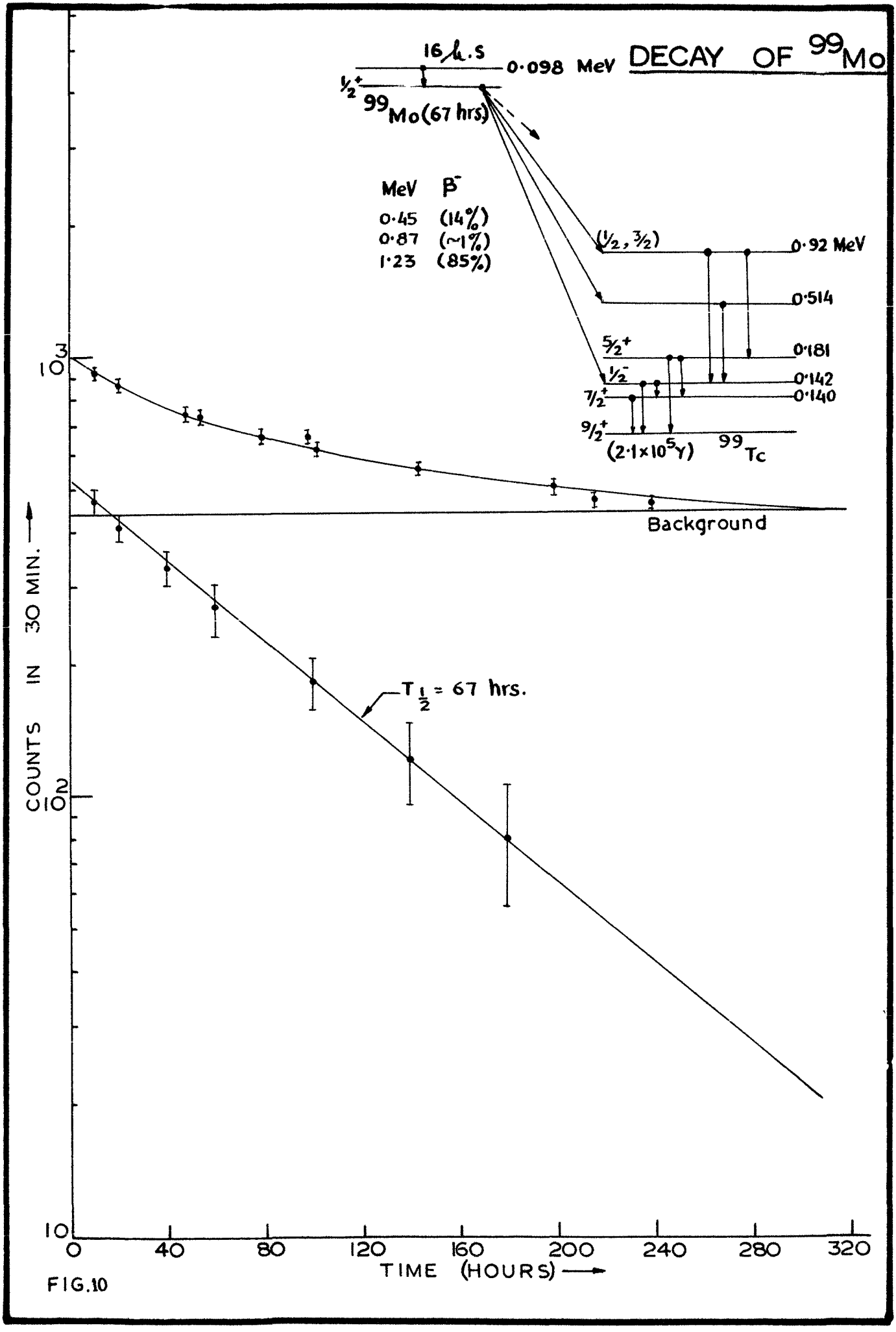
DECAY OF ^{99}Mo
16 h.s
0·098 MeV
$\frac{1}{2}^+$
^{99}Mo(67 hrs)
MeV β⁻
0·45 (14%)
0·87 (~1%)
1·23 (85%)
(1/2, 3/2)
0·92 MeV
0·514
5/2⁺
0·181
1/2⁻
0·142
7/2⁺
0·140
9/2⁺
(2·1×10⁵Y) ^{99}Tc
Background
$T_{\frac{1}{2}}$ = 67 hrs.
COUNTS IN 30 MIN.
10³
10²
10
0
40
80
120
160
200
240
280
320
TIME (HOURS)

FIG.10

$^{89}Y(n,\gamma)\ ^{90}Y$ - Reactions

The sample was prepared by using 0.0410 grams of Y_2O_3. Yetterium is monoisotopic. Sample assembly was irradiated for 134.75 hrs. Decay curve as plotted in Fig.9 shows 64 hrs. halflife.

$\Phi.G_e =$	0.368×10^5	n/sec
$N_o =$	2.185×10^{20}	
$(1-e^{-\lambda t_e}) =$	0.768	
$\epsilon =$	0.911	
$C_{t=o} =$	240	counts/30 min
$\sigma =$	25 ± 5	mb.

$^{98}Mo(n,\gamma)\ ^{99}Mo$ - Reaction

MoO_3 was used for the preparation of sample and its mass was 0.2098 grams. The sample assembly was irradiated for 120 hours. The counting of the activity was started after 9 hrs. from the stop of irradiation. This eliminates any background activity ($T_{\frac{1}{2}}$ = 14.6 min.) due to ^{101}Mo formed by the $^{100}Mo(n,\gamma)\ ^{101}Mo$ reaction. The decay of the induced activity shows 67 hrs. halflife. (See Fig.10)

$\Phi G_e =$	0.401×10^5	n/sec
$N_o =$	2.114×10^{20}	
$(1-e^{-\lambda t_e}) =$	0.711	
$\epsilon =$	0.468	
$C_{t=o} =$	520	counts/30 min.
$\sigma =$	110 ± 15	mb.

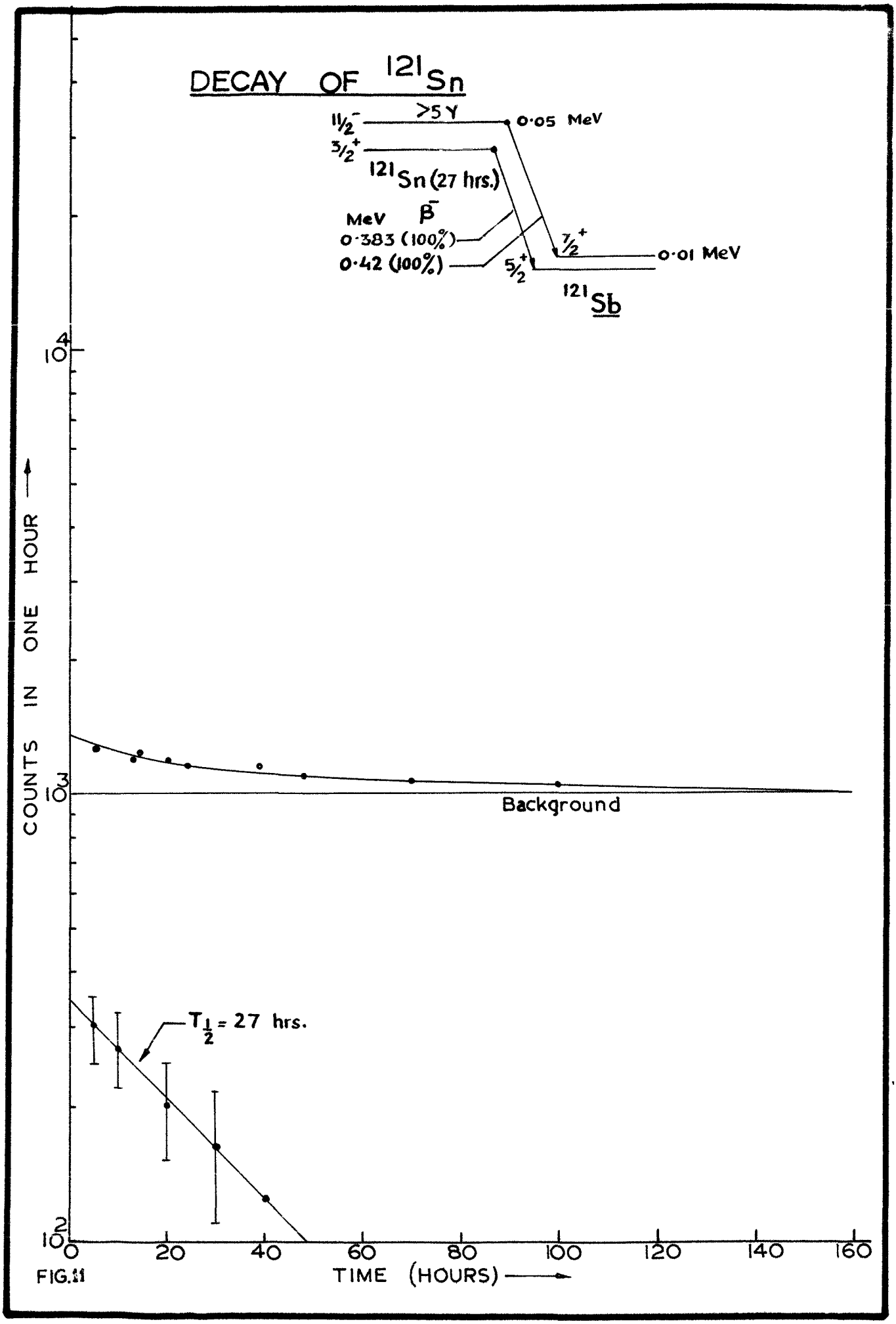
DECAY OF ^{121}Sn
$11/2^-$
>5 Y
0·05 MeV
$3/2^+$
^{121}Sn (27 hrs.)
MeV β⁻
0·383 (100%)
0·42 (100%)
$7/2^+$
$5/2^+$
0·01 MeV
^{121}Sb
COUNTS IN ONE HOUR
10^4
10^3
10^2
Background
$T_{\frac{1}{2}}$ = 27 hrs.
0
20
40
60
80
100
120
140
160
TIME (HOURS)

FIG.11

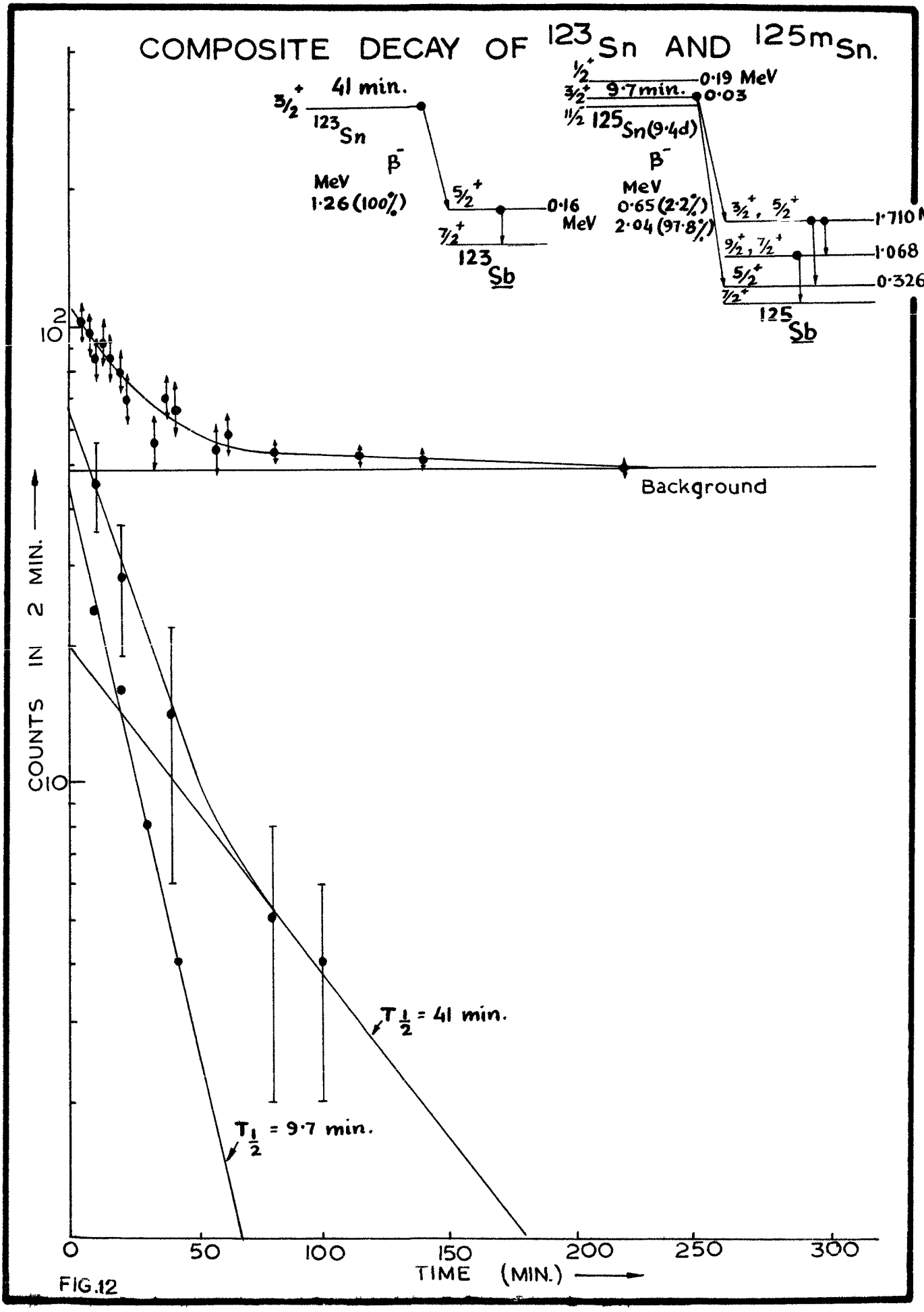
COMPOSITE DECAY OF 123Sn AND 125mSn.
3/2+ 41 min.
123Sn
β⁻
MeV
1·26 (100%)
5/2+
0·16 MeV
7/2+
123Sb
1/2+
9·7 min.
0·19 MeV
0·03
3/2+
11/2 125Sn (9·4d)
β⁻
MeV
0·65 (2·2%)
2·04 (97·8%)
3/2+, 5/2+
1·710 MeV
9/2+, 7/2+
1·068
5/2+
0·326
7/2+
125Sb
10²
Background
COUNTS IN 2 MIN.
10
T 1/2 = 41 min.
T 1/2 = 9·7 min.
0
50
100
150
200
250
300
TIME (MIN.)

FIG.12

$^{120}Sn(n,\gamma)\ ^{121g}Sn$, $^{122}Sn(n,\gamma)\ ^{123g}Sn$ and $^{124}Sn\ (n,\gamma)\ ^{125m}Sn$ - Reactions

0.068 grams of SnO_2 was used for the preparation of the sample. The percentage abundances of ^{120}Sn, ^{122}Sn & ^{124}Sn isotopes in natural element are 32.75%, 4.75% and 6.01% respectively. The measurements were made for two irradiation times. Firstly sample assembly was irradiated for shorter duration i.e. 127 min. The admixture of the two activities i.e. 9.7 min. activity corresponding to $^{124}Sn(n,\gamma)\ ^{125m}Sn$ reaction and 41 min. activity corresponding to $^{122}Sn\ (n,\gamma)\ ^{123g}Sn$ reaction was obtained. The shorter duration of irradiation helped us in eliminating large background build up due to ^{121g}Sn formed by the reaction $^{120}Sn(n,\gamma)\ ^{121g}Sn$. In second case sample assembly was irradiated for 29 hrs. and 50 min. The counting was started after 5 hrs. from the stop of irradiation so that the short lived activities may decay. Fig.12 shows the two activities of halflife 9.7 min. and 41 min. due to ^{125m}Sn and ^{123g}Sn. In Fig.11 is shown the decay of ^{121g}Sn with halflife 27 hrs.

$^{120}Sn(n,\gamma)\ ^{121g}Sn$ -

ΦG_e =	1.182×10^5	n/sec.
N_o =	8.853×10^{19}	
$(1-e^{-\lambda t_e})$ =	0.535	
ϵ =	0.220	
$C_{t=0}$ =	350	counts/Hour
σ =	77 ± 11	mb.

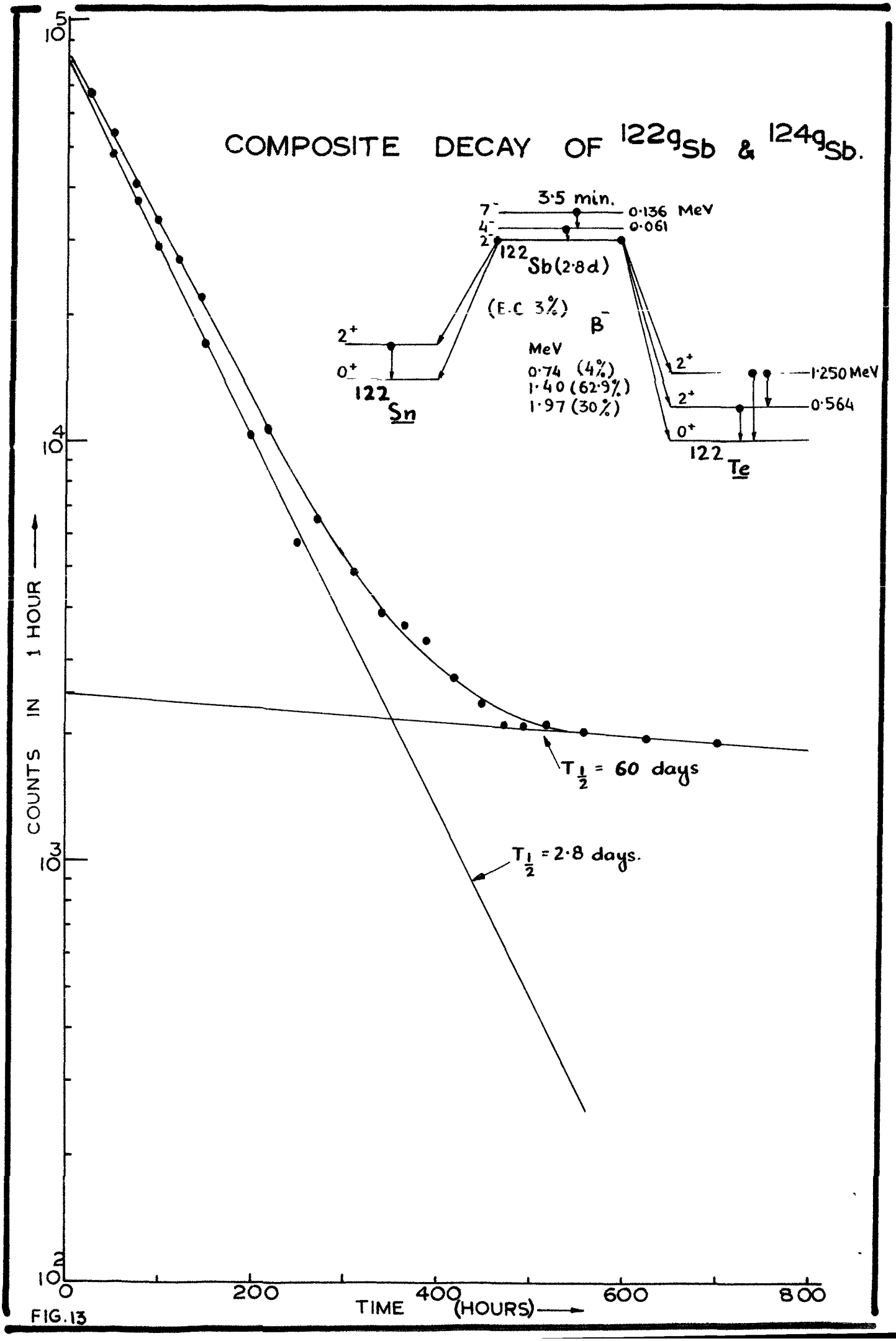
COMPOSITE DECAY OF 122g Sb & 124g Sb.
3·5 min.
7⁻
4⁻
2⁻
0·136 MeV
0·061
122 Sb (2·8 d)
(E.C 3%)
β⁻
MeV
0·74 (4%)
1·40 (62·9%)
1·97 (30%)
2⁺
0⁺
122 Sn
2⁺
2⁺
0⁺
1·250 MeV
0·564
122 Te
T½ = 60 days
T½ = 2·8 days.
COUNTS IN 1 HOUR
10⁵
10⁴
10³
10²
0
200
400
600
800
TIME (HOURS)

FIG. 13

$^{122}Sn\ (n,\gamma)\ ^{123g}Sn$ -

$\Phi.Ge =$	1.243×10^{5}	n/sec.
$N_o =$	1.247×10^{19}	
$(1-e^{-\lambda t_e}) =$	0.878	
$\epsilon =$	0.756	
$C_{t=o} =$	20	counts/ 2 min.
$\sigma =$	162 ± 81	mb.

$^{124}Sn\ (n,\gamma)\ ^{125m}Sn$ -

$\Phi.Ge =$	1.243×10^{5}	n/sec
$N_o =$	1.557×10^{19}	
$(1-e^{-\lambda t_e}) =$	1.00	
$\epsilon =$	0.866	
$C_{t=o} =$	45	counts/ 2 min.
$\sigma =$	220 ± 55	mb.

$^{121}Sb\ (n,\gamma)\ ^{122(m+g)}Sb$ and $^{123}Sb(n,\gamma)\ ^{124g}Sb$ - Reactions

Metallic antimony sponge weighing 0.2664 gms. was used for the sample preparation. The percentage abundances of ^{121}Sb and ^{123}Sb isotopes in elemental antimony are 57.25% and 42.75% respectively. The sample assembly was irradiated for 136.5 hrs. Counting was started after 25 hrs. from the stop of irradiation. During this time short lived activities due to the reactions $^{123}Sb(n,\gamma)\ ^{124m_1,m_2}Sb$ had decayed. Resolved activities (halflives 2.8 days and 60 days) correspon-

ding to ^{121}Sb (n,γ) ^{122g}Sb and ^{123}Sb (n,γ) ^{124g}Sb reaction products are shown in Fig.13. In case of ^{121}Sb (n,γ) $^{122m,g}Sb$, the isomeric state decays directly to the ground state through the isomeric transition. The 2.8 days ground state activity also contains the contribution due to the isomeric state activity and hence the calculated cross-section is the sum of the cross-sections corresponding to isomeric state and the ground state.

$^{121}Sb(n,\gamma)$ $^{122(m+g)}Sb$ -

Φ Ge =	1.144×10^5	n/sec
N_o =	7.762×10^{20}	
$(1-e^{-\lambda t_e})$ =	0.755	
ϵ =	0.475	
$C_{t=o}$ =	80000	counts/hour
σ =	700 $\pm$ 70	mb.

^{123}Sb (n,γ) ^{124g}Sb -

Φ. Ge =	1.144×10^5	n/sec.
N_o =	5.585×10^{20}	
$(1-e^{-\lambda t_e})$ =	0.062	
ϵ =	0.306	
$C_{t=o}$ =	2500	counts/hour
σ =	575 $\pm$ 50	mb.

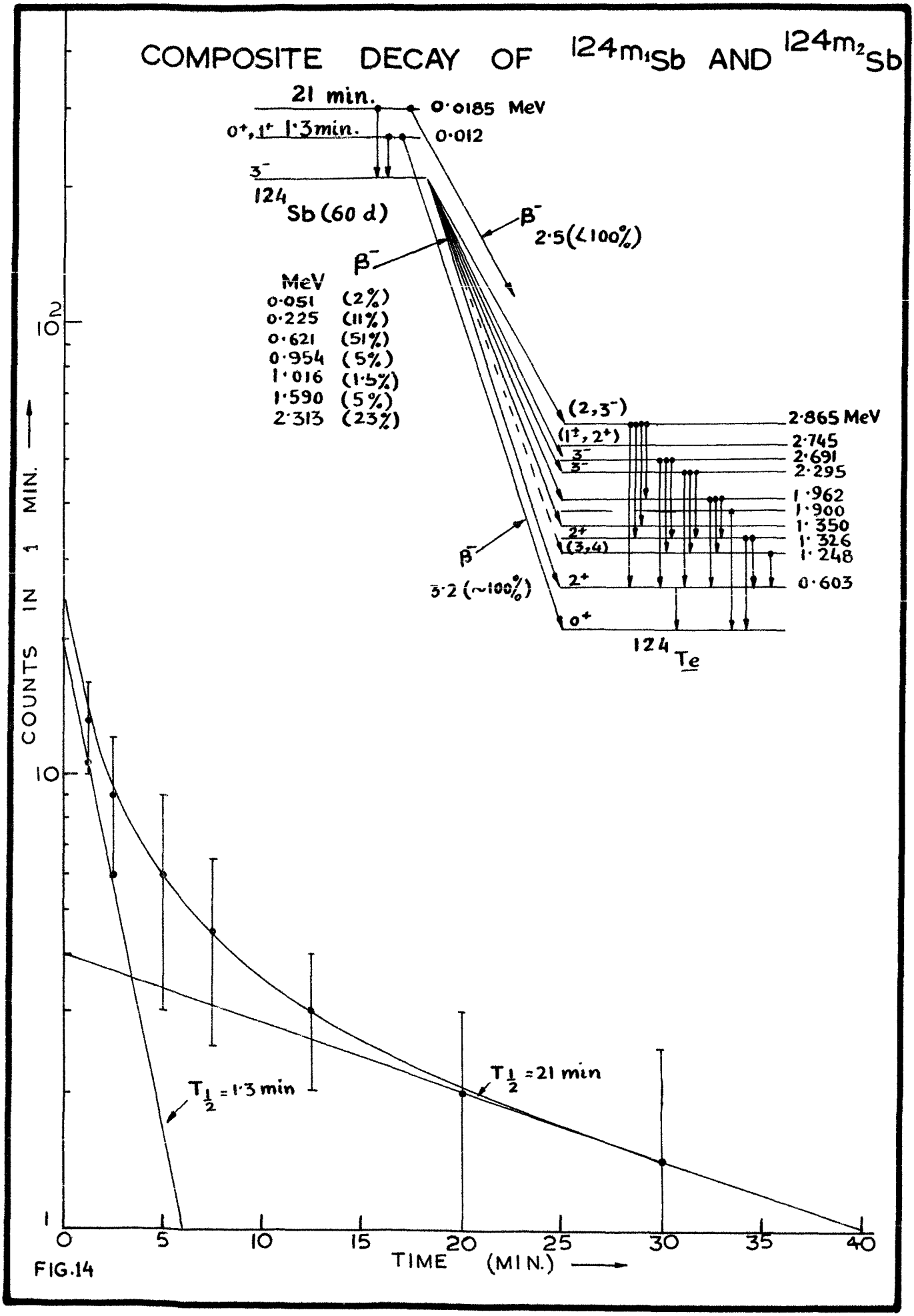
COMPOSITE DECAY OF 124m1Sb AND 124m2Sb
21 min.
0·0185 MeV
0+, 1+ 1·3min.
0·012
3⁻
124Sb (60 d)
β⁻
2·5(<100%)
β⁻
MeV
0·051 (2%)
0·225 (11%)
0·621 (51%)
0·954 (5%)
1·016 (1·5%)
1·590 (5%)
2·313 (23%)
(2,3⁻)
2·865 MeV
(1±, 2⁺)
2·745
3⁻
2·691
3⁻
2·295
1·962
1·900
2⁺
1·350
(3,4)
1·326
1·248
β⁻
3·2 (~100%)
2⁺
0·603
0⁺
124Te
COUNTS IN 1 MIN.
10²
10
1
T½ = 1·3 min
T½ = 21 min
0
5
10
15
20
25
30
35
40
TIME (MIN.)

FIG.14

$^{123}Sb\ (n,\gamma)\ ^{124m_1,m_2}Sb$ - Reactions

In these measurements a thicker sample of metallic antimony sponge, weighing 1.1992 grams, was prepared. From the decay scheme of ^{124}Sb one can see that both the isomeric states decay through β-particle emission separately. Energy of the β-particles involved in these measurements are quite high i.e. 2.5 MeV and 3.2 MeV and so use of thicker sample was possible. Thicker sample was needed because the induced activities were very weak. The sample assembly was irradiated for 21 min. only to avoid build-up of the long lived activities. The measurements were repeated several times to improve statistical counting error.

The mean of the decay curves with same irradiation time (21 min.) is shown in Fig.14. The two resolved halflives 1.3 min. and 21 min. correspond to the $^{124m_2}Sb$ and $^{124m_1}Sb$ activities respectively.

$^{123}Sb(n,\gamma)\ ^{124m1}Sb$ (21 min) -

$\Phi_{Ge} = 4.765 \times 10^{4}$ n/sec

$N_o = 2.508 \times 10^{21}$

$(1-e^{-\lambda t}) = 0.500$

$\epsilon = 0.359$

$C_{t=o} = 4$ counts/min

$\sigma = 3.1 \pm 1.5$ mb.

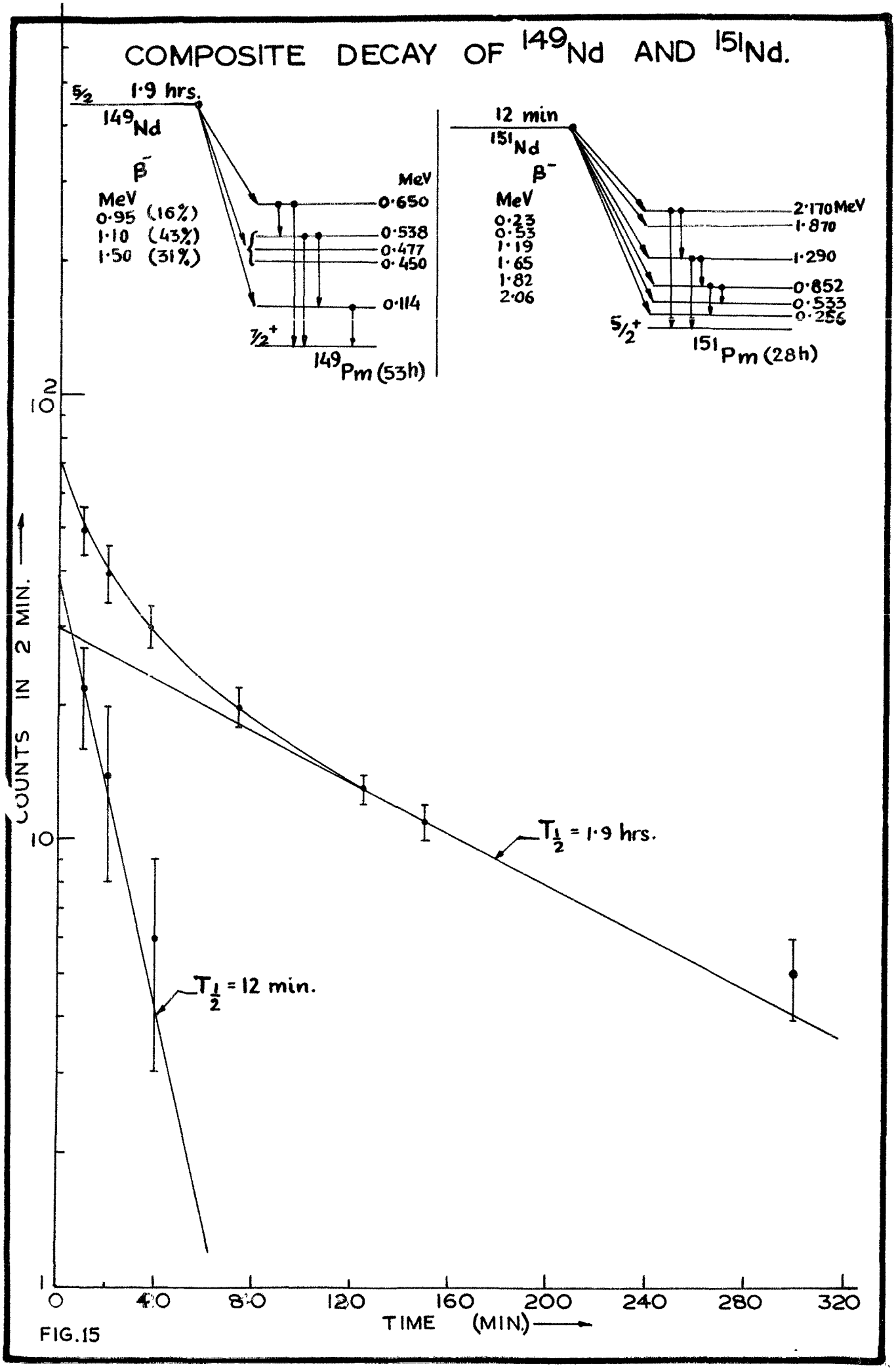
COMPOSITE DECAY OF 149Nd AND 151Nd.
5/2
1·9 hrs.
149Nd
β⁻
MeV
0·95 (16%)
1·10 (43%)
1·50 (31%)
MeV
0·650
0·538
0·477
0·450
0·114
7/2+
149Pm (53h)
12 min
151Nd
β⁻
MeV
0·23
0·53
1·19
1·65
1·82
2·06
2·170 MeV
1·870
1·290
0·852
0·533
0·256
5/2+
151Pm (28h)
COUNTS IN 2 MIN.
10²
10
1
T½ = 1·9 hrs.
T½ = 12 min.
0
40
80
120
160
200
240
280
320
TIME (MIN.)

FIG.15

$^{123}Sb\ (n,\gamma)\ ^{124m2}Sb(1.3\ min)$ -

$\Phi.G_e = 4.765 \times 10^4$ n/sec.

$N_o = 2.508 \times 10^{21}$

$(1-e^{-\lambda t_e}) = 1.000$

$\epsilon = 0.515$

$C_{t=o} = 20$ counts/min

$\sigma = 5.4 \pm 1.3$ mb.

$^{148}Nd\ (n,\gamma)\ ^{149}Nd$ and $^{150}Nd\ (n,\gamma)\ ^{151}Nd$ - Reactions

0.1944 gram Nd_2O_3 was used for the sample preparation. Irradiation of the sample assembly was carried out for 250 min. The composite decay curve obtained after subtracting the background gives 12 min. and 1.9 hrs. activities corresponding to the reaction products of $^{150}Nd\ (n,\gamma)\ ^{151}Nd$ and $^{148}Nd\ (n,\gamma)\ ^{149}Nd$ reactions respectively (See Fig.15).

$^{148}Nd\ (n,\gamma)\ ^{149}Nd$ -

$\Phi.G_e = 0.940 \times 10^5$ n/sec

$N_o = 3.880 \times 10^{19}$

$(1-e^{-\lambda t_e}) = 0.782$

$\epsilon = 0.534$

$C_{t=o} = 30$ counts/ 2 min.

$\sigma = 165 \pm 35$ mb.

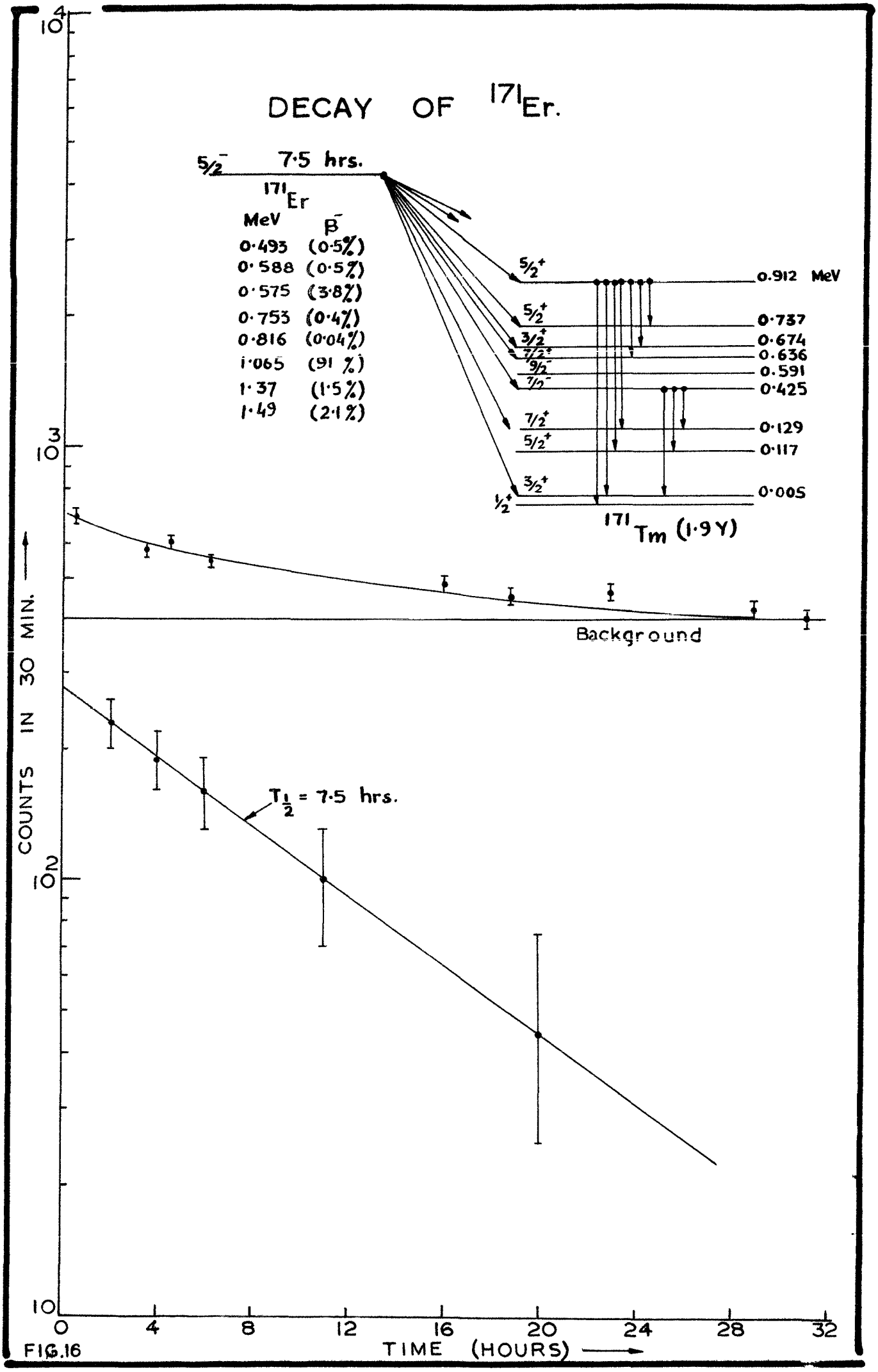
DECAY OF 171Er.
5/2⁻ 7·5 hrs.
171Er
MeV β⁻
0·495 (0·5%)
0·588 (0·5%)
0·575 (3·8%)
0·753 (0·4%)
0·816 (0·04%)
1·065 (91 %)
1·37 (1·5%)
1·49 (2·1%)
5/2⁺ 0.912 MeV
5/2⁺ 0·737
3/2⁺ 0·674
7/2⁺ 0·636
9/2⁻ 0·591
7/2⁻ 0·425
7/2⁺ 0·129
5/2⁺ 0·117
3/2⁺ 0·005
1/2⁺
171Tm (1·9 Y)
Background
T½ = 7·5 hrs.
COUNTS IN 30 MIN.
10⁴
10³
10²
10
0
4
8
12
16
20
24
28
32
TIME (HOURS)

FIG.16

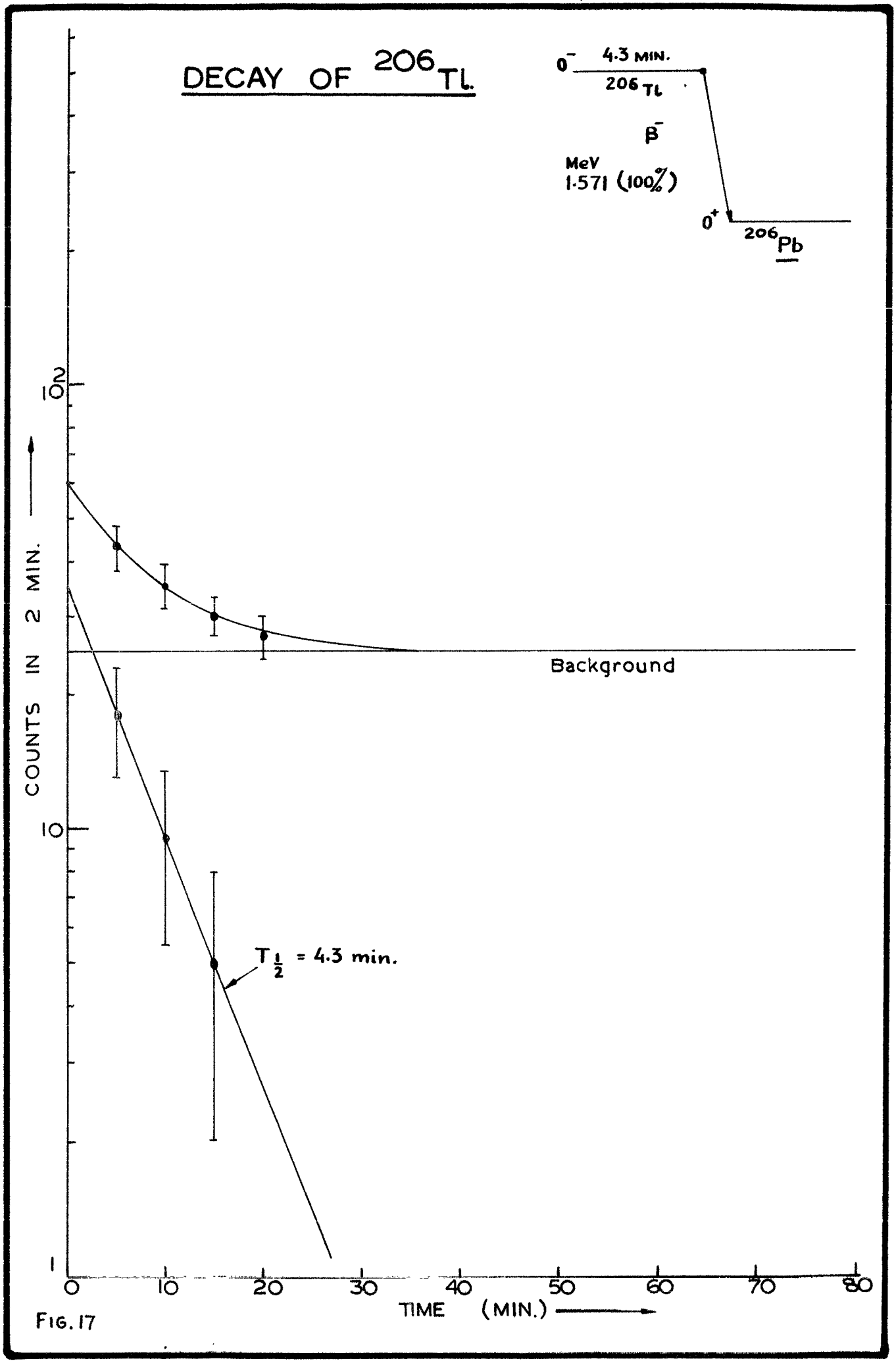
DECAY OF 206Tl.
0⁻ 4.3 MIN.
206Tl
β⁻
MeV
1.571 (100%)
0⁺
206Pb
COUNTS IN 2 MIN.
10²
10
1
Background
T½ = 4.3 min.
0
10
20
30
40
50
60
70
80
TIME (MIN.)

FIG. 17

$^{150}Nd(n,\gamma)\ ^{151}Nd$ -

$\Phi.Ge =$	0.940×10^{5}	n/sec.
$N_o =$	3.743×10^{19}	
$(1-e^{-\lambda t_e}) =$	1.000	
$\epsilon =$	0.763	
$C_{t=o} =$	40	counts/2 min.
$\sigma \geq$	125	mb.

$^{170}Er(n,\gamma)\ ^{171}Er$ - Reaction

Er_2O_3 weighing 0.0162 grams, was used for preparing the sample. Sample assembly was irradiated for 24 hrs. The decay curve gives 7.5 hrs. halflife corresponding to ^{170}Er $(n,\gamma)\ ^{171}Er$ reaction product as shown in Fig.16.

$\Phi.Ge =$	0.353×10^{5}	n/sec
$N_o =$	2.820×10^{19}	
$(1-e^{-\lambda t_e}) =$	0.867	
$\epsilon =$	0.754	
$C_{t=o} =$	280	counts/30 min.
$\sigma =$	255 ± 30	mb.

$^{205}Tl(n,\gamma)\ ^{206}Tl$ - Reaction

0.2006 grams TlCl was used for the sample preparation. Natural abundance of ^{205}Tl isotope is 70.5%. Sample assembly was irradiated for 20 min. Measurements were repeated

several times with the same irradiation time to improve the statistical counting error. The mean decay curve from these measurements is shown in Fig.17.

$\phi G_e = 0.372 \times 10^5$ n/sec.

$N_o = 3.970 \times 10^{20}$

$(1-e^{-\lambda t_e}) = 0.954$

$\epsilon = 0.678$

$C_{t=o} = 35$ counts/2 min.

$\sigma = 30 \pm 8$ mb.

Table - I gives the results of the present measurements (column 3) alongwith earlier reported values (column.4) wherever they are known.

3.3 Statistical Theory at 24-keV Neutron Energy:

Bohr's compound nucleus theory [46] is the antithesis of the single particle model and assumes that all the neucleons forming the target nucleus or incident upon it interact strongly. As a consequence of the strong interaction, the incident particle and the target nucleus coalesce forming a compound state in which all or many nucleons participate collectively. These compound nuclear states are quasi-stationary. They have a finite lifetime, since they can decay by re-emission of the incident particle, gamma-rays or otherwise The experimentally observed closely spaced resonances in the low energy neutron experiments are the compound nucleus levels.

TABLE - I: Neutron Radiative Capture Cross-section At 24 keV.

Target Nucleus X	Half-life of X + 1	Cross-section σ (mb.)	Earlier Reported σ (mb.) Values
^{23}Na	15 h	1.65 ± 0.48	1.0 ± 0.2[11], 1.72 ± 0.34[16]
^{27}Al	2.3 min	3.36 ± 1	1.4 ± 0.2[11], 2.6 ± 0.22[15]
^{37}Cl	38 min	3.12 ± 1	1.1 ± 0.2[11], 3.71 ± 0.74[16]
^{63}Cu	13 h	110 ± 10	116 ± 12[11], 105 ± 21[12]
^{75}As	26.5 h	310 ± 20	740 ± 70[11], 650 ± 160[12]
^{87}Rb	18 min	25 ± 5	75 ± 15[11], 29 ± 6[16]
^{89}Y	64 h	25 ± 5	28 ± 7[12]
^{98}Mo	67 h	110 ± 15	209 ± 21[11], 415 ± 98[15]
^{120}Sn	27 h	77 ± 11	
^{122}Sn	41 min.	162 ± 81	
^{124}Sn	9.7 min.	220 ± 55	
^{121}Sb	2.8d + ? 3.5 min	700 ± 70	950 ± 100[11], 810 ± 250[12]
^{123}Sb	1.3 min.	5.4 ± 1.3	
^{123}Sb	21 min	3.1 ± 1.5	
^{123}Sb	60 d	575 ± 50	456 ± 46[11], 230 ± 100[12]
^{148}Nd	1.9 h	165 ± 35	
^{150}Nd	12 min	>125	
^{170}Er	7.5 hrs	255 ± 30	298 ± 30[11]
^{205}Tl	4.3 min	30 ± 8	

Quasi-stationary compound nuclear states wave functions must have time dependent factor $e^{-i(\epsilon_0 - i\Gamma/2)t/\hbar}$ where ϵ_0 is the energy corresponding to a certain resonance (compound nucleus level) and Γ is the width of the resonance. The use of Heisenberg uncertainty relation, relates the life time of the compound nucleus states (τ) and its width (Γ). The relation between the two may be given as :

$$\tau = \frac{.66 \times 10^{-15}}{\Gamma(eV)} \text{ Sec.} \qquad \ldots\ldots \quad (1)$$

The widths of the observed resonances are of the order of e.V or so. The corresponding lifetime comes out to be of the order of 10^{-14} seconds. The lifetime of the compound nuclear states are comparable to the typical electromagnetic transition time (10^{-14} - 10^{-15} sec). Thus compound nucleus reaction mechanism could very easily explain the results of low energy neutron experiments as it can account for the observed closely spaced resonances and the actual predominance of capture over scattering in low energy resonances.

With increasing neutron energy, the compound nucleus levels become closer and closer. Also the widths of the levels go on increasing with the increasing energy, as at higher energies more reaction channels are open and each contribute to the width of the level. Due to this reason at higher neutron energies compound nucleus levels start overlapping.

In this energy region the cross-section depends largely upon the phase relations between the overlapping compound states and description in terms of individual compound states becomes impracticable.

Bohr generalised his theory for the energy region of overlapping compound nucleus state, by making the following assumptions. The nuclear reaction can be divided in two steps: the formation of the compound nucleus and its subsequent decay. The decay of the compound nucleus is independent of its mode of formation. With this assumption one can write cross-section for a certain reaction (a,b) as:

$$\sigma(a,b) = \sigma_c(a) \quad (\Gamma_b/\Gamma)_c \qquad \ldots\ldots \quad (2)$$

Where σ_c (a) is the cross-section for the formation of the compound nucleus by the incident particle 'a' and $(\Gamma_b/\Gamma)_c$ is the probability that particle 'b' is emitted by the compound state.

However, in the region of considerable overlapping of the compound states, independence hypothesis is by no way obvious. In this case incident particle of fixed energy excites several compound states and the relative phase of the states will depend upon the nature of excitation. The emission probability of these linear combinations of states would depend upon their phase relation and hence upon their mode of excitation.

Bohr introduced another assumption to justify the independence hypothesis. When the density of the compound nucleus states is very large, many compound nucleus states are excited simultaneously. So many states and so many phases are involved in the reason that they may act in respect to the decay process as if they are random. It is then possible that the second stage of the nuclear reaction appears independent of the first stage i.e. mode of formation.

Still independence hypothesis requires justification for the intermediate energies. The certain spread in the energy of the incident particle beam can satisfactorily account for the applicability of independence hypothesis. Though at a fixed energy of the neutrons, in the intermediate energy range, the number of compound nucleus state excited is not very large, but within the energy spread of the incident neutrons the number of excited states becomes very large and hence independence hypothesis may be valid.

A look on the above fact allows us the use of compound nuclear reaction mechanism to calculate (n,γ) reaction cross-section at 24 keV neutron energy when the inherent spread in the energy is 3 keV.

3.4 Capture Cross-section from Statistical Theory :

Margolis[47] has derived an expression for the (n,γ) cross-section based on the statistical theory. The expression gives the actual cross-section in the overlap region, where

it is smooth function of energy. A brief outline of Margolis formalism may be given as follows. :

Let 'I' be the spin of the target nucleus. This spin combines with the neutron spin to give us a "channel spin" $j = j^{\pm} = I \pm 1/2$. The components (m) of j along the Z-axis (the direction of the incident neutron beam) are -j. (-j+1) ... . , (j-1), (j). Following Hauser and Feshbech[48], the cross-section for the formation of the compound nucleus with spin 'J' by the incident neutron of angular momentum 'ℓ' and energy 'E' in the channel of spin j and Z-component 'm' may be given as

$$\sigma(\ell,j,J,mE) = (2\ell+1)\,\pi\lambda^2\, T(E) \times |(\ell j 0\ m\ |Jm)|^2 \quad \ldots\ (3)$$

$2\pi\lambda$ is the wavelength of the incident neutron, $(\ell j 0 m | j\ m)$ is the Clebsch-Gordan coefficient relating to the probability that ℓ and j with Z-component 0 and m combine vectorially to give spin J with Z-component m, and $T_\ell(E)$ is the transmission coefficient for the neutrons.

Now the partial decay probability of the compound state with spin J and excitation energy (B+E) (B is the last neutron binding energy in the compound nucleus) through γ-emission may be given as :

$$(\ell,j,J,m,E) \times \left[\Gamma_\gamma^J\ (B+E) / \Gamma^J\ (B+E) \right] \qquad \ldots\ (4)$$

where $\Gamma_\gamma^J(E+B)$ and $\Gamma^J(B+E)$ are the partial radiation width and total width respectively of the compound state with spin J and excitation energy (E+B). Summing expression (4) over the possible J's and ℓ's, and averaging over all j and m we get

$$\sigma_{cap} = \frac{\pi \lambda^2}{2(2I+1)} \sum_{\ell=0}^{\infty} T_\ell(E) \left[\sum_{J=0}^{\infty} \frac{\epsilon_{j\ell}^J (2J+1)\, \Gamma_\gamma^J(B+E)}{\Gamma^J(B+E)} \right] \quad \ldots\ldots \quad (5)$$

where

$$\epsilon_{j\ell}^J = 2, \quad |J-\ell| \le j \le J+\ell \quad \text{for both } j\text{'s}$$
$$= 1, \quad |J-\ell| \le j \le J+\ell \quad \text{for one of the two } j\text{'s only}$$
$$= 0 \text{ otherwise}$$

Margolis used a form of the level density

$$\rho(E) = C \exp 2(aE)^{1/2} \quad \ldots\ldots \quad (6)$$

to calculate (Γ_γ/Γ). The expression derived by him is given by

$$\Gamma_n^{(J,\ell')}(E') \Big/ \Gamma_\gamma^J(B+E) = \xi_J T_{\ell'}(E') f_\lambda(E) \quad \ldots\ldots \quad (7)$$

Where $\Gamma_n^{(J,\ell')}(E')$ is the width for the neutron emission of angular momentum ℓ' and energy E' from the compound state of spin J and excitation energy (B+E) and

$$f_\lambda = \int_0^B \epsilon^{2\lambda+1} \rho(B-\epsilon)\, d\epsilon \Big/ \int_0^{B+E} \epsilon^{2\lambda+1} \rho(B+E-\epsilon)\, d\epsilon \quad \ldots\ldots \quad (8)$$

λ being the multipolarity of the γ-rays emitted and

$$\xi_J = D^J(B) \Big/ 2\pi\, \Gamma_\gamma^J(B) \quad \ldots\ldots \quad (9)$$

where $D^J(B)$ is the spacing of the compound nucleus levels of spin J at excitation energy (B).

On the assumption that at the value of the excitation energy concerned compound nucleus can decay by neutron emission or by γ-emission one can write for (n, γ) reaction cross-section using equations (5) and (7),

$$\sigma_{cap}(E) \simeq \frac{\pi \lambda^2}{2(2I+1)} \sum_{l=0}^{\infty} \left[T_l(E) \times \sum_{J=0}^{\infty} \frac{\epsilon^J_{jl} (2J+1)}{1 + \xi_J f_\lambda(E) \sum_{l'} \sum_{n} \epsilon^J_{jnl'} T_{l'}(E-E_n)} \right] \quad \ldots\ldots\ldots \quad (10)$$

Where E_n is the energy of the nth excited state of the target nucleus and $j_n = i_n \pm \frac{1}{2}$ where i_n is the spin of the nth excited state of the target nucleus. The sum over l' includes only those values for which parity of the system remains conserved. The sum over E_n includes only those states for which $E_n < E$.

3.5. The Mode of Calculations:

In equation (10) for the (n, γ) cross-section a parameter ξ_J appears. For the reasons given by Margolis ξ_J can be taken as independent of J and one can write

$$\xi_J = \xi_\gamma = D / 2\pi \Gamma_\gamma \quad \ldots\ldots\ldots \quad (11)$$

Where D is the spacing between the compound nucleus levels of the same spin and Γ_γ is the radiation width at the appropriate excitation energy of the compound nucleus. ξ_γ is calculated from equation (10) by putting our experimental values of $\sigma(n, \gamma)$ in the equation.

The factor f_λ accounts for the energy and level-density dependence of the width Γ_γ. It is found[49] that dipole emission predominates over other higher multipoles, the ratio of the two is of the order of 10^{-5}. So only dipole emission is assumed. Previous workers[19] have shown that at this energy of neutrons the value of f_λ can be taken as 0.944. The same value of f_λ is used in the present calculations.

The expression for the de-Broglic wavelength of incident neutrons may be given as:

$$\lambda = \frac{2\times(3.142)\times 4.55\times 10^{-10}}{2\pi\sqrt{E_n(eV)}} \text{ cm} \quad \ldots\ldots \quad (12)$$

Neutron transmission coefficients are taken from the literature.[50] These transmission coefficients are calculated using Saxon Wood type complex potential i.e.:

$$V = -V_0 (1+i\xi) \{1+ \exp. 2(r-R)/d\}^{-1} \ldots\ldots \quad (13)$$

the parameter V_0 is taken 52 MeV, as it fits most of the experimental data.

Observed Value of ξ (ξ_{obs}) -

The value ξ_{obs} is obtained from low energy neutron resonance experiments. The experimental value of $\overline{\Gamma_\gamma}$ and D are taken from literature.[51-53] In some cases where $\overline{\Gamma_\gamma}$ is not known experimentally it is estimated from a graph plotted between $\overline{\Gamma_\gamma}$ and N (the neutron number). For s-wave resonances the two spins of the compound nucleus $J = I \pm \frac{1}{2}$ (for $I \neq 0$) are formed. These

two levels are generally too close to be resolved experimentally and so the observed average level spacing D must be related to the actual average level spacing D_o of the compound nucleus by the relation :

$$1/D = 1/D^+ + 1/D^- = 2/D_o$$

or $D_o = 2D$ where $D^+ = D^- \simeq D_o$

Hence for the target nuclei with spins other than zero the value of D_o must be double of the experimentally observed values (D).

3.6 Discussion of the Results :

Table - II gives us the values of ξ_{cal} obtained from experimental values of (n,γ) cross-sections. For comparison, the values of ξ_{obs} obtained from the low energy resonances are also given in the same table. Column(5) in the same table gives us other open channels (from Q-value considerations)[54] for 24 keV neutrons. These open channels are in addition to the γ-emission and neutron emission channels. From this table one finds that for nuclei ^{63}Cu, ^{87}Rb, ^{148}Nd and ^{150}Nd values of ξ_{cal} and ξ_{obs} are in agreement. For the nuclei ^{75}As, ^{122}Sn, ^{124}Sn, ^{121}Sb and ^{123}Sb values of ξ_{obs} are larger than ξ_{cal}. Probably this is due to the fact that the values of D obtained for these cases from low energy resonance experiments are high, due to some missing levels which could not be resolved experimentally. For nuclei ^{89}Y, ^{98}Mo and ^{120}Sn values of ξ_{cal} are

TABLE - II; Values of ξ_{Cal} (Obtained From STATISTICAL Theory) And ξ_{obs} (Obtained From Low Energy Resonance Parameter)

Target Nucleus	∇ (mb.)	ξ_{Cal}	ξ_{obs}	Open Channel other than (n, γ) at 24 keV
^{23}Na	1.65 ± 0.48	56000^{-12000}_{+30000}		
^{27}Al	3.36 ± 1	22500^{-5000}_{+8000}		
^{37}Cl	3.12 ± 1	29000^{-7500}_{+14500}		
^{63}Cu	110 ± 10	600^{-100}_{+60}	720 ± 220	
^{75}As	310 ± 20	175^{-15}_{+20}	720 ± 120	
^{87}Rb	25 ± 5	3400^{-600}_{-900}	4800 ± 1550	
^{89}Y	25 ± 5	3750^{-650}_{+1000}	1700 ± 500	(n, α)
^{98}Mo	110 ± 15	1050^{-75}_{+75}	550 ± 165	(n, α)
^{120}Sn	77 ± 11	1350^{-175}_{+250}	640 ± 175	(n, α)
^{122}Sn	162 ± 81	580^{-230}_{+620}	1660 ± 455	

TABLE - II: (Contd.)

1.	2.	3.	4.	5.
^{124}Sn	220 ± 55	390 $^{-100}_{+170}$	2060 ± 565	
^{121}Sb	700 ± 70	60 $^{-9}_{+12}$	406 ± 50	(n, α)
^{123}Sb	583 ± 55	70 $^{-8}_{+11}$	130 ± 26	(n, α)
^{148}Nd	165 ± 35	540 $^{-120}_{+240}$	505 ± 200	(n, α)
^{150}Nd	125	840 $^{-190}_{+310}$	520 ± 210	
^{170}Er	255 ± 30	320 $^{-50}_{+60}$		
^{205}Tl	30 ± 8	3500 $^{-800}_{+1200}$		

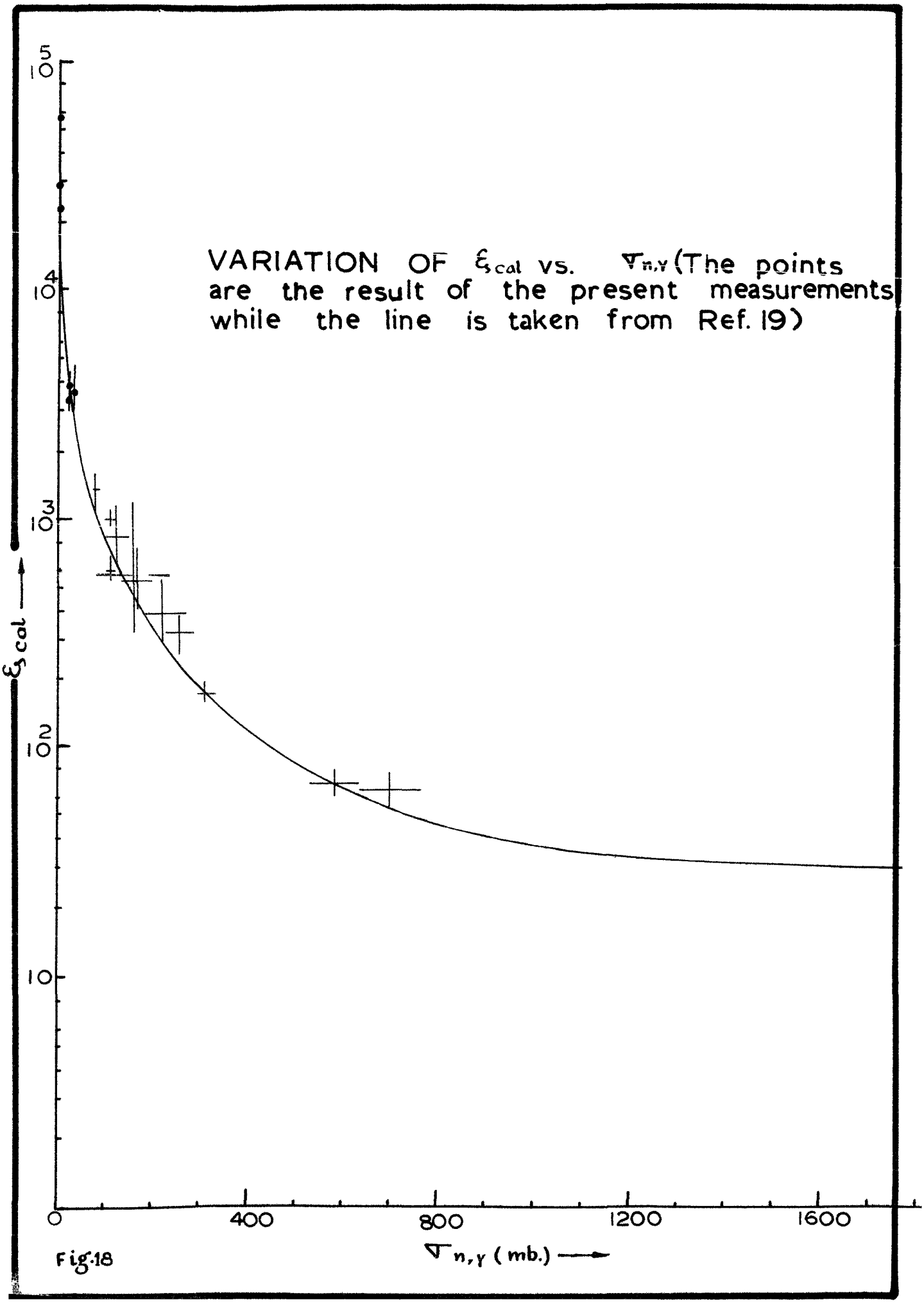
VARIATION OF ξ_{cal} vs. $\sigma_{n,\gamma}$ (The points are the result of the present measurements while the line is taken from Ref. 19)
10^5
10^4
10^3
10^2
10
ξ_{cal}
0
400
800
1200
1600
$\sigma_{n,\gamma}$ (mb.)

Fig.18

larger than ξ_{obs} . In all these cases (n,α) channel for 24 keV neutrons is open, hence the assumption in the derivation of equation (10) i.e.

$$\Gamma = \Gamma_\gamma + \Gamma_n$$

is not valid and $\sigma_0(n,\gamma)$ must decrease by some amount, to account for the contribution of α-emission width (Γ_α) in the total width Γ .

In the view of the above discussion one can say statistical theory can be applied to the 24-keV neutron capture cross-sections. However, a proper knowledge of resonance parameter is pre-requisite for the application of the statistical theory.

3.7 Variation of ξ_{cal} Vs $\sigma_0(n,\gamma)$:

In an attempt to correlate $\sigma_0(n,\gamma)$ with resonance parameter, σ_0 was plotted as a function of log ξ as shown in Fig.18. Our σ_0 values show a similar behaviour as was suggested in earlier works.[19] It is clear from the figure, log ξ increases somewhat exponentially with the decrease in the value of σ_0 .

For small values of σ_0, the corresponding value of ξ is very large. Most of the points in the region of large value of ξ either correspond to the lighter nuclei or to

those nuclei for which neutron or proton number happens to be near the magic numbers. The large value of ' ξ ' is mostly due to large value of 'D' for such cases, as the value of $\overline{\Gamma}_\gamma$ does not change considerably with atomic weight. Thus $\sigma(n,\gamma)$ has large dependence upon the value of D and increases with the decrease in the value of D i.e. the increase in value of level density.

R E F E R E N C E S :

1. G. Gamow, Revs. Mod. Phys. 21 (1949) 367
2. W.A. Fowler et al., Astrophys. J. 122 (1955) 271
3. W.A. Fowler et al., Astrophys. J., suppl. 17 2 (1955) 167
4. E.M. Burbidge et al., Revs. Mod. Phys. 29 (1957) 547
5. R.L. Macklin and J.H. Gibbons, Phys. Rev. 159 (1967) 1007
6. A. Wattenberg, Phys. Rev. 71 (1947) 497
7. Field et al., Phys. Rev. 71 (1947) 508
8. L.E. Beghain et al., Nature 163 (1949) 366
9. V. Hummel and B. Hamermesh, Phys. Rev. 82 (1951) 67
10. C. Kimbal and B. Hamermesh, Phys. Rev. 89 (1953) 1306
11. R.L. Macklin et al., Phys. Rev. 107 (1957) 504
12. R. Booth et al., Phys. Rev. 112 (1958) 226
13. F. Gabbard et al., Phys. Rev. 114 (1959) 201
14. W.S. Lyon and R.L. Macklin, Phys. Rev. 114 (1959) 1619
15. J.F. Vervier , Nucl. Phys. 9 (1959) 569
16. V.N. Kononov et al., J. Nucl. Energy A 11 (1959) 46
17. J.C. Robertson , Nucl. Phys. 71 (1965) 417
18. A.K. Chaubey and M.L. Sehgal, Nucl. Phys. 66 (1965) 267
19. A.K. Chaubey and M.L. Sehgal, Phys. Rev. 152 (1965) 1055
20. A.O. Hansen; Loas Alamos Scientific Laboratory Report LA - 276, 1945 (unpublished)
21. H. Bethe et al., J.Nucl. Energy 3 (1956) 207 and 273; 4(1957) 147
22. T.S. Belanova, J.E.T.P. (USSR) 34 (1958) 574;translation - Soviet Phys. J.E.T.P. 34 (1958) 397

23. H.W. Schimitt and C.W. Cook, Nuc. Phys. 20 (1960) 202

24. Huges et al., Phys. Rev. 75 (1949) 1781; 78 (1950) 632; 91 (1953) 1423

25. R.L. Hankel and H.H. Barschell, Phys. Rev. 80 (1950) 145

26. H.C. Martin and R.F. Toschek, Phys. Rev. 89 (1953) 1302

27. S.J. Bame and R.L. Cubit; Phys. Rev. 113 (1959) 256

28. A.L. Lipunsky et al., Proc. Conf. Peaceful Use of the Atomic Energy (GENEVA), (1958) P/2219

29. M.V. Pesechnic et al., Proc. Conf. Peaceful Use of the Atomic Energy (GENEVA), (1958) P/2030

30. A.E. Johnsurd et al., Phys. Rev. 116 (1959) 927

31. J.A. Miskel et al., Bull. Amm. Phys. Soc. 4 (1959) 475

32. A.T.G. Ferguson and E.B. Paul, J. Nucl. Energy A10 (1959) 19

33. E.G. Bilpuch et al., Ann. Phys. 10 (1960) 455

34. L.W. Weslon et al., Ann. Phys. 10 (1960) 477

35. S.A. Cox , Phys. Rev. 122 (1961) 1280

36. J.A. Miskel et al , Phys. Rev. 128 (1962) 2717

37. S.A. Cox , Phys. Rev. 133B (1964) 378

38. D.C. Stupegia et al., J. Nucl. Energy 22 (1968) 267

39. J.S. Brozosko. , Nucl. Phys. A 123 (1969) 603

40. B.C. Diven et al., Proc. Peaceful Use of Atomic Energy (GENEVA), (1958) 667

41. J.H. Gibbons et al. , Phys. Rev. 122 (1961) 182.

42. R.L. Macklin et al., Phys. Rev. 129 (1962) 2695

43. L.M. Spitz and E. Bernard, Nucl. Phys. A 121(1968) 655

44. W.P. Poenitz et al., J. Nucl. Energy 22 (1968) 505

45. Nuc. Data Sheets (1959-65), Academic Press, New York, London

46. F.L. Friedman and V.F. Weisskopf , Neils Bohr and the Development of Physics, Peragaman Press (1955)

47. B. Margolis, Phys. Rev. 88 (1952) 327

48. W. Hauser and H. Feshbech, Phys. Rev. 87 (1952) 366

49. B.B. Kinsey and G.A. Bartholomev, Phys.Rev. 93 (1954) 1260

50. E.J. Campbell et al. , MIT Laboratory for Nuclear Science and Technology, Report 73 (1960)

51. Neutron Cross-sections, B.N.L. - 325 Second Edition, Supp. No 1 (1960)

52. K.K. Seth , Nucl. Data A 2 (1966)

53. R.N. Alves , Nucl. Phys. A 134 (1969) 118

54. C. Maples et al, Nuclear Reaction Q-Values. UCRL - 1694 (1966)

CHAPTER-IV

"NEUTRON RADIATION CAPTURE AT 14.8 MeV"

4.1 Introduction:

Neutron radiative capture studies at energies above 1-MeV are quite sparse, though in the keV energy region the measurements made by different workers are quite large. Only a few workers[1-8] have measured (n,γ) reaction cross-sections at isolated energies around 14 MeV using neutrons from $^{3}_{1}H(d,n)^{4}_{2}He$ reaction. In the energy region between 5-14 MeV no measurements have been reported so far, except those reported by Menlove et al.[6] in the energy region extending from 1.0 to 19.4 MeV. The lack of neutron radiative capture cross-section measurements at higher energies is due to various complications involved in these measurements.

Of the three methods for (n,γ) cross-section measurements (details given in Chapter II), spherical shell transmission method can only be used with isotropic neutron sources. Capture γ-ray studies have their own limitations. The generally used technique is the activation technique. (n,γ) cross-section measurements by activation technique have some special limitations at higher energies. These limitations are mainly due to: a) large number of open channels for the compound system to decay b) low (n,γ) cross-section at higher energies of neutrons. Since the captured state can decay through different channels i.e. (n,2n), (n,p), (n,α), (n,γ) and many others, the

irradiated sample would have the admixture of various activities, each corresponding to a certain specific channel. In case where (n, γ) reaction gives a product nucleus which is also formed by (n,2n) or (n,3n) reaction with some other isotope of the same element, cross-section measurement is not possible using natural element. This fact restricts the choice of target nuclei to those isotopes where the natural abundance is either 100% or where enriched isotopes are available. In some cases it may also happen that (n, γ) activity may be swamped in the activity produced due to (n,2n), (n,p) and (n, α) reactions with the same isotope or some other isotope of the same element. This happens either due to the fact that the reaction products of the competing reactions have nearly equal halflives or (n, γ) activity is too small to be separated from the admixture.

Neutron radiative capture cross-section measurements at higher energies are of greater interest, as they can provide a check to the various proposed reaction mechanisms. Neutron radiative capture data in the low energy region where sharp resonances appear is fairly well understood by the Breit-Wigner single level formula. In the keV energy region statistical theory approach gives fairly good agreement with the experimental data. In the energy region of 1 to 5 MeV statistical theory partially accounts for the experimentally observed values of (n, γ) cross-sections, while at energies higher than $\sim$ 5 MeV

statistical theory completely fails to account the experi - mentally measured (n, γ) cross-section values.

In nuclear reaction studies, based on Feshbech, Porter and Weisskopf's[10] optical potential model, an incident particle does not always form a compound nucleus at the instant of its entry into the target nucleus. The compound nucleus formation probability is large only after a certain time when the entering particle has traversed a certain distance (K^{-1}) within the nucleus. For incident particle of energy E and the complex potential well - $[V_o(Y) + i\ V_1(Y)]$ K is given as:[11]

$$K = \left\{\frac{m}{2(E + V_o)}\right\}^{\frac{1}{2}} \times 2.\left\{\frac{V_1}{\hbar}\right\} \qquad \ldots\ldots\ (1)$$

The mean time that lapses between the instant of entry of the incident particle into the nuclear boundary and the instant when compound nucleus formation probability is large may be given as:[11] $1/2\ (\hbar/V_1)$

Theoretical physicists[12-16] have seen the possibility of another reaction mechanism, based on the optical potential model. Initially while moving in the average nuclear potential, the incident particle may radiate energy in the form of a photon and drop into a bound particle orbit. This type of capture is termed as 'direct' or one stage capture. The neutron radiative capture cross-section obtained from direct capture theory are an order of magnitude smaller than the experimental values. To account this discrepancy some

authors[17-19] have suggested a 'semidirect' or 'collective' capture mechanism. Applicability of this model has been checked by various workers by comparing experimental and theoretically calculated values. The shapes of experimentally observed γ-ray spectra have been studied by some workers[8,9] in the light of these reaction mechanisms.

/The present measurements of neutron capture cross-sections at 14.8 MeV have been performed in our laboratory as a part of research project entitled,/"(n, γ) reaction studies at different energies". Due to the difficulties associated with these measurements at 14.8 MeV neutron energy, we have made measurements only for ^{103}Rh, ^{127}I and ^{175}Lu./ The capture cross-section values obtained in the present measurements along with the experimental values (at the same neutron energy) as obtained by other workers[1-8] have been used to check how far "direct" and "semidirect" capture theories account for the same. Neutron capture cross-sections are also plotted against neutron number to see the effect of magic numbers, if any.

4.2 Experimental Procedure:

It is noted that (n, γ) cross-sections for slow neutrons are many order of magnitude larger than their values at 14.8 MeV neutron energy. Presence of these slow neutrons alongwith 14.8 MeV neutrons must significantly effect the values of (n, γ) cross-sections. To eliminate the error due to the presence of these slow neutrons one must know the ratio (X) of the slow to

14.8 MeV neutron flux. It was further thought, that measurements with sample wrapped in cadmium foil would eliminate the error partly, which might be due to the presence of the neutrons with energy lower than cadmium cutoff energy i.e. 0.4 eV only. In our case there was practically no hydrogenous material located close to the place of irradiation, and so, the neutron flux with energy lower than the cadmium cutoff must be very small (see chapter II). However, the presence of the slow neutrons with energy extending up to a keV or so is expected, which could be due to the scattering of the neutrons emitted in the backward direction.

For the estimation of the ratio of slow to 14.8 MeV neutron flux, an Indium sample was irradiated in the same geometry as other samples, and its neutron radiative capture cross-section was measured. The cross-section thus obtained also have the contribution due to the presence of the slow neutrons which arises due to scattering. Let us denote this measured cross-section by σ_{obs}. The correct value of neutron radiative capture cross-section at 14.8 MeV ($\sigma_{14.8}$) is related to σ_{obs} by the following relation -

$$(1+X)\ \sigma_{obs} = \sigma_{14.8} + X\ \bar{\sigma}_{slow}, \quad \ldots\ldots\ldots \quad (2)$$

where $x = \dfrac{\text{slow neutron flux } (\phi_{slow})}{\text{14.8 MeV neutron flux } (\phi_{14.8})}$

and $\bar{\sigma}_{slow}$ is the neutron capture cross-section averaged over energy region from 1 ev to 1 keV. $\bar{\sigma}_{slow}$ was obtained from the literature.[20]

To obtain 'x' from equation no.(2) one must know the value of $\sigma_{14.8}$. Menlove et al.[6] have measured ^{115}In (n,γ) ^{116m}In reaction cross-section at 14.8 MeV neutron energy. Their measurements appear to be accurate, as they have very carefully taken into account the effect of slow neutrons. While finding the value of (x) from equation (2), the value of the ^{115}In (n,γ) ^{116m}In reaction cross-section at 14.8 MeV is taken 5.97 mb as quoted by Menlove et al.[6] The value of x thus obtained was used to obtain $\sigma_{14.8}$ for other cases using the same equation.

All the reaction cross-sections at 14.8 MeV neutron energy are measured relative to that of ^{27}Al (n,p) ^{27}Mg or ^{27}Al (n, α) ^{24}Na reaction corss-section. The halflives of the two reaction products are 9.5 min. and 15 hrs. respectively. These reactions are chosen as standard due to the following reasons:

a) aluminum is monoisotopic.

b) halflives of all the reaction products studied in the present cases are comparable to one of the two halflives corresponding to the two activities produced in the irradiated ^{27}Al sample.

c) decay schemes of ^{27}Mg as well as ^{24}Na are both well known.

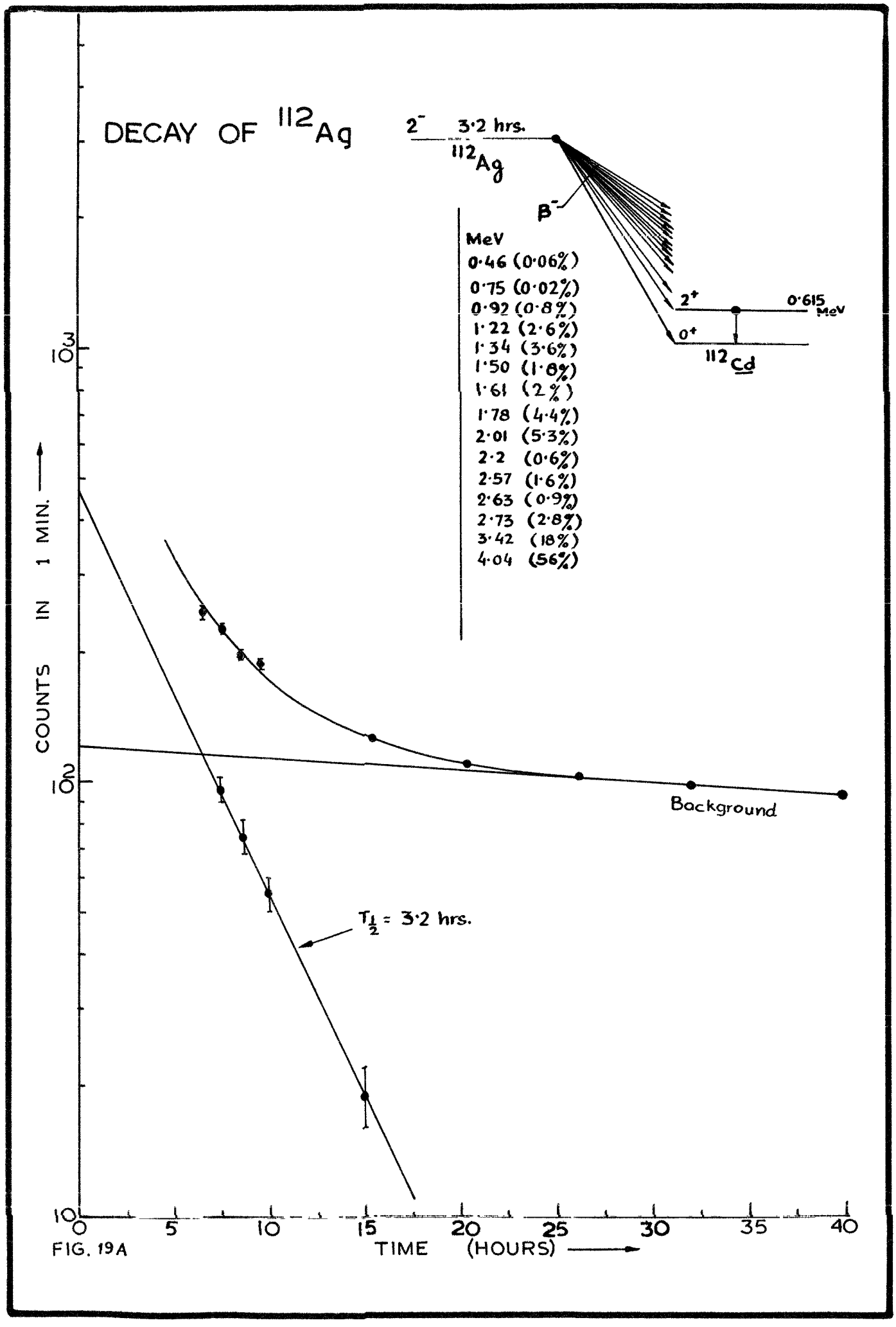
DECAY OF ^{112}Ag
2^- 3·2 hrs.
^{112}Ag
β^-
MeV
0·46 (0·06%)
0·75 (0·02%)
0·92 (0·8%)
1·22 (2·6%)
1·34 (3·6%)
1·50 (1·8%)
1·61 (2%)
1·78 (4·4%)
2·01 (5·3%)
2·2 (0·6%)
2·57 (1·6%)
2·63 (0·9%)
2·73 (2·8%)
3·42 (18%)
4·04 (56%)
2^+
0·615 MeV
0^+
^{112}Cd
COUNTS IN 1 MIN.
10^3
10^2
10
Background
$T_{\frac{1}{2}}$ = 3·2 hrs.
0
5
10
15
20
25
30
35
40
TIME (HOURS)

FIG. 19A

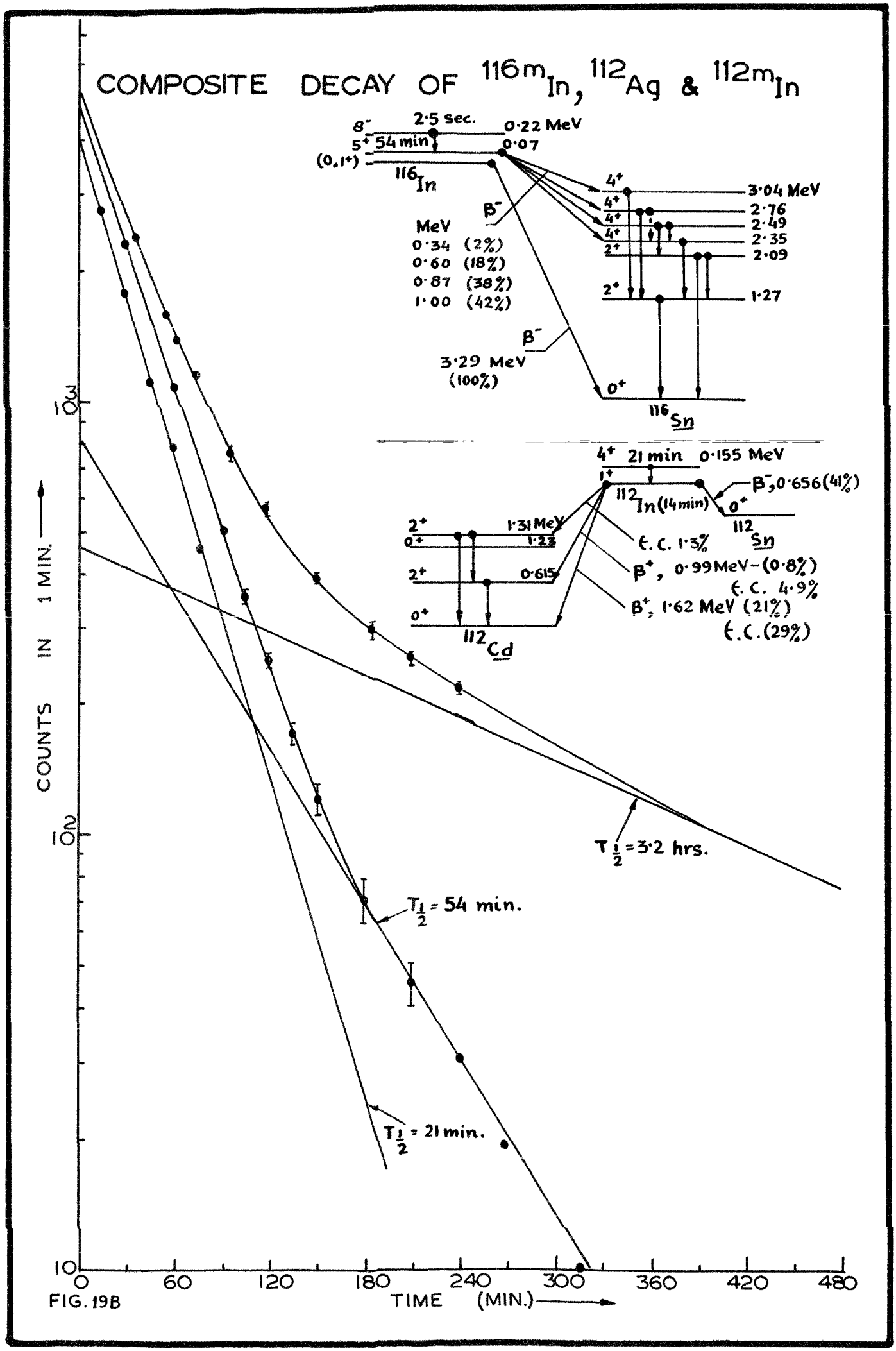
COMPOSITE DECAY OF 116m In, 112 Ag & 112m In
8⁻ 2·5 sec.
5⁺ 54 min
(0,1⁺)
116 In
0·22 MeV
0·07
β⁻
MeV
0·34 (2%)
0·60 (18%)
0·87 (38%)
1·00 (42%)
β⁻
3·29 MeV
(100%)
4⁺
4⁺
4⁺
4⁺
2⁺
2⁺
0⁺
3·04 MeV
2·76
2·49
2·35
2·09
1·27
116 Sn
4⁺ 21 min 0·155 MeV
1⁺
112 In (14 min)
β⁻, 0·656 (41%)
0⁺
112 Sn
2⁺
0⁺
2⁺
0⁺
1·31 MeV
1·23
0·615
112 Cd
ε.C. 1·3%
β⁺, 0·99 MeV – (0·8%)
ε.C. 4·9%
β⁺, 1·62 MeV (21%)
ε.C. (29%)
COUNTS IN 1 MIN.
10³
10²
10
T½ = 3·2 hrs.
T½ = 54 min.
T½ = 21 min.
0
60
120
180
240
300
360
420
480
TIME (MIN.)

FIG. 19B

d) cross-section for these two reactions have been studied extensively.[29] The values of cross-sections for the reactions $^{27}Al\ (n,p)\ ^{27}Mg$ and $^{27}Al\ (n,\alpha)\ ^{24}Na$ are taken to be 73 mb. and 115 mb. respectively.

The decay schemes of the reaction products and the natural abundances of the target nuclei are taken from Nuclear Data Sheets.[21] All the (n,γ) measurements at 14.8 MeV are performe by the counting of β-activities in the irradiated samples. Details of individual measurements are as follows.

$^{115}In\ (n,\gamma)\ ^{116m}In$ - Reaction

Metallic indium foil weighing 0.0742 grams was used as the target sample. The percentage abundance of ^{115}In isotope in elemental indium is 95.84%. The sample assembly was irradiated for 20 mins. Counting was started after 36 minutes from the stop of irradiation. During this time various short lived activities corresponding to different reactions with ^{113}In and ^{115}In had decayed. The decay of induced β-activities was followed up to forty hours. In the decay curve shown in Fig.19A, 3.2 hrs. activity corresponds to the $^{115}In\ (n,\alpha)\ ^{112}Ag$ reaction product. In Fig.19B decay curve of irradiated sample is shown after subtracting the background counts. The three resolved activities with halflives 3.2 hrs, 21 mins and 54 mins. correspond to the reaction products of $^{115}In\ (n,\alpha)\ ^{112}Ag$, $^{113}In\ (n,2n)\ ^{112m}In$ and $^{115}In(n,\gamma)\ ^{116m}In$ reactions respectively.

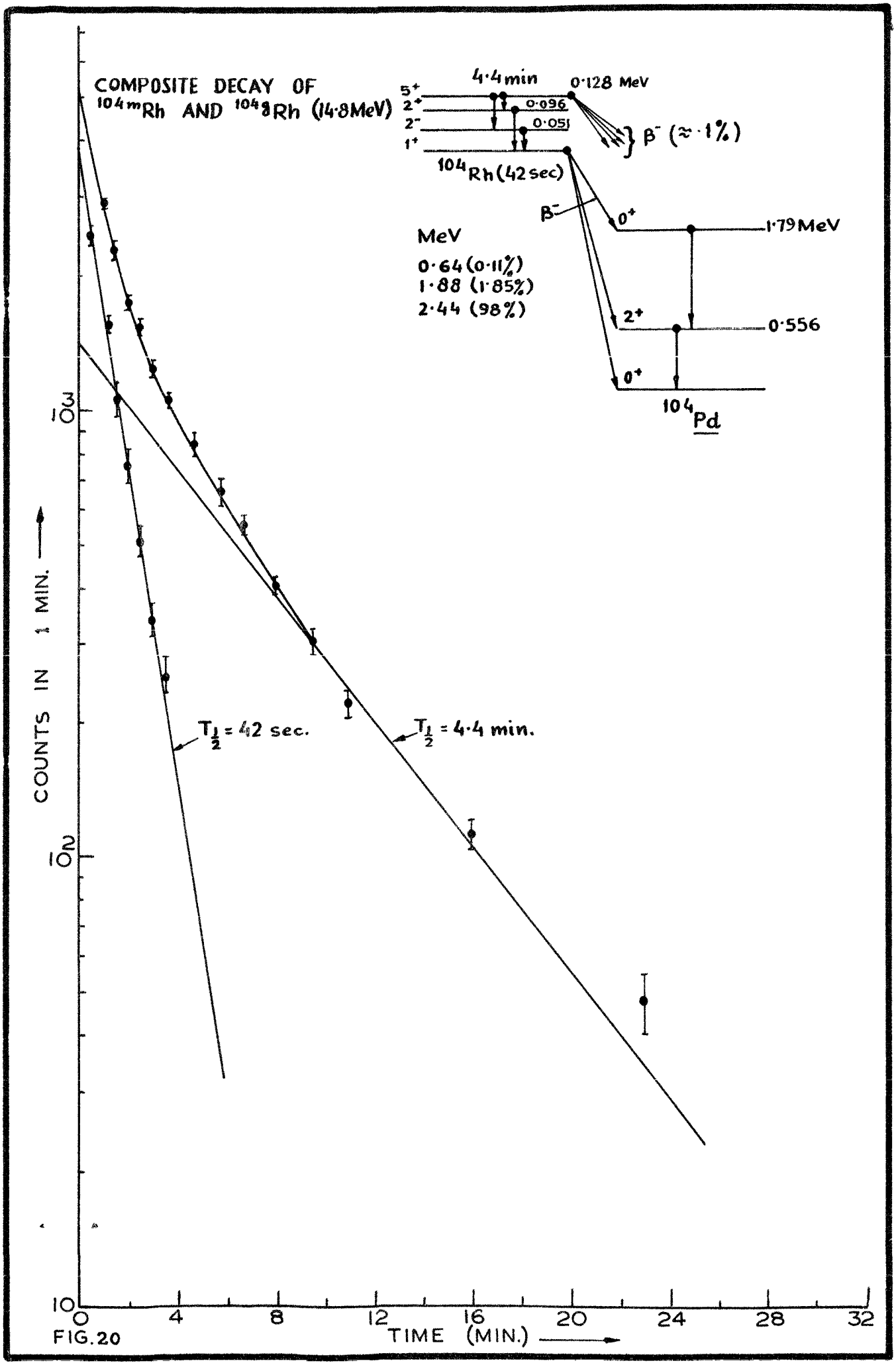
COMPOSITE DECAY OF
^{104m}Rh AND ^{104g}Rh (14·8MeV)
4·4 min
0·128 MeV
5⁺
2⁺
2⁻
1⁺
0·096
0·051
β⁻ (≈ 1%)
^{104}Rh (42 sec)
β⁻
0⁺
1·79 MeV
MeV
0·64 (0·11%)
1·88 (1·85%)
2·44 (98%)
2⁺
0·556
0⁺
^{104}Pd
COUNTS IN 1 MIN.
$T_{\frac{1}{2}}$ = 42 sec.
$T_{\frac{1}{2}}$ = 4·4 min.
10³
10²
10
0
4
8
12
16
20
24
28
32
TIME (MIN.)

FIG. 20

Φ.Ge = 1.166×10^{9} n/min

$N_o(^{115}In)$ = 3.724×10^{20}

ϵ = 0.413

$(1-e^{-\lambda t_e})$ = 0.226

$C_{t=o}$(54 min.activity = 300 counts/min.

σ_{obs} = 19.75 mb.

Value of $\sigma_{14.8}$ from literature[6] may be given as:

$\sigma_{14.8}$ = 5.97 mb

The a[illegible] radiative [illegible] cross-section for slow neutrons obt[illegible] literature[illegible] may be given as:

σ_{slow} = 12.1 mb.

Putting values of σ_{obs}, $\sigma_{14.8}$ and σ_{slow} in equation (2) we get

= 1.132×10^{-3}

This value of x is used in later measurements to eliminate the error due to the [illegible]sence of slow neutrons.

<u>$^{103}Rh(n,\gamma)\ ^{104m,g}Rh$ - Reaction.</u>

0.1662 grams elemental rhodium sponge was used for the preparation of the target sample. Assembly of the target and the standard samples was irradiated for 10 minutes. Counting of the target sample was started after one minute from the stop of irradiation. As shown in the decay scheme isomeric state of ^{104}Rh has 4.4 min. halflife and it decays to ground state through 100% isomeric transition. The induced β-activit

of the ground state is measured, which appears similar to the adminixture of two activities with halflives 4.4 min and 42 sec. The decay curve for the induced β-activity in the irradiated rhodium sample is shown in Fig.20.

No activity was observed corresponding to (n, γ) reaction. Probably the yield of this reaction at the present energy of the neutrons is small. Moreover counting was started after one minute from the stop of the irradiation, which is nearly four times larger than the halflife of (n, α) product i.e. 4.4 min.

The [illegible] calculated using eq[illegible] No.(15) of the chapter II, for the irradiation [illegible]

Φ.Ge= 3.417×10^{8} n/min

N_o= [illegible]$\times 10^{21}$

ϵ_g= 0.693

$(1-e^{-\lambda_m t_e})$= [illegible]

$(1-e^{-\lambda_g t_e})$= 1.000

$\lambda_g/\lambda_g-\lambda_m$= 1.189

Am = 1400 counts/min

Ag = 3800 counts/min

$(\sigma_m)_{obs}$ = 6.5 ± 1.5 mb.

$(\sigma_g)_{obs}$ = 18 ± 2.5 mb.

σ_{obs} = $(\sigma_m)_{obs} + (\sigma_g)_{obs}$ = 24.5 ± 3 mb.

After making correction for the slow neutron background

$\sigma_{14.8}$ = 16.8 ± 3 mb.

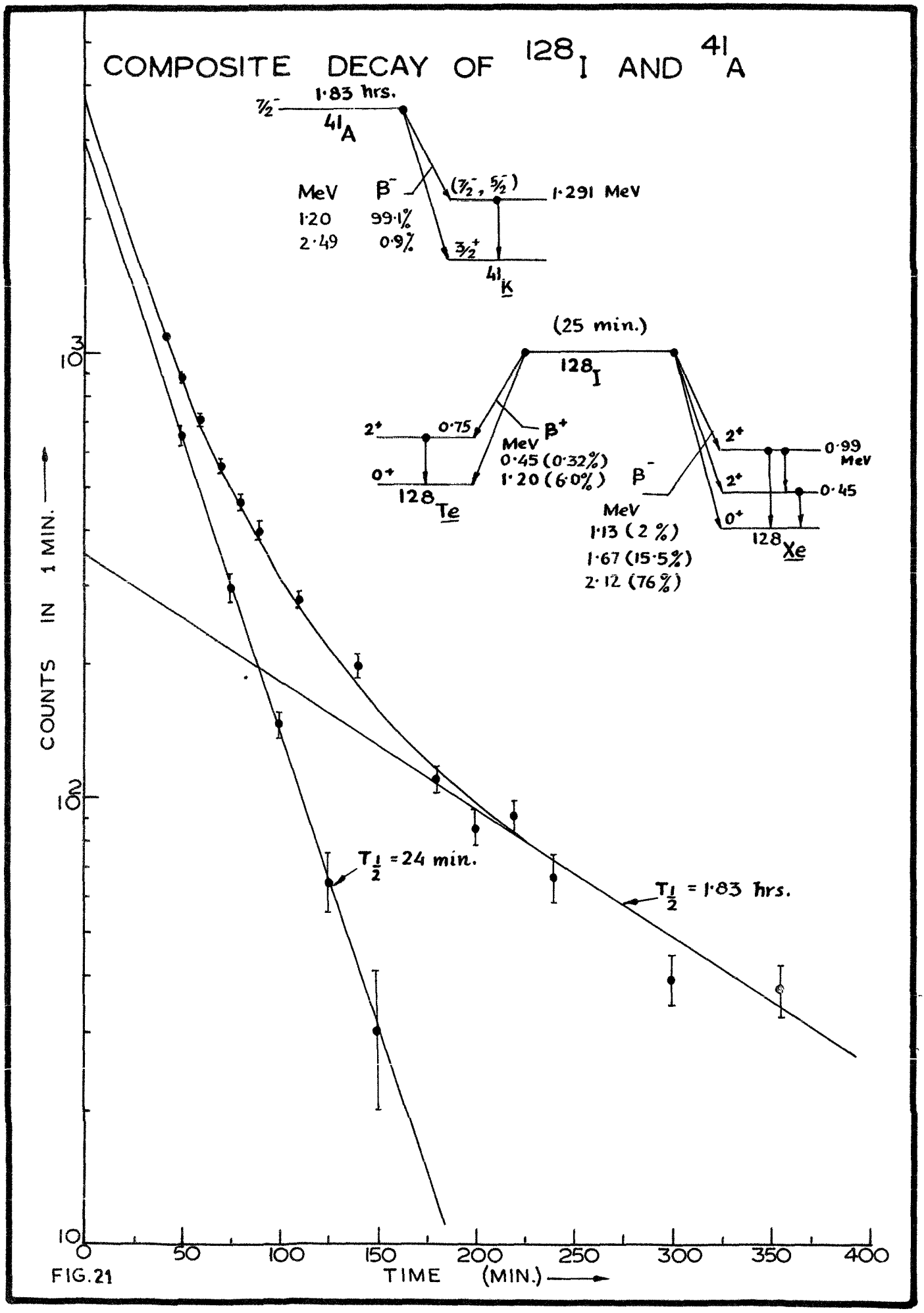
COMPOSITE DECAY OF 128I AND 41A
7/2⁻
1·83 hrs.
41A
MeV
1·20
2·49
β⁻
99·1%
0·9%
(7/2⁻, 5/2⁻)
1·291 MeV
3/2⁺
41K
(25 min.)
128I
2⁺
0·75
0⁺
128Te
MeV
0·45 (0·32%)
1·20 (6·0%)
β⁺
β⁻
MeV
1·13 (2 %)
1·67 (15·5%)
2·12 (76%)
2⁺
2⁺
0⁺
0·99 MeV
0·45
128Xe
COUNTS IN 1 MIN.
10³
10²
10
T½ = 24 min.
T½ = 1·83 hrs.
0
50
100
150
200
250
300
350
400
TIME (MIN.)

FIG. 21

$^{127}I(n,\gamma)\ ^{128}I$ - Reaction.

0.1992 grams potassium iodide was used for the preparation of the sample. The sample assembly was irradiated for 20 minutes. Counting of the sample was started after 40 mins. [illegible] stop of irradiation to enable short lived activities (due to other reactions) to decay during this time. Fig.21 shows the decay curve. Activity [illegible] halflife 1.83 hrs. corresponds to [illegible] ^{41}A reaction product, while 24 min. halflife corresponds to the composite activity $^{127}I(n,\gamma)$ ^{128}I (25 min.) and $^{127}I\ (n,\alpha)\ ^{124m}Sb$ (21 min) reactions.

$$\Phi . G_e = 1.159 \times 10^{9} \quad n/min.$$

$$N_o = 7.216 \times 10^{20}$$

β-counting efficiencies [illegible] reaction products i.e. ^{124m}Sb and ^{128}I are nearly same, [illegible] be wirtten as:

$$\epsilon = 0.548$$

$$(1-e^{-\lambda t_e}) = 0.425$$

$$C_{t=o} = 3000 \quad \text{counts/min.}$$

hence

$$\sigma_{obs}\{^{127}I(n,\gamma)\ ^{128}I\} + \sigma\{^{127}I(n,\alpha)\ ^{124m}Sb\} = 15.25 \pm 1 \text{ mb.}$$

Value of $\sigma\{^{127}I(n,\alpha)\ ^{124m}Sb\}$ as quoted in reference 22) is equal to 1.5 ± 2 mb, and so we get

$$\sigma_{obs}\{^{127}I\ (n,\gamma)\ ^{128}I\} = 13.75 \pm 3 \text{ mb}$$

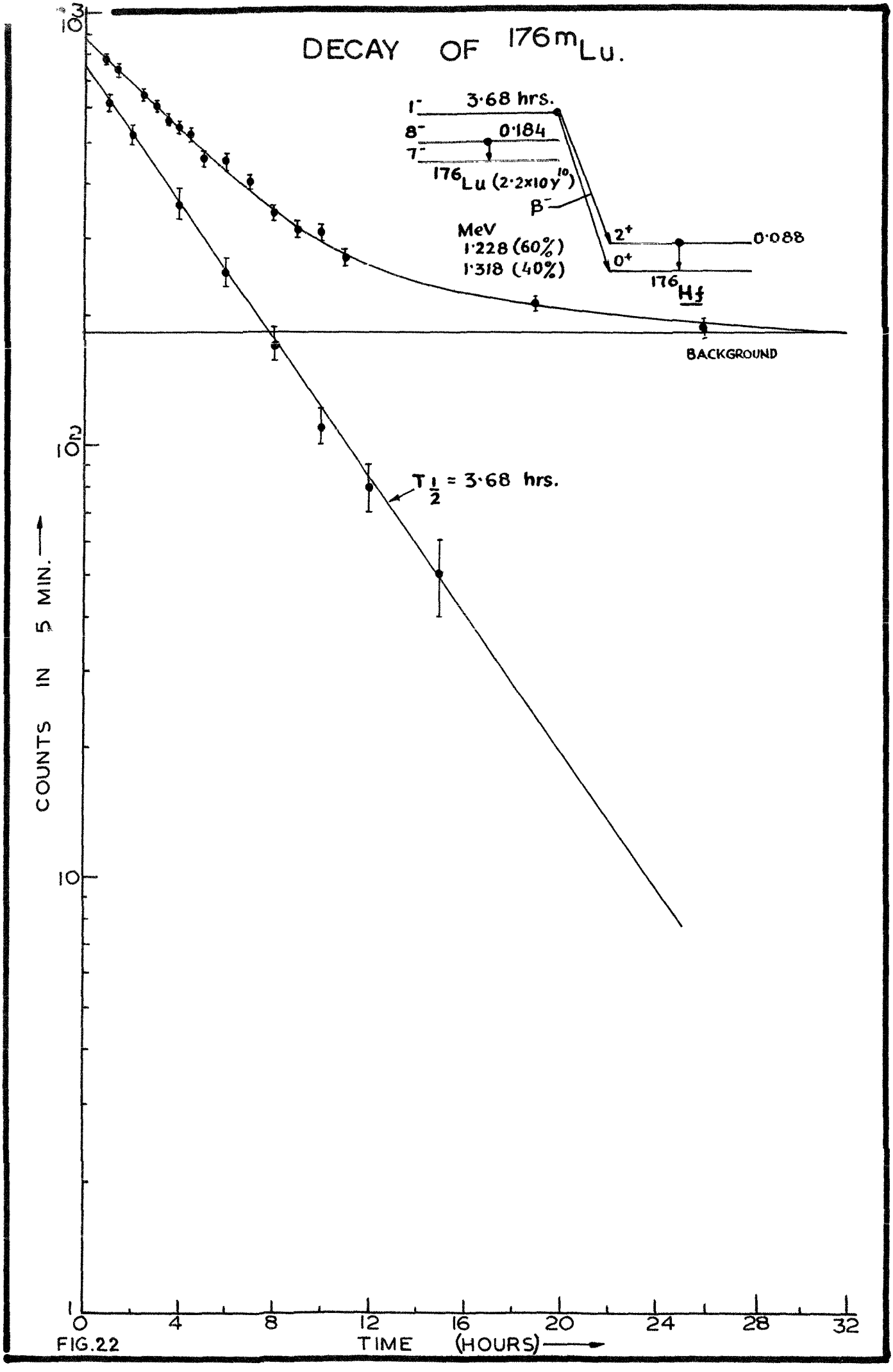
DECAY OF 176m Lu.
1⁻ 3·68 hrs.
8⁻ 0·184
7⁻
176 Lu (2·2x10y 10)
β⁻
MeV
1·228 (60%)
1·318 (40%)
2⁺
0⁺
0·088
176 Hf
BACKGROUND
T 1/2 = 3·68 hrs.
COUNTS IN 5 MIN.
10³
10²
10
1
0
4
8
12
16
20
24
28
32
TIME (HOURS)

FIG.22

Making correction for slow neutron background we get

$$\sigma_{14.8} = 7.64 \pm 3 \text{ mb.}$$

$^{175}Lu\ (n,\gamma)\ ^{176m}Lu$ - Reaction.

Lutetium oxide weighing 0.0452 grams was used for the sample preparation. The irradiation of the [illegible] assembly was carried out for a duration of 45 min. The decay of the target sample was followed up to 26 hours. Fig.22 gives decay curve of lutetium. 3.68 hrs. activity of ^{176m}Lu is obtained after subtracting th[illegible].

$\Phi . I_e = 0.828 \times 10^9$ n/min

$N_o = 1.327 \times 10^{20}$

$\epsilon = 0.692$

$(1-e^{-\lambda t_e}) =$ [illegible]

$C_{t=o} =$ counts/5 min.

$\sigma_{obs} = 15.6 \pm 2$ mb.

Making correction for the slow neutron background we get

$$\sigma_{14.8} = 2 \pm 2 \text{ mb.}$$

Experimental values of neutron radiative capture cross-section at 14.8 MeV neutron energy are given in table -III. Results of present measurements are given in column (3) of the same table, and the results of earlier measurements are

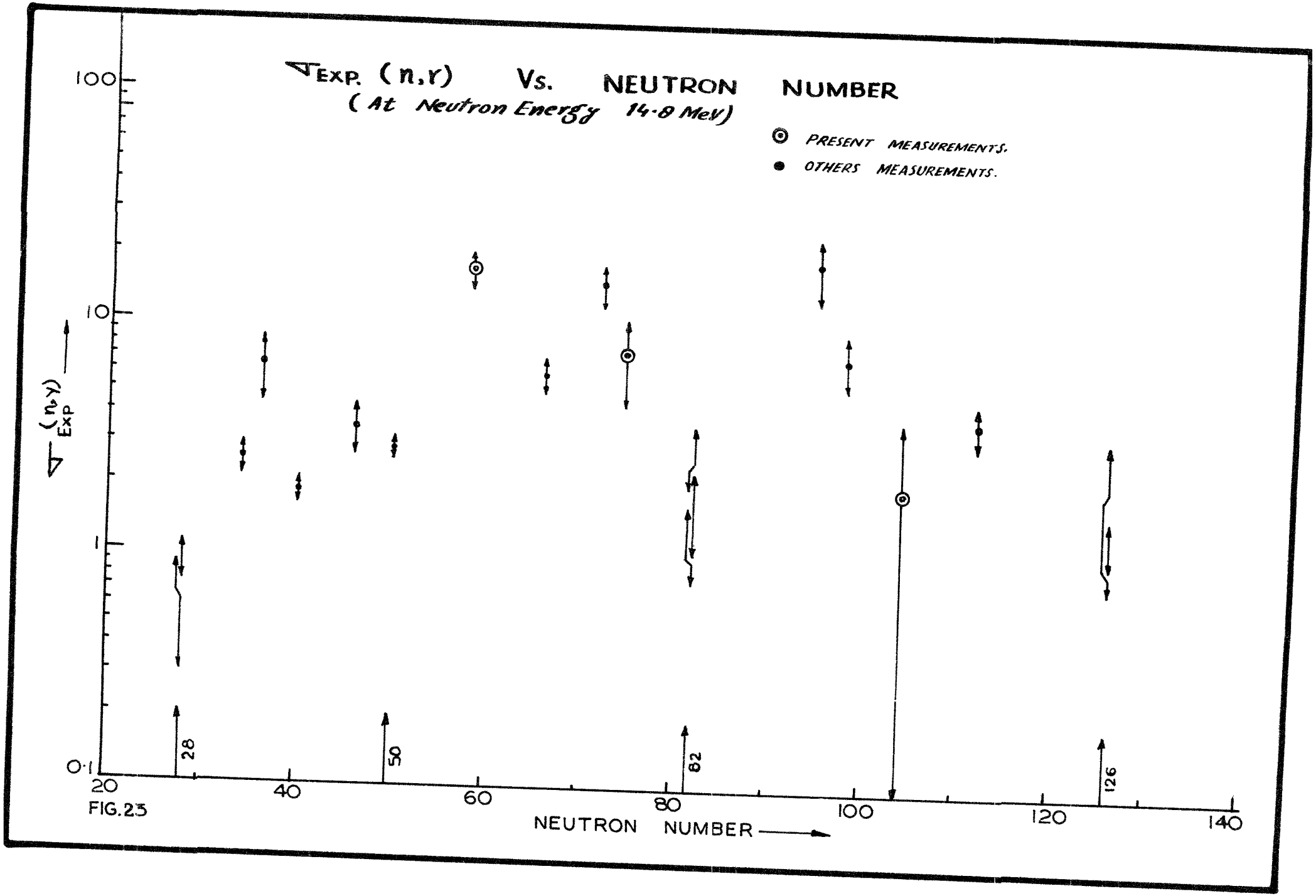
σ EXP. (n,γ) Vs. NEUTRON NUMBER
(At Neutron Energy 14·8 MeV)
PRESENT MEASUREMENTS.
OTHERS MEASUREMENTS.
σ (n,γ) EXP
100
10
1
0·1
28
50
82
126
20
40
60
80
100
120
140
NEUTRON NUMBER

FIG.23

given in column (4). Our experimental values are in fairly good agreement with the earlier reported values. In the case of iodine our value agrees with the value of Qaim and Ejaz[22] and does not agree with that of Perkin and Conner.[1]

In Fig.23 we have plotted neutron radiative capture cross-section (at 14.8 MeV) against the neutron number in the target nucleus. The two ends of the arrow show the maximum and minimum reported values. The graph explicitly shows presence of shell effects in the radiative capture cross-section at 14.8 MeV neutron energy.

4.3 Direct-Semi-Direct Capture:

Beck[12] suggested that interaction of a nucleon with the radiation field may be treated as a perturbation. The cross-section for the direct capture may be given in the form of Dirac's formula for the emission of radiations. A phenomenological expression for direct capture cross-section may be given as:

$$\sigma^{D}_{n,\gamma}(E) = (2\pi/\hbar) \sum_{b} |\langle U(E)|\mathcal{H}|\psi_b\rangle|^2 \rho \quad \ldots\ldots\ldots \quad (3)$$

where $U(E)$ is the wave function normalized to a unit flux of an incident wave of energy E, scattered by a complex potential well representing the target nucleus; ψ_b is the wave function normalized to unity over all space of the bound state b of the real part of the same potential.

Lane and Lynn[14] emphasised that the resonance theory formalism of Wigner and Eisenbud[23] and of Kapur & Peierls[24] are exact and therefore must include both 'direct' and 'compound nucleus' mechanisms for any type of reaction. Compound nucleus cross-section are extracted by making Bethe's[25] approximation that the phases of matrix elements are random. As a consequence of this approximation the cross-section depends upon the energy levels of the compound system near the excitation energy corresponding to the incident nucleon energy. Thus one can think of the other reaction mechanism to be associated with the break-down of Bethe's approximation. The problem of extracting direct cross-section from the resonance theory formalism reduces to evaluating the sum of the resonance terms from the distant levels. On these lines Lane and Lynn[14] made an attempt to extract direct capture cross-section from Kapur - Peierls formalism. They, however, came to the conclusion that this approach gives an expression for the direct capture cross-section, which is similar to the Beck's phenomenological expression.

From the phenomenological expression, direct capture evidently appears to be a mechanism in which an incident nucleon moving in a complex potential field of a target nucleus makes a direct transition to one of the unfilled bound states of the nucleus. Restricting discussion to the electric

dipole transition and using standard expression for the electromagnetic transition probability, cross-section for the direct capture of neutron may be given as[16]

$$\sigma^{D}_{n,\gamma} = \frac{8\pi M}{3k\hbar^2}\left(\frac{-Ze}{A}\right)^2 \sum_{\ell\ell'}\left(\frac{E_\gamma}{\hbar c}\right)^3 (\ell+\ell'+1)|R^{5/2} I_{\ell\ell'}|^2 \quad \ldots\ldots\ldots \quad (4)$$

where ℓ and ℓ' are the relative orbital angular momenta before and after the transition respectively; Z and A are the charge and mass number of the target; M is the reduced mass of the incident neutron; k is the incident neutron wave number; E_γ is the photon energy and is equal to the difference $(\epsilon - \epsilon'_{N'\ell'})$ between the initial and final nucleon energies; R is nuclear radius and $I_{\ell\ell'}$ is the dimensionless dipole integral which may be given as:

$$I_{\ell\ell'} = R^{-5/2} \int_0^\infty \psi_\ell(r)\, u_{N'\ell'}(r)\, r^3\, dr \quad \ldots\ldots\ldots \quad (5)$$

where $\psi_\ell(r)$ is the radial part of the incident wave of angular momentum ℓ which satisfies

$$\left\{(\hbar/2M)\left(\frac{d^2}{dr^2} + \frac{\ell(\ell+1)}{r^2}\right) + V + i\,W - \epsilon\right\} r\,\psi_\ell(r) = 0 \quad \ldots\ldots\ldots \quad (6)$$

$(V + iW)$ is the complex potential of the target nucleus. $u_{N'\ell'}(r)$ is the radial part of the final particle wave function i.e. wave function corresponding to a certain bound state of the target nucleus and satisfies the following equation

$$\left\{(\hbar/2M)\left(\frac{d^2}{dr^2} + \frac{\ell'(\ell'+1)}{r^2}\right) + V - \epsilon'_{N'\ell'}\right\} r\, u_{N'\ell'}(r) = 0 \quad \ldots\ldots\ldots \quad (7)$$

$U_{N'\ell'}$ are normalized as

$$\int_0^\infty [u_{N'\ell'}(r)]^2 r^2 dr = 1 \qquad \ldots\ldots \quad (8)$$

Evaluation of dipole integral using equations 5 to 8 is quite cumbersome.

Lane and Lynn[14] under certain approximations derived a more simpler equation to get an order of magnitude for the direct radiative capture cross-section. These approximations are listed below.

1. Instead of taking more realistic form of the complex potential a simple square well model was chosen. The imaginary part W of the complex potential (V + iW) was taken as $(2+\frac{1}{2} E_n)$ for neutron interaction, where E_n is the incident neutron energy.

2. Only contribution to the dipole integral from the internal region ($r < R$) was taken into account. External region ($r > R$) or the channel contribution was neglected.

3. The energy region of the neutron was chosen above 5-MeV, so that the ℓ-values that contribute to the cross-section are at least up to $\ell = 3$ or more.

4. The capture cross-section must clearly depend on the number of final single - particle states available for E_1 transitions from the initial ℓ-wave states. For each incident ℓ wave with $\ell \leq \ell'_{max} + 1$, there is one bound state to which E_1 transition occurs, where ℓ'_{max} is the highest ℓ' value in the bound states.

With these assumptions the expression for the direct capture cross-section becomes[14]

$$\sigma^{D}_{n,\gamma} \approx 6\left(\frac{Z}{A}\right)^{2} \frac{R^{4}\,(E_n)^{1/2}\,(E_\gamma)^{3} \times 10^{10}}{2 + \frac{1}{2} E_n + 16.8\,(E_n)^{1/2}/R} \text{ barn} \quad \ldots\ldots\ldots \quad (9)$$

where R is the radius in Fermis and is taken to be $1.4 \times A^{1/3}$. Energy of the emitted photon satisfies

$$E_n + B \geqslant E_\gamma \geqslant E_n$$

Where B is the binding energy of the last neutron. In the calculation of $\sigma^{D}_{n,\gamma}$ photon energy E_γ is taken to be $E_n + \frac{1}{2}B$.

However, one finds that equation (9) may not be true for the neutrons with energies above 20 MeV. The maximum value (in the incident wave) that contribute to the direct capture is given by

$$\ell_{max} = \ell'_{max} + 1$$

When the incident neutron energy rises above the angular momentum barrier for incident wave with $\ell = \ell'_{max} + 1$ there is no contribution from the higher ℓ's and hence increasing energy is accompanied by the decrease in cross-section.

At 14.8 MeV neutron energy radiative capture cross-sections obtained from direct capture theory are two to three orders of magnitude large than their values obtained from compound nucleus theory.[14] The comparison of the direct capture cross- sections with the experimental values reveals

the fact that the former are smaller than later by an order of magnitude. To bridge the gap between the experimental and theoretical capture cross-sections another reaction mechanism has been proposed by several authors.[17-19] The proposed capture mechanism is termed as "semi-direct" or the "collective"capture. Perhaps the idea of semi-direct capture is picked up from the experimentally observed giant dipole resonances in the (γ,n) and (γ,p) reactions.

In semi-direct process the incident nucleon and the target nucleus interact to give an intermediate state in which the former is in a bound state and the later is excited to its giant dipole state or the collective vibrational state. This dipole state decays by the emission of γ-ray. For neutron energies between 10 to 20 MeV semi-direct capture is quite significant. At neutron energies near the giant dipole resonance ($\sim$15 MeV) collective mode of capture is dominant.

Brown[17] considered the case of photo nucleon emission which is the inverse of the radiative capture. He considered a core and a valance nucleon and a process in which the valance nucleon is emitted by the absorption of the photon. To work out this process schematic model[26] was used. In the schematic model operation of the dipole operator on the ground state of the core produces the giant dipole state or collective vibrational state having well-defined energy E_R and width Γ .

The schematic model approach[26] can be briefly outlined as follows. In the shell model description excited states of a closed shell nucleus may be obtained by lifting a particle from one shell to another. This type of excitation is termed as particle-hole excitation. The absence of a particle from a closed shell behaves itself like a particle. So one can have a particle-hole interaction similar to the particle-particle interaction. When a γ-ray is absorbed in a closed shell nucleus, it produces particle-hole pair and hence particle-hole interaction. The solution of the secular equation giving particle-hole eigenstates shows, that all but one of the eigen-energies E are sandwiched between the unperturbed particle-hole excitation energies. The particle-hole eigen-energy not trapped between the unperturbed particle-hole excitation energies, is given by

$$E_R = E_o + \sum_{mi} \lambda D_{mi}^2 \qquad \ldots\ldots \quad (10)$$

where E_o is an average unperturbed particle-hole excitation energy. D_{mi} is the transition amplitude to certain unperturbed state. Brown[26] has shown that the eigen state with energy E_R corresponds to the vibrational (or giant dipole) state of the nucleus.

In process under consideration dipole operator when operates on core gives giant dipole state. This giant dipole state, in turn, makes a transition to the ground state by

imparting its energy to the valance nucleon. Empirically one can take for the energy and width of the dipole states the experimentally observed values. Browns'[17] approach ultimately gives us an expression for radiative capture cross-section which can be written as:

$$\sigma_{n,\gamma}^{D.S} = \sigma_{n,\gamma}^{D} \times F \qquad \ldots\ldots \quad (11)$$

where

$$F = \left| 1 + \frac{E_R - E_o}{(E_\gamma - E_R) + i\,\Gamma/2} \right|^2 \qquad \ldots\ldots \quad (12)$$

From equation (11) one can say that capture through collective vibrational mode just causes an enhancement over direct capture cross-section ($\sigma_{n,\gamma}^{D}$) by a factor F. The enhancement factor F contain two terms first term accounts for the direct capture and the second term containing $(E_R - E_o)$ accounts for the semi-direct capture and the two are added up coherently.

Clement et al.[18] developed semi-direct capture formalism by examining the coupling between the incident particle and target nucleus in more detail. It is assumed that the charge and mass densities of the nucleus are capable of shape oscillation and the nuclear potential oscillates in the same mode as these densities. Due to this oscillation of the target nucleus, the incident particle will experience a slightly deformed potential. Collective modes of the target nucleus can be excited through the interaction of the target particles

with the deformed potential of the target nucleus. Clement's approach to collective capture yields the results which agree qualitatively with those obtained by Brown using schematic model

4.4 Calculations:

We have calculated neutron radiative capture cross-sections using expressions (11) and (12) given by Brown for the direct-semi-direct capture mechanism. The order of magnitude for ($\sigma^{D}_{n,\gamma}$) is determined from Lane and Lynn's expression (9).

For the determination of Brown's enhancement factor "F" parameter E_R, Γ are taken from reference 27) **. The energy shift in giant dipole state from an average unperturbed dipole energy ($E_R - E_o$) is taken to be 7 MeV. Essentially one can write the average unperturbed dipole particle-hole excitation energy in the following form[9)]

$$E_o = \sum_i |\langle M \rangle_i|^2 E_i \; / \sum_i |\langle M \rangle_i|^2 \qquad \ldots\ldots (13)$$

where $\langle M \rangle_i$ is the matrix element for the dipole transition between the two shell model states, and E_i being the corresponding particle-hole excitation energy. Generally[17)] E_i comes out to be between 6 and 8 MeV. So an average value of E_o can be taken as :

$$E_o \approx 7 \text{ MeV}$$

** Empirical values of E_R and Γ are taken in a few cases where their experimental values are not available.

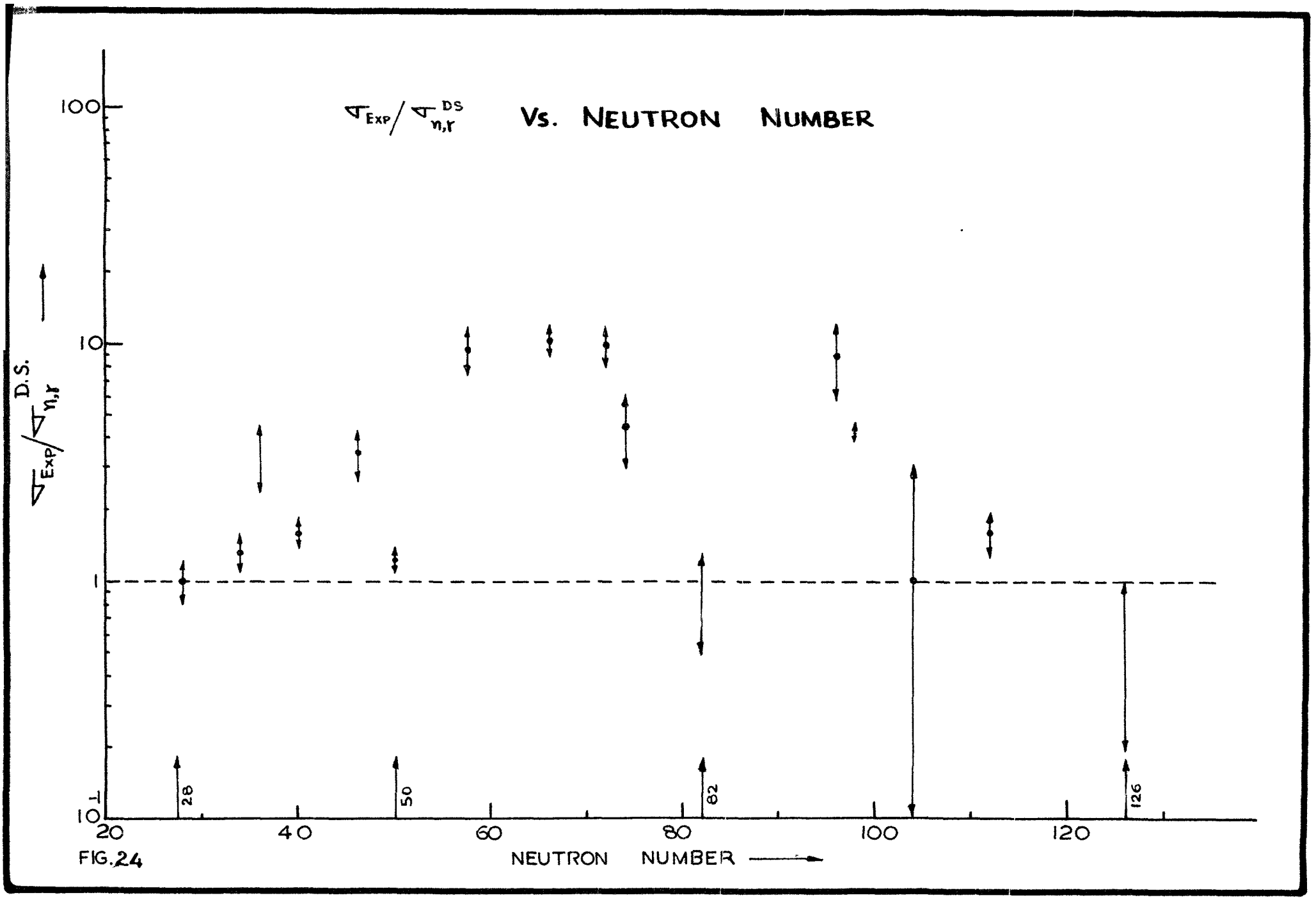
$\sigma_{Exp}/\sigma_{n,\gamma}^{DS}$ Vs. NEUTRON NUMBER
100
10
1
$\frac{1}{10}$
$\sigma_{Exp}/\sigma_{n,\gamma}^{D.S.}$
28
50
82
126
20
40
60
80
100
120
NEUTRON NUMBER

FIG. 24

also empirically one can take $E_R \approx 14$ MeV, and hence $E_R - E_o \approx 7$ MeV. For determining E_γ (= E_n + B/2), binding energies are taken from reference[28]. The values of giant dipole resonance parameters used in our calculations are tabulated in table-IV.

4.5 Discussion of the Results -

Calculated values of neutron radiative capture cross-sections obtained from direct - semi-direct theory are given in table III; column 5 & 6. They are in agreement with the experimental values, for those nuclei which are near the close neutron shells. In Fig.24 we have plotted (σ_{Exp} / $\sigma^{D.S}_{n,\gamma}$) against neutron number of the target nuclei. It is clear from this figure that the ratio of the two is equal to unity only for closed shell nuclei, and for nuclei off the close shells the ratio varies between one to eight. The calculation of neutron radiative capture cross-section from the expressions (9) and (10), basedon direct-semi-direct theory involves two types of errors.

1. The inherent errors due to several approximations in deriving the expressions for " $\sigma^{D}_{n,\gamma}$ " and 'F'
2. Errors associated with improper choices of the values of parameters E_γ, Γ and $(E_R - E_o)$.

However, the severest error comes from the neglect of channel contribution of the dipole integral, while deriving expression (9) for the direct-capture cross-section, Lane and

TABLE - III: Neutron Radiative Capture Cross-section at 14.8 MeV (σ_{Exp} denotes Experimental Values; σ_{Cal} denotes theoretically calculated values)

Target Nuc. ^{A}X	^{A+1}X	σ_{Exp} (mb.)		σ_{Cal} (mb.)	
		Present	earlier	$\sigma^{D}_{n,\gamma}$ (mb.)	$\sigma^{DS}_{n,\gamma}$ $(\sigma^{D}_{n,\gamma} \times F)$
^{51}V	^{52}V		0.73 ± 0.15 [3] 0.37 ± 0.06 [4]	0.094	0.672
^{52}Cr	^{53}Cr		0.92 ± 0.18 [3]	0.108	0.908
^{63}Cu	^{64}Cu		2.56 ± 0.38 [1]	0.145	1.909
^{65}Cu	^{66}Cu		6.3 ± 1.9 [1]	0.130	1.823
^{71}Ga	^{72}Ga		1.9 ± 0.2 [1]	0.144	1.150
^{81}Br	^{82}Br		3.5 ± 0.85 [1]	0.178	0.998
^{89}Y	^{90}Y		2.9 ± 0.3 [1]	0.205	2.361
^{103}Rh	^{104}Rh	16.8 ± 3.0	14 ± 3.0 [4]	0.261	1.773
^{115}In	^{116m}In		$5.97 + 0.81$ [6]	0.287	1.870
^{123}Sb	^{124g}Sb		15 ± 3.0 [4]	0.293	1.529

TABLE - III: (Contd.)

1.	2.	4.	6.	7.	8.
^{127}I	^{128}I	7.64 ± 3	7.2 ± 1.2[22)] 2.5 ± 0.5[1)]	0.320	1.804
^{138}Ba	^{139}Ba		1.3 ± 0.4[1)] 1.0 ± 0.2[5)]	0.283	2.574
^{139}La	^{140}La		1.9 ± 0.4[1)] 1.4 ± 0.15[2)] 1.1 ± 0.2[4)] 1.4 ± 0.3[5)]	0.302	2.383
^{141}Pr	^{142}Pr		3.33± 0.33[1)] 2.1 ± 0.1[2)] 3.0 ± 0.3[4)]	0.345	2.814
^{160}Gd	^{161}Gd		18.5± 5.5[1)] 3.0 ± 1.0[2)]	0.365	2.044
^{165}Ho	^{166}Ho		8.8 ± 0.6[4)] 6.87± 1.44[6)]	0.416	1.990
^{175}Lu	^{176m}Lu	2 ± 2	2.0 ± 1.0[2)]	0.466	2.122
^{186}W	^{187}W		4.0 ± 0.8[1)]	0.473	2.437
^{209}Bi	^{210}Bi		1.45 ± 0.16[1)] 1.2 ± 0.2[4)]	0.560	3.570
^{208}Pb	^{209}Pb		3.05± 0.45[1)] 1.0 + 0.2[4)]	0.470	3.531

TABLE - IV: Giant dipole resonance parameters & Factor "F"

Target Nuc.	E_R (MeV)	Γ (MeV)	"F"
^{51}V	18.2	5.7	7.139
^{52}Cr	18.8	5.0	8.419
^{63}Cu	17.5	4.0	13.193
^{65}Cu	17.5	4.0	14.068
^{71}Ga	16.5	5.5	8.010
^{81}Br	17.0	7.2	5.595
^{89}Y	16.3	3.8	11.534
^{103}Rh	14.4 - 17.2	3.2 - 4.2	6.800
^{115}In	14.0 - 16.2	3.0 - 3.8	6.514
^{123}Sb	15.2	7.2	5.220
^{127}I	15.3	6.6	5.632
^{138}Ba	15.5	5.0	9.089
^{139}La	15.0	5.1	7.888
^{141}Pr	15.0	4.4	8.154
^{160}Gd	13.5	5.3	5.603
^{165}Ho	12.1 - 16.0	2.6 - 4.5	4.781
^{175}Lu	16.0	8.4	4.556
^{186}W	14.5	7.0	5.152
^{209}Bi	13.7	5.1	6.375
^{208}Pd	13.5	3.8	5.723

Lynn in a later publication[16] have shown, that the inclusion of the channel contribution increases $\sigma^{D}_{n,\gamma}$ by a factor of the order of four. Longo and Seporetti[19] calculated direct-semi-direct capture cross-section using a more sophisticated expression which included a term for the interference between direct and semi-direct processes. They observed a similar behaviour in the calculated values, as in the present case i.e. their values showed agreement with the experimental values only for the closed shell nuclei.

Cvelbar et al.[8] measured γ-ray spectra from the radiative capture of 14.1 MeV neutrons in the light nuclei i.e. Mg, Si, P and Ca. They found that the absolute value of the capture cross-section is well accounted by the Brown's expression for direct-semi-direct capture. Their γ-ray spectra supports the presence of collective capture. Menlov et al[6] have measured (n,γ) cross-section for some nuclei over an energy interval 1 to 19 MeV. Their plot of cross-section against incident neutron energy shows a sort of peak, which is expected from the collective capture theory.

From the above discussion one can say that direct-semi-direct capture mechanism accounts fairly well for the order of magnitude of the experimental values of radiative capture cross-section at 14.8 MeV., particularly for the nuclei near the closed shell experimental and theoretically calculated values agree very well.

R E F E R E N C E S :

1. J.L. Perkin et al., Proc.Phys.Soc.(London) 72A (1958) 505
2. R.G. Will and R.W. Find Phys. Rev. 118 (1960) 242
3. F. Cvelbar et al., Proc.International Conf.Nucl.Struc. Antwerp (1965), C 160
4. J. Ciskai et al., Nucl. Phys. A95 (1965) 229
5. P. Cuzzocrea et al., Nuovo. Cim. 52B (1967) 476
6. H.O. Menlove et al., Phys. Rev. 163 (1967) 1299
7. E.T. Bramlitt and R.W. Fink, Phys. Rev. 131 (1963) 2649
8. F. Cvelbar et al., Nucl. Phys. A130 (1969) 401;A138(1969)412
9. F. Cvelbar et al., Nucl. Phys. A 130 (1969) 413
10. H. Feshbach et al., Phys. Rev. 96 (1954) 448
11. F.L. Friedman and V.F. Weisskopf, Niels Bohr and the development of Physics, Pergamon Press, (1955)
12. F. Beck, Proceedings of the Amsterdam Conference on Nucl. reactions (1956)
13. B.L. Cohen, Phys. Rev. 100 (1955) 206
14. A.M. Lane and J.E. Lynn, Proc.Conf.Peaceful uses of atomic energy Geneva (1958) Vol. 15 paper P/4
15. A.M. Lane, Nucl. Phys. 11 (1959) 625
16. A.M. Lane and J.E. Lynn, Nucl. 11 (1959) 640
17. G.E. Brown, Nucl. Phys. 57 (1964) 339
18. C.F. Clement et al. Nucl. Phys. 66 (1965) 273; 293
19. G. Longo and F. Saporetti, Nucl.Phys. A127 (1969) 503
20. Neutron Cross-sections, BNL-325, Second edition, 1958

21. Nuclear Data Sheets, Academic Press (1959-65)

22. S.M. Qaim and M. Ejaz, Journ.Inorg.Nucl.Chem.30(1968) 2577

23. E.P. Wigner and L. Eisenbud, Phys. Rev. 72 (1947) 29

24. P.L. Kapur and R.E. Peierls, Proc.Roy.Soc.A166 (1938) 277

25. H.A. Bethe, Revs. Mod. Phys. 9 (1937) 69

26. G.E. Brown, Unified Theory of Nuclear Models
John Wiley & Sons INC-New York, 1967

27. P. Olive and D. Prosperi, Nuovo Cim. 49B (1967) 161

28. Philip A. Seeger, Nucl. Phys. 25 (1961) 1

29. H. Liskien and Paulsen, EUR 119e- Vol 1 (1966)

****

CHAPTER -V

14.8 MeV NEUTRON CROSS-SECTION MEASUREMENTS

5.1 Introduction:

Exoergic reaction $^{3}_{1}H(d,n)\ ^{4}_{2}He$ yields high neutron flux of energy $\sim$14 MeV at deuteron bombarding energy as low as 120 keV, and hence it has proved to be a good tool for nuclear studies in the 14 MeV energy region. $\sim$14 MeV neutrons can initiate many reactions e.g. (n,γ), (n,n'), (n,α), (n,p) and (n,2n) etc. Therefore 14 MeV neutron cross-section measurements can be of much use for the understanding of the reaction mechanism of these reactions.

Salant and Ramsey[1] were the first to carry out cross-section measurements in the 14 MeV energy region. The most extensive measurements in this energy region have been performed by Paul and Clark[2] in 1953, followed by large number of measurements by various workers.[13-23,26-49] Many authors[3-10,49] have studied the systematic regularities in these cross-sections Some workers[3-5;11;12] have also given expressions for these reaction cross-sections, based on compound nucleus reaction mechanism. A comparison of the experimental and the predicted value can give some information about the applicability of the compound nucleus reaction mechanism. In quite a few cases large discrepancies appear in the cross-section values, when reported by various groups for the same reaction. Some times

this difference is as large as an order of magnitude. In table V we have tabulated some of the literature values of the reaction cross-sections at 14 MeV, which have large discrepancies.

The following are the possible causes which may introduce errors in the measurements of the cross-section.

1. In the 14 MeV energy region many reaction channels are open to the incident neutrons. So in a certain irradiated sample a mixture of many activities (each corresponding to certain specific reaction product) is produced. These different activities when separated have large statistical errors, especially in cases where natural elements have many stable isotopes.
2. Large spread in the energy of the neutrons used and the presence of slow neutron background (due to the scattering of fast neutrons with the walls and other scattering material near the place of irradiation) also introduces large errors, particularly in the measurements of (n, γ) cross-section in the 14 MeV energy region.
3. Errors may also be introduced in the process of normalization to a given standard, erroneus determination of neutron flux and branching ratios etc.

Keeping in view the above facts, it was decided to perform measurements using enriched isotopes of some elements which have many stable isotopes. A standard was chosen whose

TABLE - V ; 14.8 MeV Neutron Cross-sections (with large discrepancies)

Reaction	Reported values of cross-section (mb.)	Reference
$^{86}Kr(n,2n)^{85m}Kr$	350 ± 35	(13)
	65	(14)
$^{109}Ag(n,2n)^{108m}Ag$	1000 ± 100	(15)
	311 ± 150	(20)
$^{97}Mo(n,p)^{97}Nb$	108 ± 54	(2)
	17.7± 1.5	(16)
$^{128}Te(n,p)^{128m}Sb$	65 ± 19	(17)
	1.0± 0.1	(18)
$^{160}Gd(n,\gamma)^{161}Gd$	18.5± 5.5	(19)
	3 ± 1	(20)
$^{81}Br(n,\alpha)^{78}As$	103 ± 20	(2)
	10 ± 1	(21)
$^{68}Zn(n,\alpha)^{65}Ni$	51 ± 10	(22)
	7.6± 0.8	(23)

cross-section had been studied quite extensively.[24] The latest available decay schemes data[25] is used to minimize the errors due to uncertainties in the determination of branching ratios etc.

5.2 Experimental Procedure:

In present measurements we have used enriched isotopes (^{82}Se, ^{92}Mo, ^{117}Sn, ^{128}Te and ^{130}Te). The percentage abundance of the various isotopes in the enriched samples used presently are given in table VI. These isotopes are selected because of the fact that either their experimental cross-section values have large discrepancies or their cross-sections could not be measured due to the small isotopic abundance in the natural elements. The enriched isotopes were obtained from ONL, Oak Ridge, Tennessee, U.S.A. Some of the cross-section reported here, are obtained as a by-product from the activities produced during (n,γ) measurements at the same energy(chap.IV).

^{27}Al (n,p) ^{27}Mg and ^{27}Al (n,α) ^{24}Na reactions were chosen as standard and their cross-section were taken from the compilation of Liskein and Paulsen[24]. The various reasons for choosing these reactions as standard are given in Chap.IV alongwith the adopted values for these reaction cross-sections.

The beam current used in our measurements varied between 50-100 μa and the corresponding neutron flux were around 10^9 neutrons/min. ZnS crystal was used to monitor the neutron flux during irradiations. The details of the individual measurements are given below.

TABLE - VI: Percentage Abundances of the Various Isotopes in the Enriched Samples.

Se enriched in ^{82}Se	Mo enriched in ^{92}Mo	SnO_2 enriched in ^{117}Sn	Te enriched in ^{128}Te	Te enriched in ^{130}Te
^{74}Se (0.23%)	^{92}Mo (98.27%)	^{112}Sn (0.03%)	^{120}Te (< 0.05%)	^{120}Te (< 0.02%)
^{76}Se (2.21%)	^{94}Mo (0.46%)	^{114}Sn (0.03%)	^{122}Te (< 0.05%)	^{122}Te (0.04%)
^{77}Se (1.87%)	^{95}Mo (0.37%)	^{115}Sn (0.06%)	^{123}Te (< 0.05%)	^{123}Te (0.02%)
^{78}Se (6.78%)	^{96}Mo (0.26%)	^{116}Sn (2.57%)	^{124}Te (< 0.05%)	^{124}Te (0.02%)
^{80}Se (13.62%)	^{97}Mo (0.13%)	^{117}Sn (78.8%)	^{125}Te (0.23%)	^{125}Te (0.03%)
^{82}Se (75.31%)	^{98}Mo (0.27%)	^{118}Sn (8.03%)	^{126}Te (1.2%)	^{126}Te (0.1%)
	^{100}Mo (0.25%)	^{119}Sn (7.19%)	^{128}Te (93.05%)	^{128}Te (0.3%)
		^{120}Sn (2.84%)	^{130}Te (5.52%)	^{130}Te (99.49%)
		^{122}Sn (0.24%)		
		^{124}Sn (0.20%)		

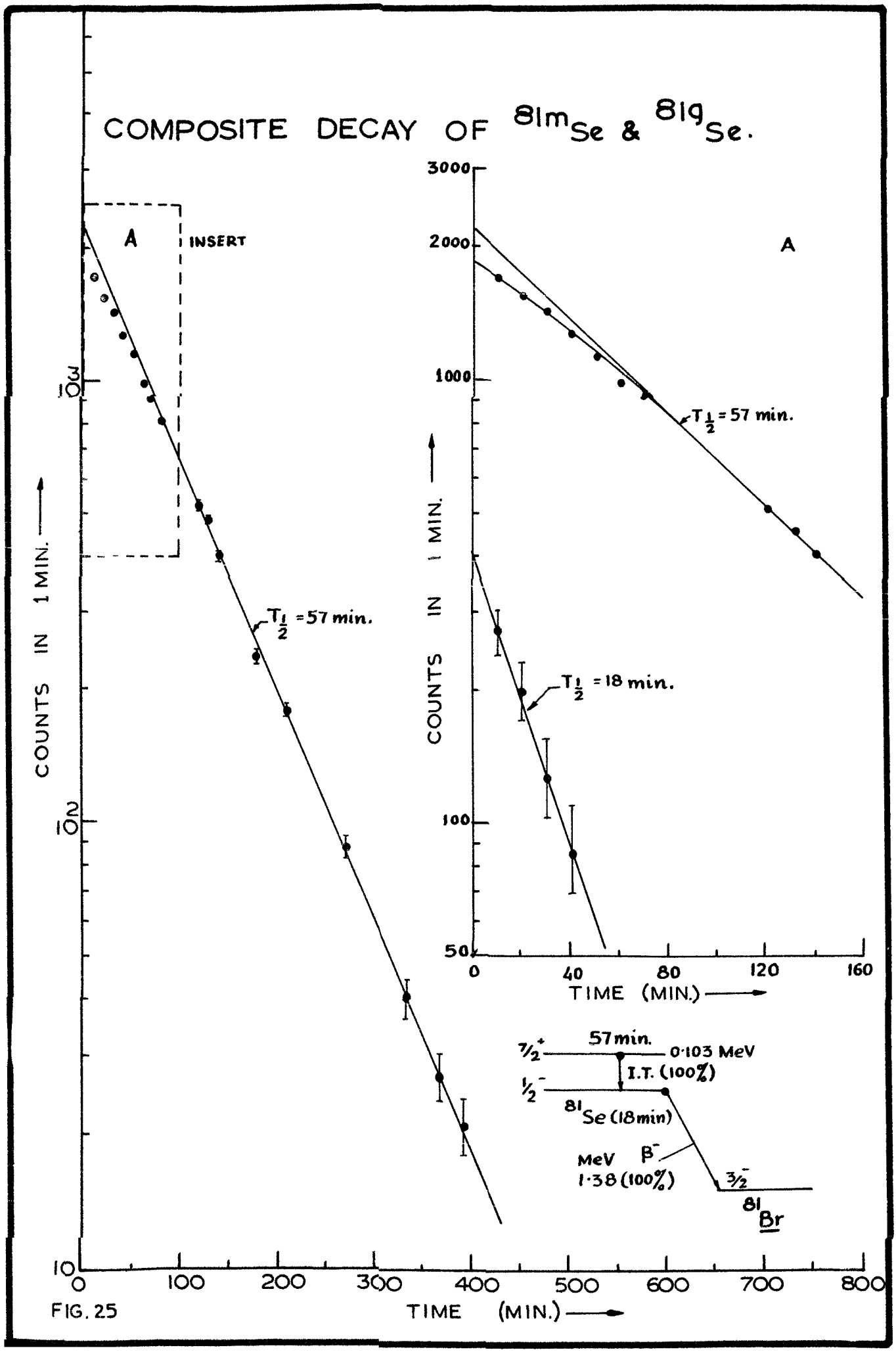
COMPOSITE DECAY OF ^{81m}Se & ^{81g}Se.
A
INSERT
$T_{\frac{1}{2}}$ = 57 min.
$T_{\frac{1}{2}}$ = 18 min.
COUNTS IN 1 MIN.
TIME (MIN.)
3000
2000
1000
100
50
10
0
40
80
120
160
100
200
300
400
500
600
700
800
57 min.
0·103 MeV
I.T. (100%)
^{81}Se (18 min)
MeV
1·38 (100%)
^{81}Br

FIG. 25

$^{82}Se\ (n,2n)\ ^{81m,g}Se$ - Reaction.

Metallic selenium enriched in ^{82}Se isotope (75.3%) was used for the sample preparation. The mass of the sample was 0.0102 grams. Sample assembly was irradiated for 10 minutes. Decay curve of the irradiated sample is shown in Fig.25. The (n,2n) reaction product of ^{82}Se isotope has two isomers ^{81m}Se (57 min) and ^{81g}Se (18 min.). The ratio of $\sigma\{^{82}Se\ (n,2n)\ ^{81m}Se\}$ to $\sigma\{^{82}Se\ (n,2n)\ ^{81g}Se\}$ is such that the ground state β-activity appears to grow during the initial counting period and later it shows 57 min. halflife. 57 min. activity is extrapolated back to zero time and then the initial composite curve is subtracted from 57 min activity to get the 18 min. activity (see Chap.II, equation 15 A &18) The two resolved activities with halflives 57 and 18 min are also shown in Fig.25.

$\Phi.Ge$	=	3.411×10^{8}	n/min.
N_o	=	0.564×10^{20}	
ϵ_g	=	0.861	
λ_g	=	0.038	min^{-1}
λ_m	=	0.012	min^{-1}
$\lambda_g/\lambda_g-\lambda_m$	=	1.458	
$(1-e^{-\lambda_m t_e})$	=	0.114	
$(1-e^{-\lambda_g t_e})$	=	0.320	
$(C_m)_{t=o}$	=	2200	counts/min
$(C_g')_{t=o}$	=	410	counts/min
σ_m	=	850 ± 50	mb.
σ_g	=	310 ± 25	mb.

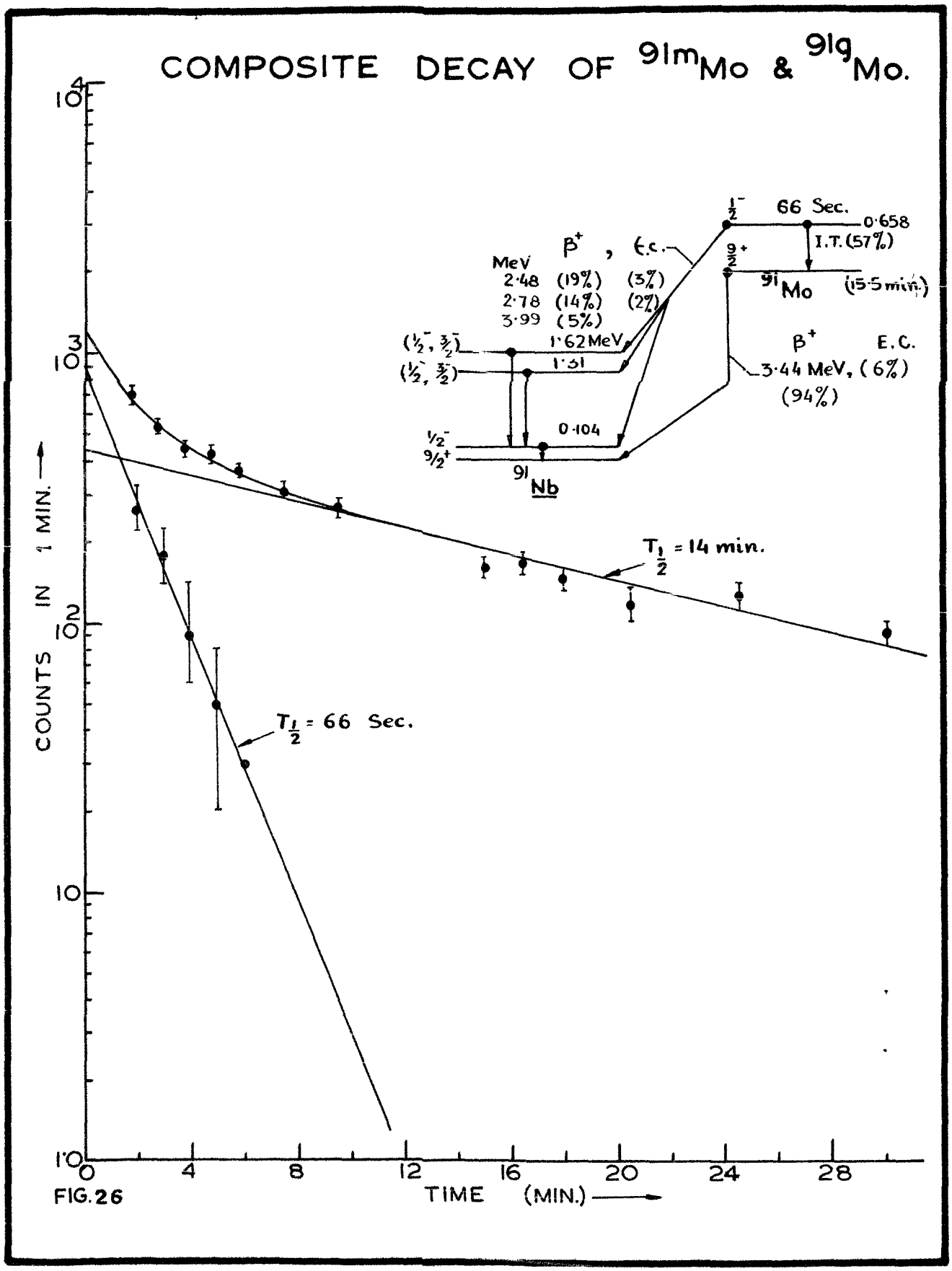
COMPOSITE DECAY OF 91mMo & 91gMo.
COUNTS IN 1 MIN.
TIME (MIN.)
$T_{\frac{1}{2}}$ = 14 min.
$T_{\frac{1}{2}}$ = 66 Sec.
β+ , E.C.
MeV
2·48 (19%) (3%)
2·78 (14%) (2%)
3·99 (5%)
1·62 MeV
1·31
0·104
91Nb
1/2⁻ 66 Sec.
0·658
I.T. (57%)
9/2+
91Mo (15·5 min.)
β+ E.C.
3·44 MeV, (6%)
(94%)

FIG. 26

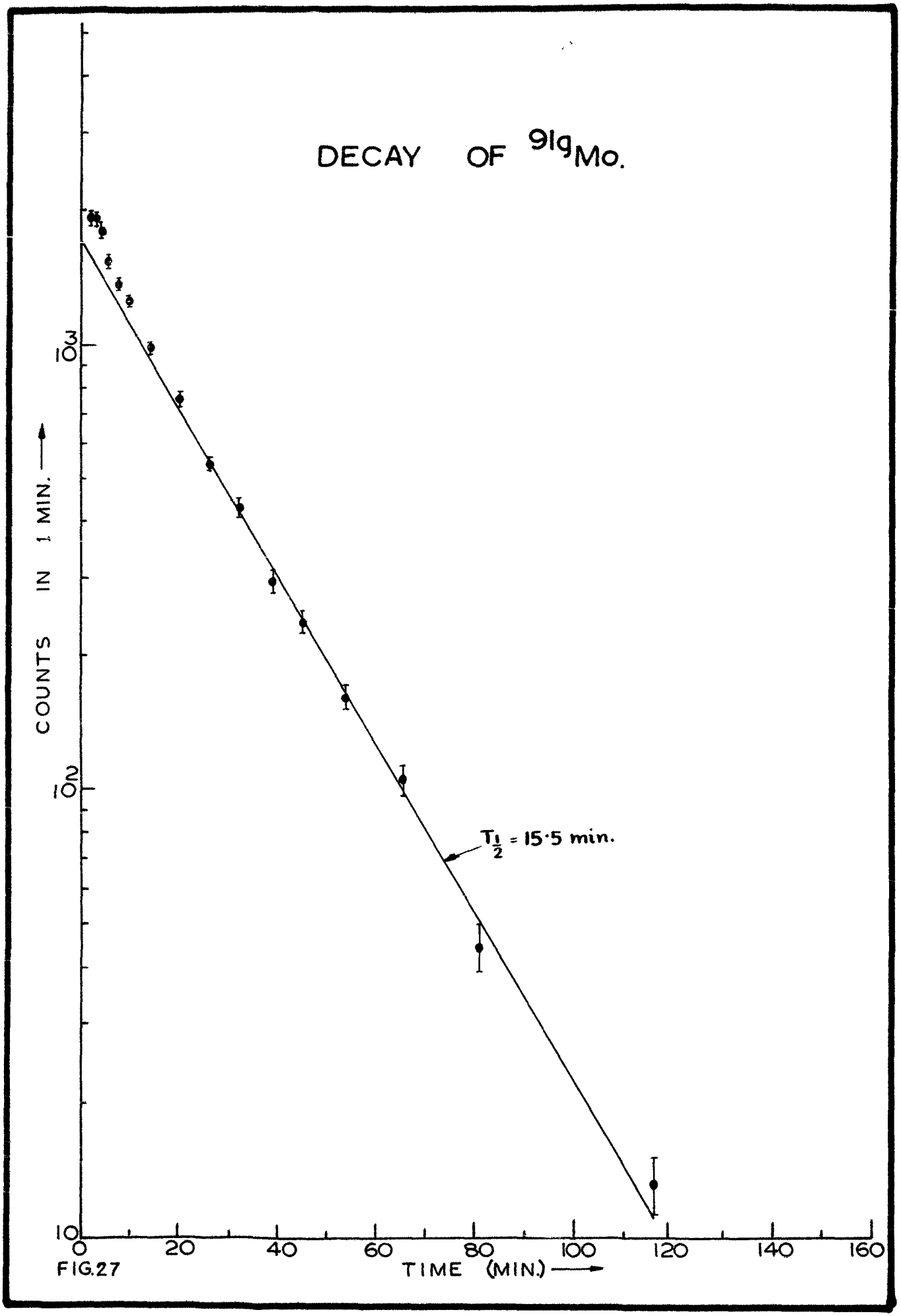
DECAY OF 91g Mo.
COUNTS IN 1 MIN.
10³
10²
10
$T_{\frac{1}{2}}$ = 15·5 min.
0
20
40
60
80
100
120
140
160
TIME (MIN.)

FIG.27

$^{92}Mo(n,2n)\ ^{91m}Mo$ Reaction.

0.0412 gram molybdenum enriched in ^{92}Mo isotope (98.27%) was used for the sample preparation. Sample assembly was irradiated for a short duration of 1.5 min only to reduce the build up of the longer lived activities. As can be seen from the decay scheme, isomeric state of $^{92}Mo(n,2n)$ reaction product ^{91m}Mo (66 sec) decays 43% by β-ray emission and the rest of it decays to the ground state ^{91g}Mo (15.5 min) by isomeric transition. The cross-section for the isomeric state can be directly measured by counting its β-rays. The decay curve is shown in Fig. 26. 66 sec. activity extracted from the decay curve, corresponds to the β-decay of the isomeric state. Another activity having roughly 14 min. halflife is due to poorly populated ^{91g}Mo state and has large statistical errors.

$\Phi.G\epsilon = 1.298 \times 10^{8}$ n/min

$N_o = 2.647 \times 10^{20}$

$\epsilon_m = 0.339$

$(1-e^{-\lambda_m t_e}) = 0.611$

$(C_m)_{t=o} = 850$ counts/min

$\sigma_m = 120 \pm 12$ mb.

$^{92}Mo\ (n,2n)\ ^{91g}Mo$ Reaction.

For this measurement ^{92}Mo sample was irradiated for 30 min. The ground state β-activity was counted. The decay curve

DECAY OF 127g Te.
T½ = 9·3 hrs.
COUNTS IN 1 MIN.
10
1·0
0
4
8
12
16
20
24
28
32
TIME (HOURS)

FIG. 28A

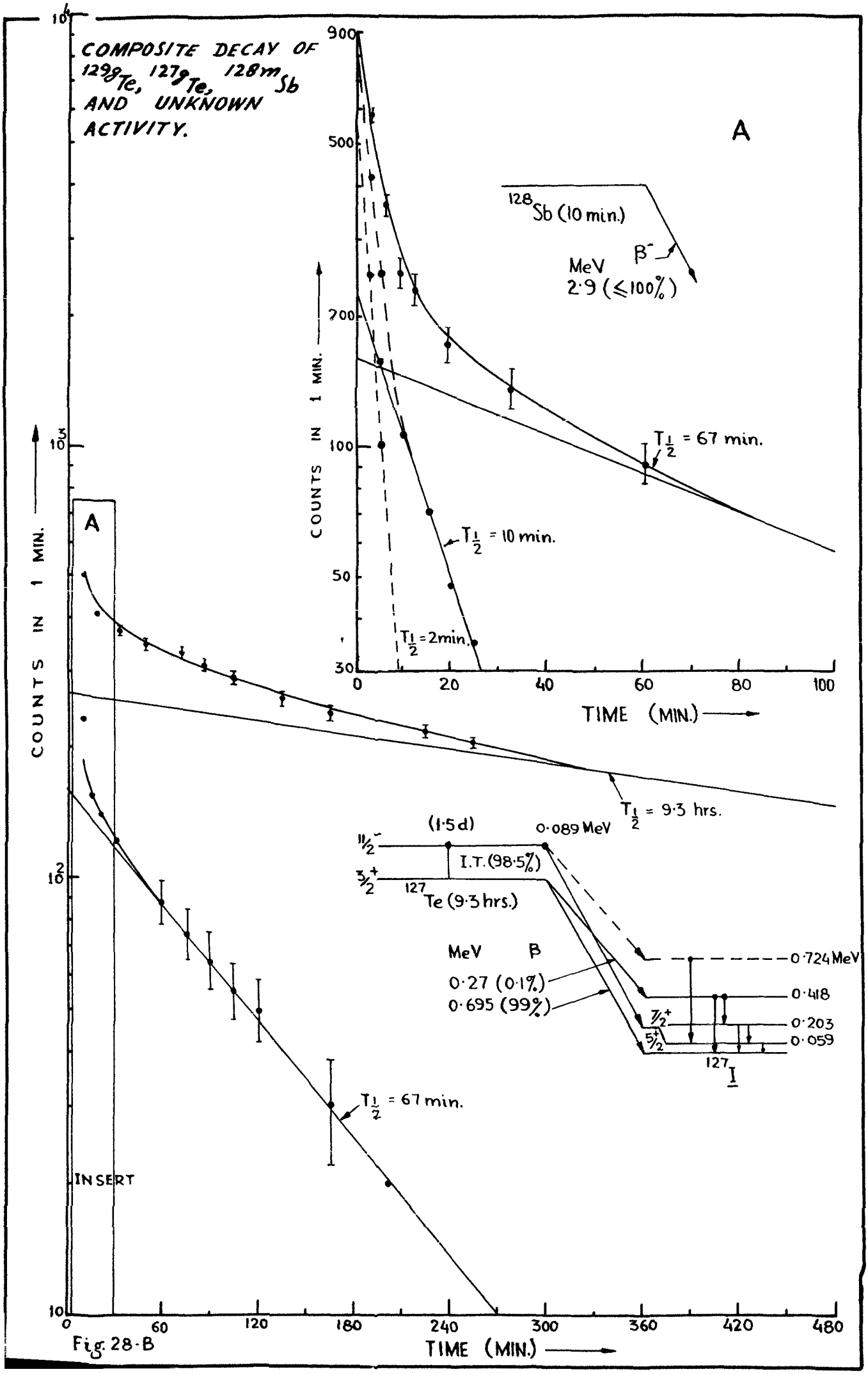
COMPOSITE DECAY OF 129gTe, 127gTe, 128mSb AND UNKNOWN ACTIVITY.
A
128Sb (10 min.)
β⁻
MeV
2·9 (≤100%)
COUNTS IN 1 MIN.
T½ = 67 min.
T½ = 10 min.
T½ = 2min.
TIME (MIN.)
T½ = 9·3 hrs.
(1·5 d)
0·089 MeV
11/2⁻
I.T. (98·5%)
3/2⁺
127Te (9·3 hrs.)
MeV β
0·27 (0·1%)
0·695 (99%)
0·724 MeV
0·418
7/2⁺
0·203
5/2⁺
0·059
127I
INSERT
Fig. 28·B

shown in Fig. 27 shows 15.5 mins. halflife. The zero time activity corresponding to 15.5 mins. halflife is the sum of the ground state activity and 57% of the populated isomeric state

$\Phi . G_e = 5.653 \times 10^7$ n/min

$N_o = 2.647 \times 10^{20}$

$\epsilon_g = 0.868$

$(1-e^{-\lambda_g t_e}) = 0.727$

$(C_g)_{t=o} = 0.1700$ counts/min

$(\sigma_g + 0.57\,\sigma_m) = 180 \pm 12$ mb.

$\sigma_m = 112 \pm 14$ mb.

^{128}Te (n,2n) ^{127g}Te and ^{128}(n,p) ^{128}Sb Reaction.

Tellurium enriched in ^{128}Te isotope (93.05%) and weighing 0.0202 grams was used for the sample preparation. Irradiation of the sample was carried out for one hour. Decay curve of the β-activity in the irradiated sample is shown in Fig.28 A & B. Of the four resolved activities in Fig.28B, 9.3 hrs. activity corresponds to ^{128}Te (n,2n) ^{127g}Te reaction product; 10 min. activity corresponds to the sum of $^{128}Te(n,\alpha)$ ^{125}Sn and ^{128}Te (n,p) ^{128g}Sb reaction products and 67 min. activity corresponds to ^{130}Te (n,2n) ^{129g}Te reaction product. A two min. activity observed is an unknown activity, as it could not be associated with any possible reaction product

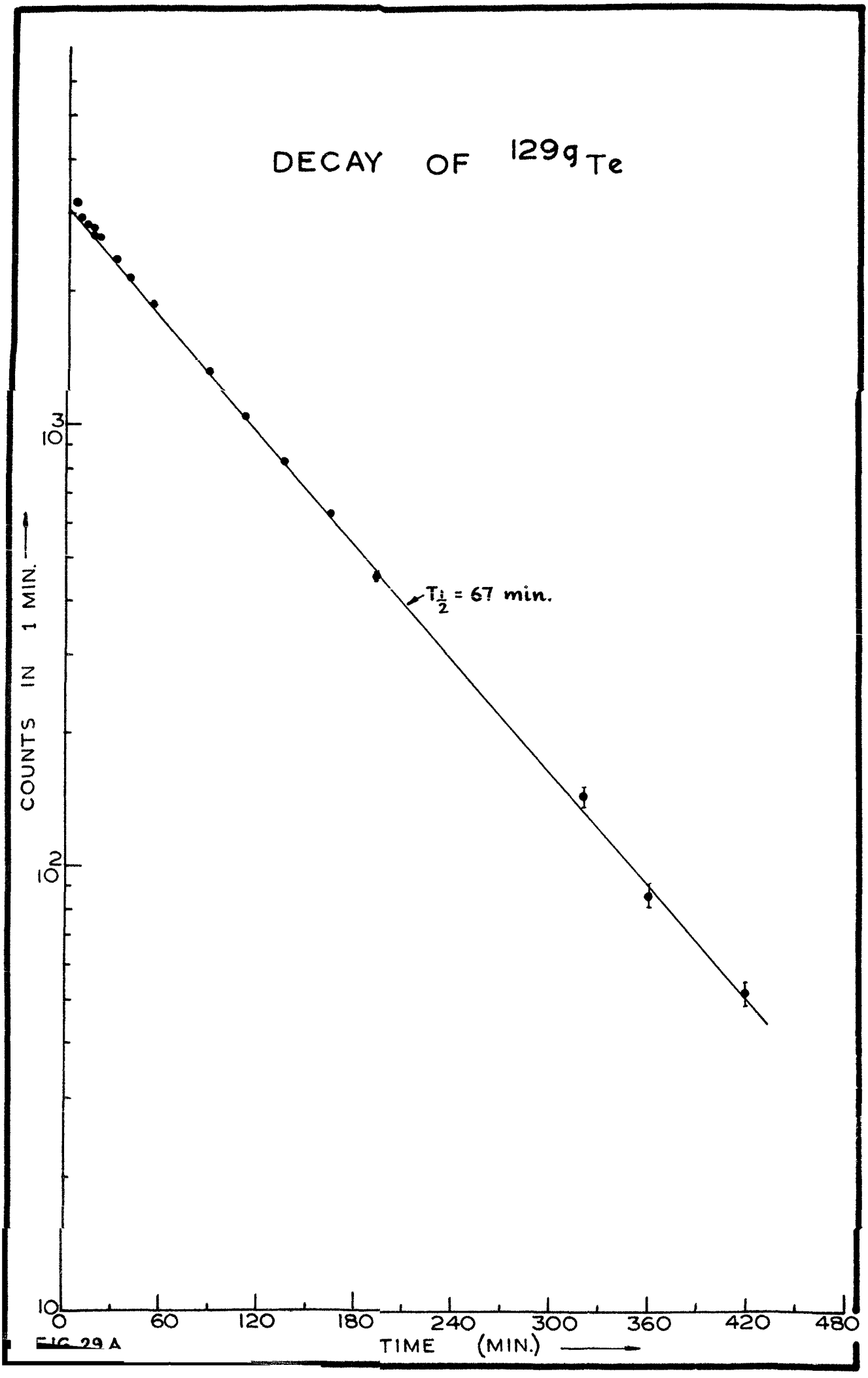
DECAY OF ^{129g}Te
COUNTS IN 1 MIN.
10^3
10^2
10
$T_{\frac{1}{2}}$ = 67 min.
0
60
120
180
240
300
360
420
480
TIME (MIN.)

FIG. 29 A

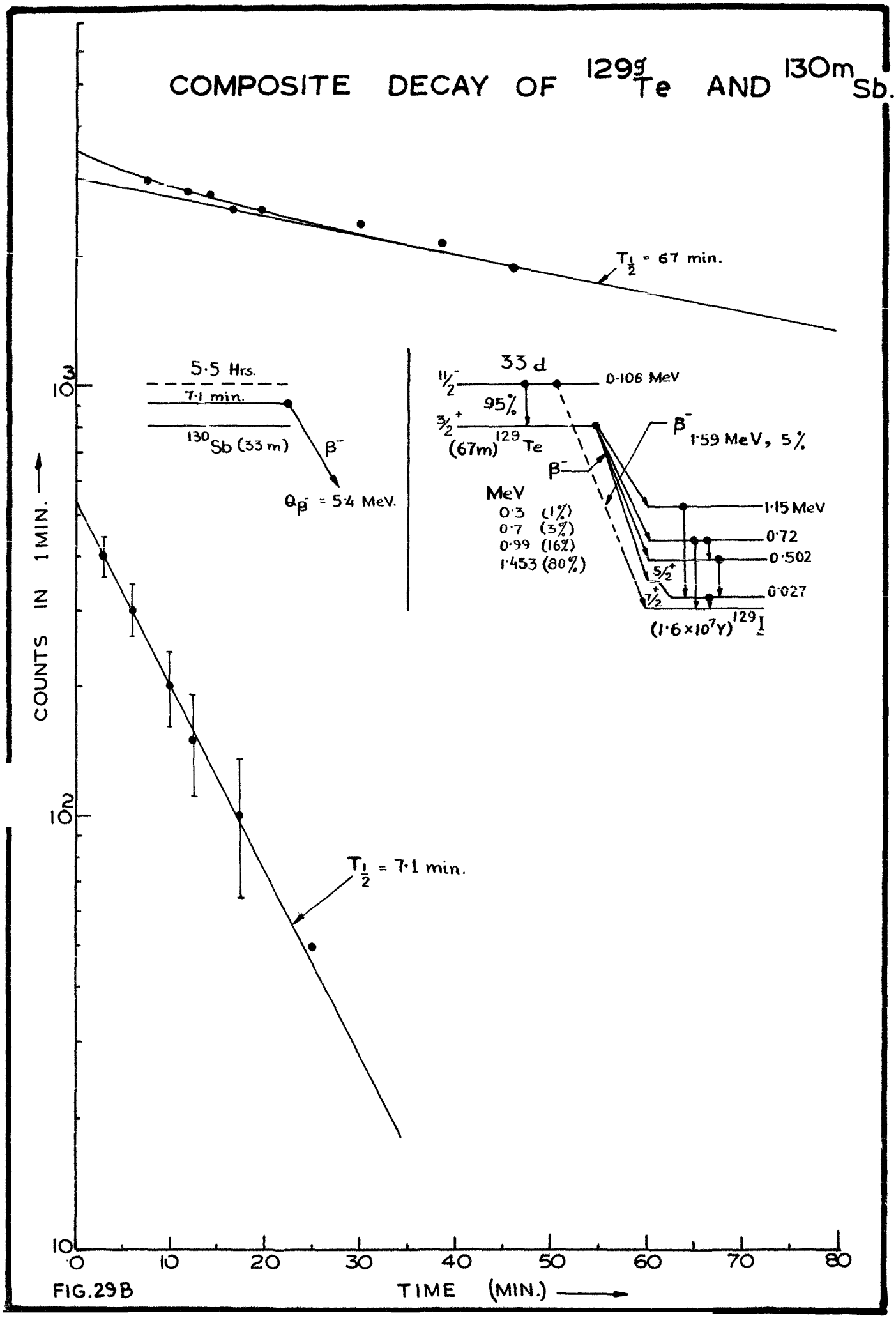
COMPOSITE DECAY OF 129g Te AND 130m Sb.
T½ = 67 min.
5·5 Hrs.
7·1 min.
130Sb (33 m)
β⁻
Qβ⁻ = 5·4 MeV.
33 d
11/2⁻
0·106 MeV
95%
3/2⁺
(67m) 129 Te
β⁻
β⁻ 1·59 MeV, 5%
MeV
0·3 (1%)
0·7 (3%)
0·99 (16%)
1·453 (80%)
1·15 MeV
0·72
0·502
5/2⁺
0·027
7/2⁺
(1·6×10⁷Y) 129 I
COUNTS IN 1 MIN.
10³
10²
10
T½ = 7·1 min.
0
10
20
30
40
50
60
70
80
TIME (MIN.)

FIG.29B

$^{128}Te\ (n,2n)\ ^{127g}Te$ -

$\Phi . Ge = 1.294 \times 10^{8}$ n/min.

$N_o = 0.886 \times 10^{20}$

$\epsilon_g = 0.568$

$(1-e^{-\lambda_g t_e}) = 0.072$

$(C_g)_{t=o} = 270$ counts/min.

$\sigma_g = 580 \pm 45$ mb.

$^{128}Te(n,p)\ ^{128g}Sb$ -

$\Phi . Ge = 1.294 \times 10^{8}$ n/min

$N_o = 0.886 \times 10^{20}$

$\epsilon = 0.872$

$(1-e^{-\lambda_g t_e}) = 0.986$

$C_{t=o} = 220$ counts/min.

$\sigma \left\{ \begin{matrix} ^{128}Te(n,\alpha) + \\ ^{128}Te(n,p) \end{matrix} \right\} = 24 \pm 4$ mb.

The quoted[18,34] values of cross-section for $^{128}Te(n,\alpha)\ ^{125m}Sn$ reaction are between 0.55 to 0.8 mb. and hence one can write

$$\sigma \left\{ ^{128}Te(n,p)\ ^{128g}Sb \right\} = 24 \pm 4 \text{ mb.}$$

<u>$^{130}Te(n,2n)\ ^{129g}Te$ and $^{130}Te\ (n,p)\ ^{130m}Sb$ Reactions.</u>

0.0182 grams of tellurium enriched in ^{130}Te isotope (99.49%) was used for the sample preparation. Sample assembly

was irradiated for one hour. β -activity of the activated sample was followed up to background level. The decay curve gives two activities with 67 min. and 7.1 min. halflives corresponding to ^{130}Te (n,2n) ^{129g}Te and ^{130}Te (n,p) ^{130m}Sb reaction products respectively (see Fig.29 A&B). As the energy of the β -rays corresponding to ^{130m}Sb decay is not known, it was taken equal to Q_B. The value of Q_B as given in Ref.50 is 5.4 MeV.

^{130}Te (n,2n) ^{129g}Te -

$\Phi . G_e = 1.464 \times 10^8$ n/min

$N_o = 0.834 \times 10^{20}$

$\epsilon_g = 0.799$

$(1-e^{-\lambda_g t_e}) = 0.462$

$(C_g)_{t=o} = 3000$ counts/min.

$\sigma_g = 660 \pm 40$ mb.

^{130}Te (n,p) ^{130m}Sb -

$\Phi . G_e = 1.464 \times 10^8$ n/min.

$N_o = 0.834 \times 10^{20}$

$\epsilon_m = 0.997$

$(1-e^{-\lambda_m t_e}) = 1$

$(C_m)_{t=o} = 540$ counts/min.

$\sigma_m \geq 44$ mb.

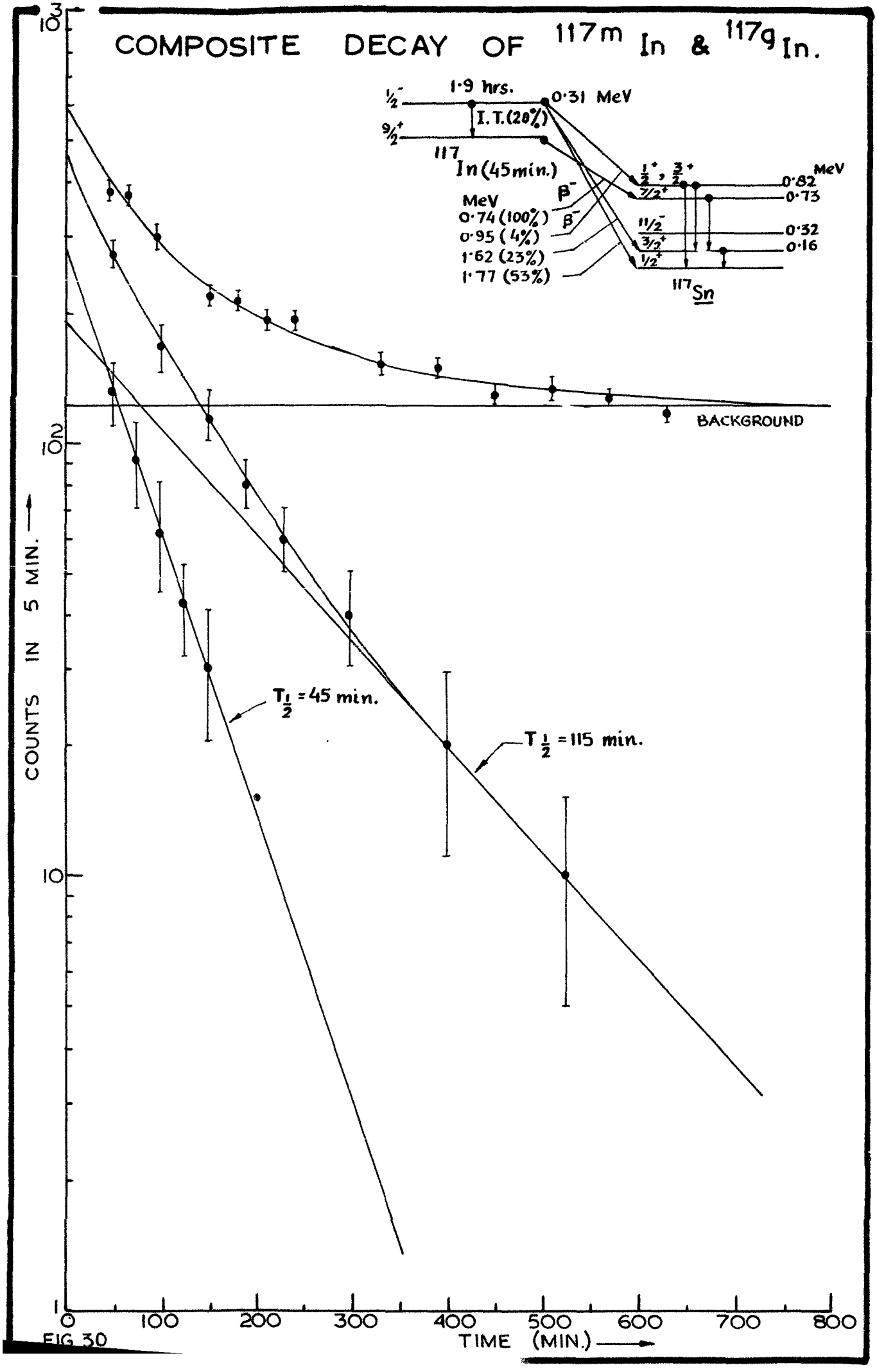
COMPOSITE DECAY OF 117m In & 117g In.
1·9 hrs.
0·31 MeV
I.T.(20%)
117 In (45min.)
MeV
0·74 (100%)
0·95 (4%)
1·62 (23%)
1·77 (53%)
β⁻
β⁻
MeV
0·82
0·73
0·32
0·16
117Sn
BACKGROUND
T½ = 45 min.
T½ = 115 min.
COUNTS IN 5 MIN.
TIME (MIN.)
10³
10²
10
1
0
100
200
300
400
500
600
700
800

FIG 30

$^{117}Sn(n,p)\ ^{117m,g}In$ Reaction -

SnO_2 enriched in ^{117}Sn isotope (78.8%) was used for the sample preparation. Mass of SnO_2 used was 0.0224 grams. Sample assembly was irradiated for one hour. β-activity in the irradiated sample was counted. The decay curve and the decay scheme are shown in Fig.30

$\Phi . G_e =$	1.464×10^8	n/sec
$N_o =$	0.712×10^{20}	
$\lambda_m =$	0.365	hrs^{-1}
$\lambda_g =$	0.924	hrs^{-1}
$\lambda_g/\lambda_g - \lambda_m =$	1.652	
$\epsilon_m =$	0.672	
$\epsilon_g =$	0.583	
$=$	0.306	
$(1-e^{-\lambda_m t_e}) =$	0.603	
$(1-e^{-\lambda_g t_e}) =$	190	counts/5 min.
$(C_m)_{t=0} =$	280	counts/5 min.
$(C_g)_{t=0}$		
$\sigma_m =$	14 ± 2	mb.
$\sigma_g =$	16.5 ± 2	mb.

$^{113}In\ (n,2n)\ ^{112m}In$ and $^{115}In(n,\alpha)\ ^{112}Ag$ Reactions.

The two activities with half-lives 3.2 hrs. and 21 min. were obtained in decay of irradiated Indium, while measuring

^{115}In (n, γ) ^{116m}In reaction cross-section (see Fig.19 A&B). The decay schemes for these reaction products are also given in the same Figure.

^{113}In (n,2n) ^{112m}In -

$\Phi . G_e$ =	1.166×10^9	n/min.
N_o =	0.162×10^{20}	
λ_m =	0.033	min^{-1}
λ_g =	0.049	min^{-1}
$\lambda_g/\lambda_g-\lambda_m$ =	2.982	
$(1-e^{-\lambda_m t_e})$ =	0.483	
ϵ_g =	0.259	
$(C_m)_{t=o}$ =	4000	counts/min.
σ_m =	570 $\pm$ 40	mb.

$^{115}In(n,\alpha)$ ^{112}Ag -

$\Phi . G_e$ =	1.166×10^9	n/min.
N_o =	3.723×10^{20}	
ϵ =	0.853	
$(1-e^{-\lambda t_e})$ =	0.070	
$C_{t=o}$ =	450	counts/min
σ =	17.4 $\pm$ 2	mb.

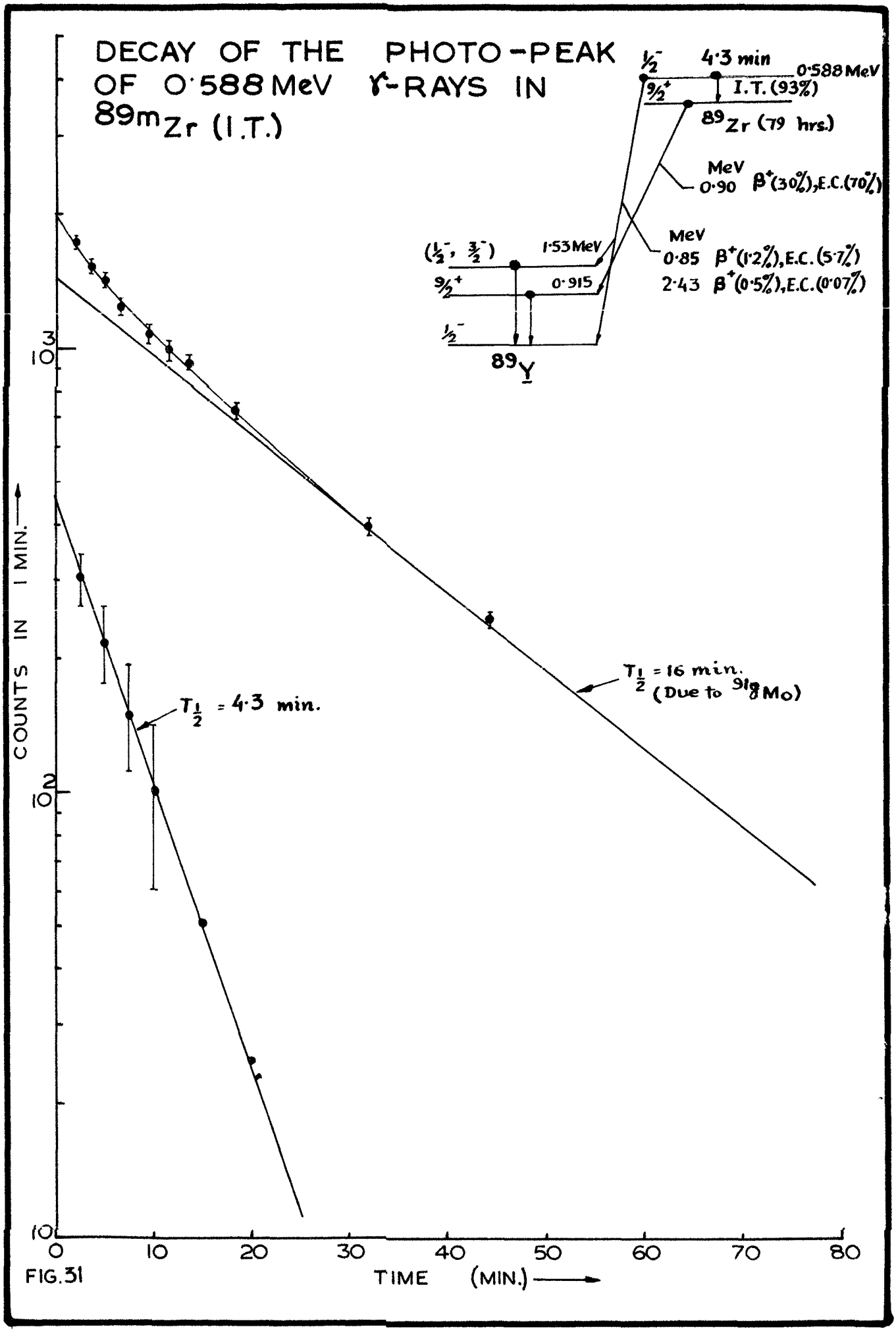
DECAY OF THE PHOTO-PEAK OF 0·588 MeV γ-RAYS IN 89mZr (I.T.)
½⁻ 4·3 min
0·588 MeV
9/2⁺ I.T. (93%)
89Zr (79 hrs.)
MeV
0·90 β⁺(30%), E.C.(70%)
MeV
0·85 β⁺(1·2%), E.C.(5·7%)
2·43 β⁺(0·5%), E.C.(0·07%)
(½⁻, 3/2⁻) 1·53 MeV
9/2⁺ 0·915
½⁻
89Y
COUNTS IN 1 MIN.
T½ = 16 min. (Due to 91g Mo)
T½ = 4·3 min.
TIME (MIN.)
FIG. 31

^{41}K (n,p) ^{41}A Reaction

This activity is observed in ^{127}I (n,γ) ^{128}I reaction cross-section measurement (see Fig. 21).

$\phi . G_e = 1.159 \times 10^9$ n/min.

$N_o = 0.498 \times 10^{20}$

$\epsilon = 0.310$

$(1-e^{-\lambda_m t_e}) = 0.116$

$C_{t=o} = 350$ counts/min.

$\sigma = 165 \pm 40$ mb.

^{92}Mo (n,α) ^{89m}Zr Reaction

Sample of ^{92}Mo (enriched) was irradiated for 8 min. ^{92}Mo (n,α) reaction product has two isomers. The isomeric state has 4.3 min. half-life and 93% of it decays to ground state by isomeric transitions. The decay scheme is shown in Fig.31. Photo-peak of the 0.588 MeV γ-ray corresponding to the isomeric transition was counted. However,in the decay curve a 16 min. activity is also observed alongwith 4.3 min. activity (see Fig.31). This 16 min. activity is observed due to $^{92}Mo(n,2n)$ ^{91g}Mo reaction product which decays through β-rays of 3.44 MeV.

$\phi . G_e = 5.163 \times 10^9$ n/min.

$N_o = 2.647 \times 10^{20}$

Photo-peak efficiency P(E) = 0.350

absorption correction ($e^{\mu t}$) = 1.022

$(1-e^{-\lambda te}) = 0.725$

detection efficiency D(E) = 0.619

Internal conversion correction $(1 + \alpha_T) = 1.076$

$C_{t=o}$ = 450 counts/min.

σ = 2.48 ± 0.3 mb.

4.3 Results and Discussions:

A) (n,2n) reaction cross-section.

The results of the present (n,2n) cross-section measurements are given in table VII column (1), (2) and (3) give target nuclei, product nuclei and halflives of the product nuclei respectively; column (4) gives cross-section values determined presently. In column (5) earlier reported values of the cross-section are given for the sake of comparison with the present measurements. Present value of $^{82}Se(n,2n)\ ^{81m}Se$ reaction cross-section is in close agreement with that of Rao and Fink.[26] The value of $^{82}Se(n,2n)\ ^{81g}Se$ reaction cross-section lies between two values reported by Rao and Fink[26] and Minetti and Pasquarelli[27]. In case of $^{92}Mo\ (n,2n)\ ^{91m}Mo$ reaction our value of cross-section is much higher than the earlier reported values. However, the value of $(\sigma_g + 0.57\ \sigma_m)$ obtained from ground state β-activity is in good agreement with all the earlier reported values. Present value of $^{128}Te(n,2n)\ ^{127g}Te$ reaction

TABLE - VII ; (n,2n) Cross-sections at 14.8 MeV

(1) Target Nuc.	(2) Product Nuc.	(3) Product Halflife	σ_{Exp} (mb.) (4) Present	σ_{Exp} (mb.) (5) Others	(6) $\sigma_t(n,2n) = \sigma_m + \sigma_g$ (mb.)	σ (mb.) predicted (Ref.11)
^{82}Se	^{81m}Se	57 min.	850 ± 50	894 ± 89 [26] 1077 ± 30 [27] 1870 ± 250 [28] 1500 ± 500 [2] 1600 ± 160 [29]		
	^{81g}Se	18 min.	310 ± 25	225 ± 45 [26] 385 ± 20 [27] < 100 [29]		
^{92}Mo	^{91m}Mo	66 sec.	120 ± 12	15 ± 1.5 [30] 7 ± 2 [31] 51 ± 10 [32]	1160 ± 60	1400
	^{91g}Mo	15.5 min.	112 ± 14	159 ± 16 [30] 158 ± 5 [16] 106 ± 7.5 [33] 163 ± 12 [31] 205 ± 25 [32]	232 ± 16	500
^{128}Te	^{127g}Te	9.3 hrs.	580 + 45	238 ± 36 [34] 760 ± 100 [18] 779 ± 233 [2] 640 ± 23 [35]		

TABLE - VII (Contd.)

(1)	(2)	(3)	(4)	(5)	(6)	(7)
^{130}Te	^{129m}Te	33 days	- - - -	241 ± 30[18] 247 ± 74[36] *528 ± 100[34]		
	^{129g}Te	67 min.	660 ± 40	435 ± 50[18] 210 ± 46[36] 225 ± 28[34] 599 ± 120[2]		
^{113}In	^{112m}In	21 min.	570 ± 60	1490 ± 150[37] 800[38]	1188 ± 110	1825
	^{112g}In	14 min.	- - - -	300 ± 30[37] *700[38]	1270 ± 60	1500

* Literature values taken to find out $\sigma_t(n,2n)$

cross-section agrees with that of Bonazzola et al[35] and the value of ^{130}Te (n,2n) ^{129g}Te reaction cross-section agrees with the value of Paul and Clark.[2] Value for ^{113}In (n,2n) ^{112m}In is quite close to the value reported in Ref.38).

For the sake of comparison theoretically predicted values of (n,2n) cross-sections are also given in column (7) of the table VII. These predicted values are the one given by Pearlstein[11] based on relatively crude statistical model. In the case of $^{130}Te(n,2n)$ $^{129mg}Te$, $^{113}In(n,2n)$ $^{112m,g}In$ and $^{128}Te(n,2n)$ $^{127m,g}Te$ reactions, cross-section is measured only for one of the two isomeric states. For the other state literature values are taken. Cross-section for $^{128}Te(n,2n)$ ^{127m}Te has not been reported so far and so comparison of predicted and experimental value is not possible. However, it is noted that experimental results lie within 70% of the theoretical predications. It shows the applicability of statistical theory for (n,2n) reactions at 14.8 MeV neutron energy, and is in agreement with the predictions of other workers.[13,16] The isomeric cross-section ratios for (n,2n) reactions measured presently are used to calculate spin cutoff parameter (see Chap. VI).

B) (n,p) and (n,α) Reaction Cross-sections.-

The values of (n,p) cross-sections measured presently are given in table VIII. Column (1), (2) and (3) give target

TABLE - VIII ; (n,p) and (n, α) Cross-sections at 14.8 MeV

(1) Reaction	(2) Product Nuc.	(3) halflife of product	σ_{Exp} (mb.) (4) Present	(5) Others	(6) σ (mb.) predicted
^{41}K (n,p)	^{41}A	1.83 hrs.	165 ± 40	81 ± 32 [2] 52 ± 4 [39]	113.9 Ref.5)
^{117}Sn(n,p)	^{117m}In	1.9 hrs.	14 ± 2	3.7± 0.5 [40] 5.1+ 1.6 [36]	
	^{117g}In	45 min.	16.5± 2	5.9± 0.4 [40] 10.7 ± 2.6 [36]	
^{128}Te(n,p)	^{128m}Sb	10 min.	$(\sigma_m + \sigma_g)$=30.5±3 24±4	1.0 ± 0.1 [18] 65 ± 19 [17]	24.3 Ref.5)
^{130}Te(n,p)	^{130m}Sb	7 min.	⩾ 44		
^{92}Mo(n, α)	^{89m}Zr	4.3 min.	2.48 + 0.3		
^{115}In (n, α)	^{112}Ag	3.2 hrs.	17.4 ± 2		

nuclei, product nuclei, and halflives of the reaction products respectively. In column (4) are given (n,p) cross-section values measured presently. For comparison earlier reported values of (n,p) cross-sections are also given in column (5). Generally agreement between present values and earlier reported values is poor. In case of ^{128}Te (n,p) ^{128m}Sb reaction our cross-section value is in between the two values reported by the earlier workers.[17,18] No literature value for $^{130}Te(n,p)$ ^{130}Sb reaction cross-section is available. Most probably this cross-section is not reported yet. Cross-section for $^{41}K(n,p)$ ^{41}A and $^{117}Sn(n,p)$ $^{117m,g}In$ reactions are compared with the Gardners[5] prediction based on statistical model. The agreement between experimental and predicted values is within 80%. Valuesof (n,α) reaction cross-sections measured presently are also given in table VIII.

C) Unknown Activity-

While following the β -activity of the irradiated ^{128}Te sample, a two min. activity was observed. Even after a thorough study this activity could not be assigned to any possible reaction. From the counting rate a lower limit of 60 mb. can be put for the cross-section of the reaction responsible for this activity. Majumdar and Chatterjee[34] also observed this 2 min activity in their measurements and suspected it to be due to $^{130}Te(n,\alpha)$ reaction. However, in

our measurement no activity with 2 min. halflife was observed, when β -rays from irradiated ^{130}Te isotopes were counted. Hence this activity could not be assigned to ^{130}Te (n, α) reaction.

R E F E R E N C E S :

1. E.O. Salant and N.F. Ramsey, Phys.Rev. 57 (1940) 1047
2. E.B. Paul and R.L. Clark, Can. J.Phys. 31 (1953) 267
3. D.G. Gardner, Nucl. Phys. 29 (1962) 373
4. D.G. Gardner and Y.W. Yu, Nucl. Phys. 60 (1964) 49
5. D.G. Gardner and S. Rosenblum, Nucl.Phys. A96 (1967) 121
6. V.N. Levkovskii, JETP (USSR) 33 (1957) 1520
7. A. Chatterjee, Nucl. Phys. 47 (1963) 511
8. A. Chatterjee, Nucl. Phys. 60 (1964) 273
9. A. Chatterjee, Nucl. Phys. 49 (1963) 686
10. P. Hill, Nucl. Phys. A107 (1968) 49
11. S. Pearlstein, Nucl. Data A3 (1967) 327
12. J.M. Blatt and V.F. Weisskopf, Theoretical Nuclear Physics, John Wiley & Sons, N.Y.
13. E. Kondaiah et al., Nucl. Phys. 120 (1968) 337
14. E. Husain, Nucl.Chem.Symp., American Chemical Society, South West Regional Meeting, Little Rock, Arkanass (Dec. 1967)
15. S.G. Forbes, Phys. Rev. 88 (1952) 1309
16. P. Cuzzocrea et al., Nucl. Phys. A103 (1967) 616
17. J. Brozosko et al, Nucl. Phys. 45 (1963) 579
18. L. Husain and P. Kuroda, Nucl. Phys. A 114 (1968) 663
19. J.L. Perkin and L.P.O. Conner, Proc.Phys.Soc.72(1958) 505

20. R.G. Wille and R.W. Fink, Phys. Rev. 118, (1960) 242

21. S.K. Mukherjee et al., Proc.Phys.Soc. 77 (1961) 508

22. I.L. Preiss and R.W. Fink, Nucl. Phys. 15 (1960) 326

23. H.G. Blosser et al., Phys.Rev.100(1955) 429; 110(1958) 531

24. H. Liskien and A. Paulsen, EUR 119e-Vol.1 (1966)

25. Nuclear Data Sheets, Academic Press (1959-65)

26. P.V. Rao and R.W. Fink, Phys. Rev. 154 (1967) 1023

27. B. Minetti and A. Pasquarelli, Nucl.Phys. A100(1967) 186

28. V.V. Ivanenko and K.A. Perlzhak, Yadarnayo Fizika (USSR) 9 (1969) 258

29. C.S. Khurana and S.K. Mangal, Nucl.Phys.69 (1965) 158

30. J. Bacso et al., Acta. Phys. Hung. 18 (1965) 295

31. B. Minetti and A. Pasquarelli, Nucl.Phys. A118 (1968) 449

32. R. Prasad and D.C. Sarkar, Nucl. Phys. A94 (1967) 476

33. M. Cevolani, Nuovo Cim. 26 (1962) 1328

34. N.K. Majumdar and A. Chatterjee, Nucl.Phys. 41 (1963) 192

35. G.C. Bonazzola et al., Nucl. Phys. 51 (1964) 337

36. J. Brozosko et al, Nucl. Phys. 74 (1965) 438

37. H. Rotzer, Nucl. Phys. A109 (1968) 694

38. J. Csikai et al., Atomic Energy Review 8 (1969) 93

39. R. Prasad, Ph.D. Thesis Submitted to AMU., Aligarh (1967)

40. L. Lulic et al., Nucl. Phys. A119 (1968) 517

41. E. Bramlitt and R.W. Fink, Phys. Rev. 131 (1963) 2649

42. D. Crumpton et al., Journ.Inorg.Nucl.Chem.(GB) 31(1969) 1

43. J. Karolyi et al., Nucl. Phys. A122 (1968) 234

44. P. Rama Prasad et al., Nucl.Phys.A125 (1969) 57

45. J.K. Temperly, Phys. Rev., 178 (1969) 1904

46. V.N. Levkovskii et al, Yadrenaya Fizika (USSR) 10 (1969) 44

47. M. Bormann and I. Riehle, Z. Phys. $^{207}_{A}$ (1967) 64

48. H.O. Menlove et al., Phys. Rev. 163 (1967) 1308

49. M. Bormann, Nucl. Phys. 65 (1965) 257

50. J.H.E. MATTAUCH et al., Nucl. Phys. 67 (1965) 1.

****

CHAPTER - VI

"SPIN CUT OFF PARAMETER STUDIES"

6.1 Introduction:

The ratio of the cross-sections leading to the neighbouring isomeric states in a particular isotope can be used to complement the knowledge about the nuclear reactions, since the relative probability of forming each state of an isomeric pair seems to be governed mainly by the spin difference between the state which decays to the isomers and the spins of the isomeric states themselves. In γ-ray de-excitation of the excited nucleus, the multipolarity of the radiations is mainly dipole in character,[9-11] so the relative population of the isomeric states can be a valuable guide to the spins of the states participating in the γ-cascade and the initial states.

Isomeric ratio for neutron capture have been used by some workers[1-3] to decide which isomeric level has a spin close to that of the capturing state. Huizenga and Vandenbosch[4,5] have tried to explain quantitatively the isomeric cross-section ratios using the spin dependence of the nuclear level density.

The important parameter to study, is the spin dependent part of the level density, through the analysis of the isomeric cross-section ratios. The total angular momentum of the nucleus may be thought of as a vector sum of the spin angular momenta and orbital angular momenta of the nucleons. The shell model[6] approach gives a reasonably good prediction of the angular momentum of the ground state as well as of the few low lying

excited states. For higher excitation energies description of individual levels and their spins become impracticable due to overlapping of states etc. At such excitation energies statistical model approach is adopted and then one speaks of angualr momentum distribution of the levels in a certain small energy interval. On the assumption of random coupling of angular momenta of the nucleons within the nucleus, a simpler form of the spin dependent level density was predicted theoretically as:[7,8]

$$\rho(E,J) = \rho(E)\ (2J+1)\ \mathrm{Exp}\left\{-(J+\tfrac{1}{2})^2/2\,\sigma^2_{sp}\right\} \ldots\ldots\ldots (1)$$

where $\rho(E,J)$ denotes the density of levels with angular momentum J at excitation energy E. The quantity $\rho(E)$ depends only on the excitation energy and to a good approximation it is equal to $\rho(E,O)$ i.e. the density of the levels at excitation energy E, with angular momentum J=o. The spin distribution is characterized by the parameter " σ_{sp}", which is termed as spin cutoff parameter. Theoretically σ^2_{sp} is proportional to the product of the moment of inertia of the nucleus and the thermodynamic temperature, and it may depend on the excitation energy.

Presently we have used Huizenga and Vandenbosch[4,5] method for the analysis of isomeric cross-section ratios, to study the energy dependence of " σ_{sp}". Isomeric cross-section ratio for $^{103}Rh(n,\gamma)\ ^{103m,g}Rh$ reaction has been measured at different

neutron energies. The value of " σ_{sp} " at different excitation energies have been calculated so as to study its variation with energy. Isomeric cross-sections measured for (n,2n) reactions at 14.8 MeV have been analysed to give $(\sigma_{sp})_{Exp}$ The value of $(\sigma_{sp})_{rig}$ have been calculated, taking moment of inertia of the nucleus as the one corresponding to a rigid sphere. Comparison of $(\sigma_{sp})_{Exp}$ and $(\sigma_{sp})_{rig}$ give valuable information about the effect of excitation energy on nuclear moment of inertia.

6.2 Measurements:

Isomeric cross-section ratios for $^{103}Rh\ (n,\gamma)\ ^{104m,g}Rh$ reaction at neutron energies 2.0 MeV, 2.6 MeV and 2.8 MeV have been measured using neutrons from endoergic reaction $^{3}_{1}H\ (p,n)\ ^{3}_{2}He$. At 14.8 MeV isomeric cross-section ratio has been measured using neutrons from the exoergic reaction $^{3}_{1}H\ (d,n)\ ^{4}_{2}He$ (details given in chap.IV). For the production of neutrons in the 2-3MeV region, thin tritium target was bombarded with accelerated proton beam, obtained from the Van-de-Graaff accelerator, B.A.R.C., Trombay, India. Neutrons were monitored using ZnS detector coupled optically to a 6342-A photo-multiplier tube.

Sample of elemental Rhodium sponge (99.99% pure, obtained from M/S Johnson Mathey and Co. Ltd., London) were irradiated in zero degree forward direction relative to the proton beam. Since we were interested exclusively in the isomeric cross-section ratios, calibration of the neutron flux was not necessary for

the present measurements. As can be seen from the decay scheme[12] in Fig.20, isomeric state of ^{104}Rh decays to its ground state through ~ 100% isomeric transition. Halflife of the isomeric state (4.4 min.) is longer than that of the ground state (42 sec.). Hence it was possible to determine isomeric cross-section ratio by counting β-activity corresponding to the ground state decay.

Ground state β-activity of ^{104}Rh was measured using plastic scintillator in conjunction with a 6342A photomultiplier tube and a four hundred channel analyzer in the multiscaler mode. Due to large area of the plastic scintillator, background counts in present measurements were large and consequently increased statistical counting error. The decay curves of irradiated Rhodium obtained at incident neutron energies 2.0 MeV, 2.6 MeV and 2.8 MeV, are shown in Fig. 32 to 34. At energies 2.6 and 2.8 MeV a 16 sec. activity is also obtained which corresponds to the ^{103}Rh (n,α) ^{100}Tc reaction product. The expression used for the determination of isomeric cross-section ratio is given below:[14]

$$\sigma_g/\sigma_m = \frac{A_g \lambda_g (1-e^{-\lambda_m t_e}) + A_m \lambda_m (1-e^{-\lambda_g t_e})}{A_m (\lambda_g - \lambda_m)(1-e^{-\lambda_g t_e})} \quad \ldots\ldots\ldots \quad (2)$$

Where the various symbols have the same meanings as described in chap. II, sec.3. Details of individual measurements at different energies are given below:

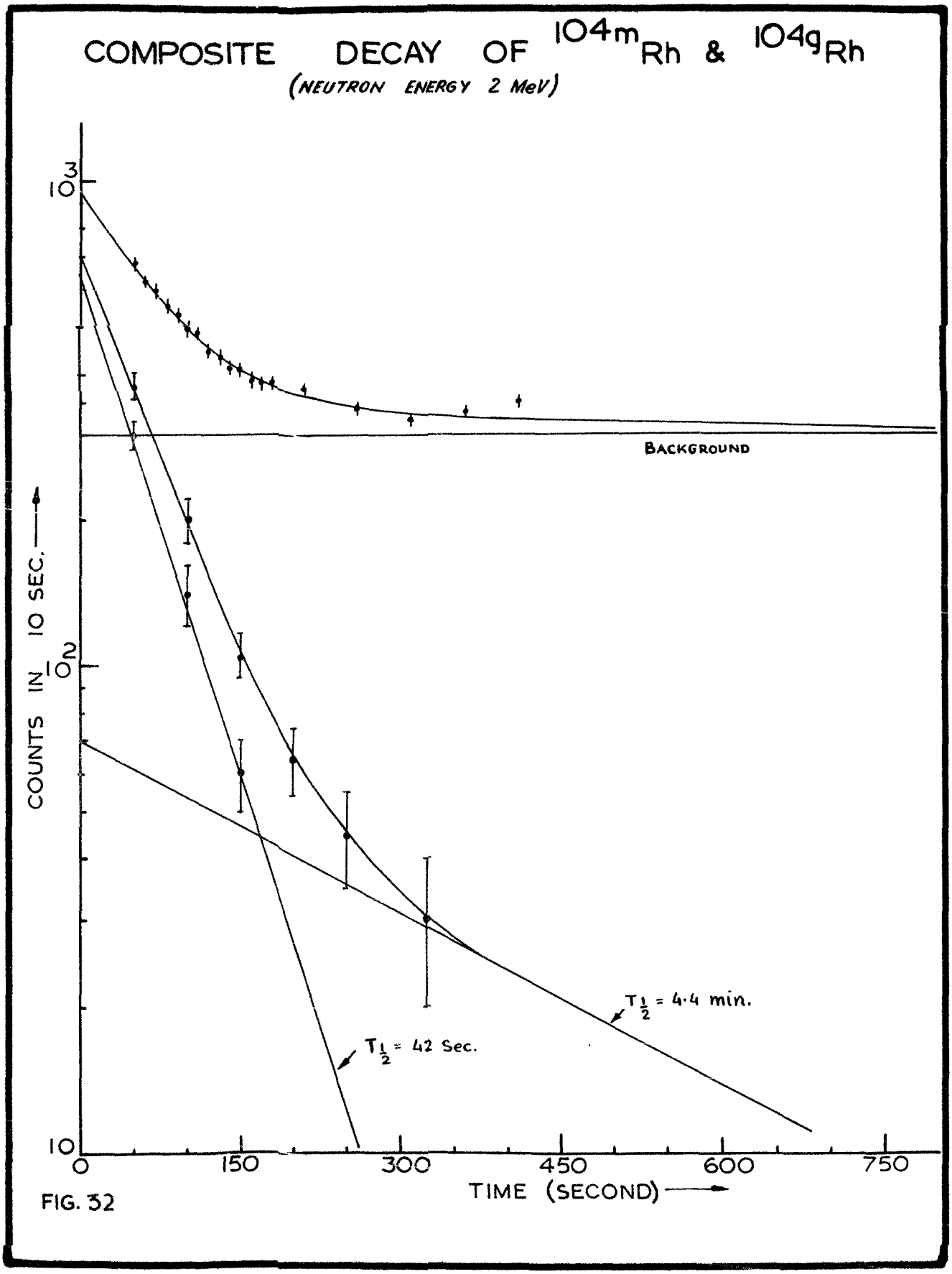
COMPOSITE DECAY OF 104m Rh & 104g Rh
(NEUTRON ENERGY 2 MeV)
BACKGROUND
COUNTS IN 10 SEC.
10³
10²
10
0
150
300
450
600
750
TIME (SECOND)
T½ = 4·4 min.
T½ = 42 Sec.

FIG. 32

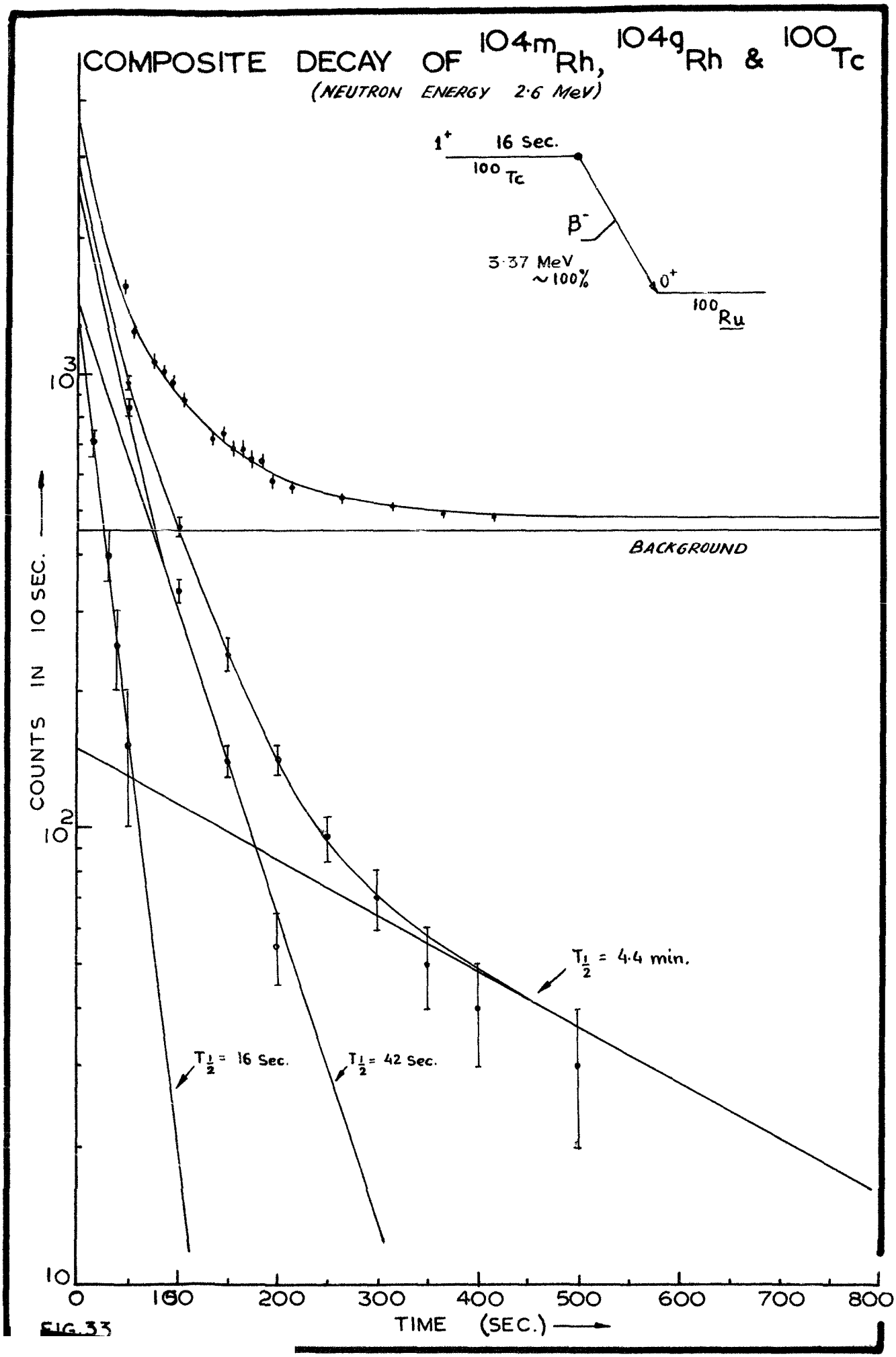
COMPOSITE DECAY OF 104m Rh, 104g Rh & 100 Tc
(NEUTRON ENERGY 2·6 MeV)
1+ 16 Sec.
100 Tc
β-
3·37 MeV
~100%
0+
100 Ru
BACKGROUND
COUNTS IN 10 SEC.
10³
10²
10
T½ = 4·4 min.
T½ = 16 Sec.
T½ = 42 Sec.
0
100
200
300
400
500
600
700
800
TIME (SEC.)

FIG. 33

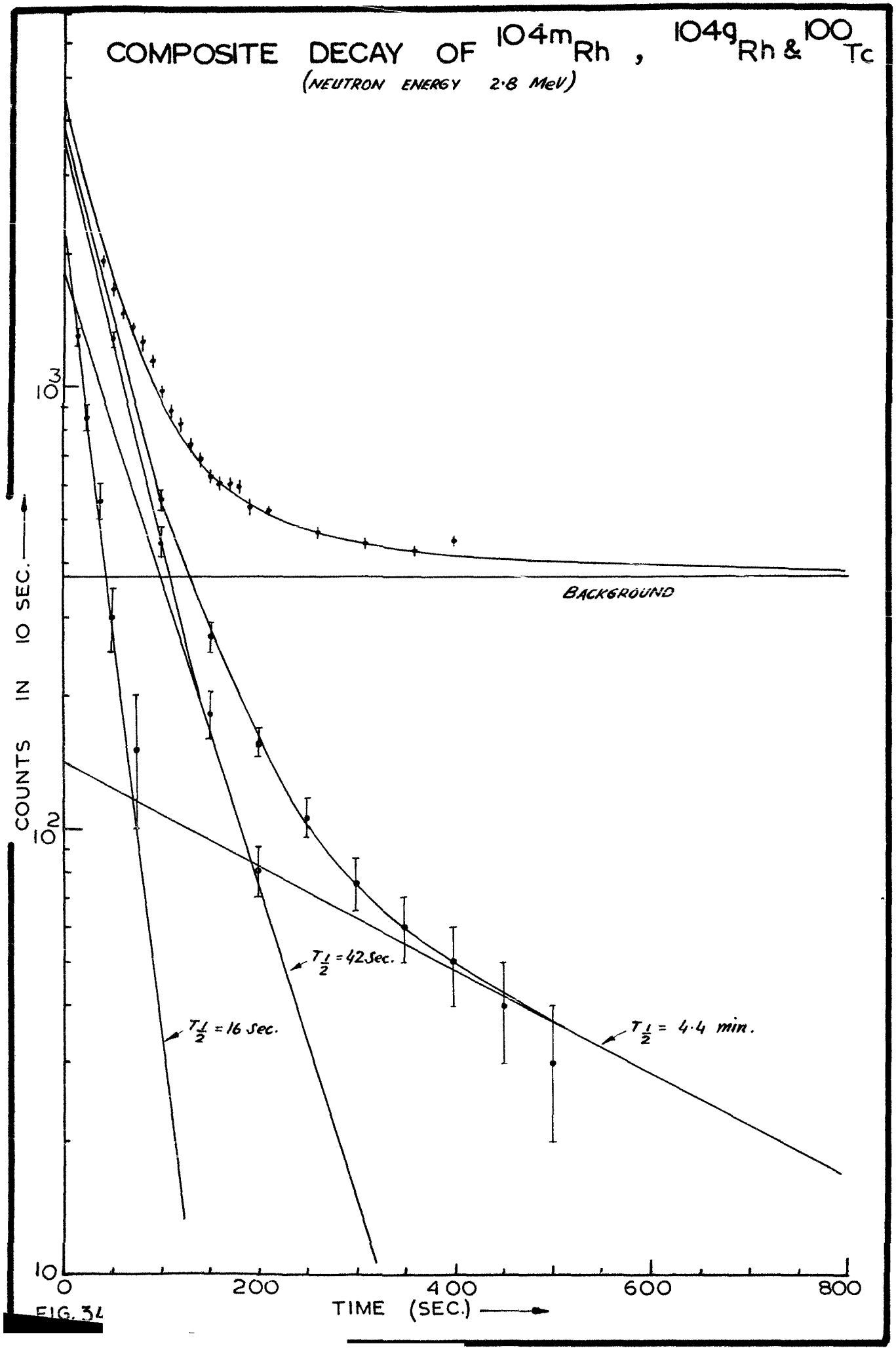
COMPOSITE DECAY OF 104m Rh , 104g Rh & 100 Tc
(NEUTRON ENERGY 2·8 MeV)
BACKGROUND
$T_{\frac{1}{2}}$ = 16 Sec.
$T_{\frac{1}{2}}$ = 42 Sec.
$T_{\frac{1}{2}}$ = 4·4 min.
COUNTS IN 10 SEC.
10³
10²
10
0
200
400
600
800
TIME (SEC.)

FIG. 31

Neutron Energy - 2 MeV

$te = 10$ min.

$(1-e^{-\lambda_g te}) = 1.000$

$(1-e^{-\lambda_m te}) = 0.793$

$\lambda_g - \lambda_m = 0.832$

$Ag = 640 \pm 40$

$Am = 70 \pm 30$

$\sigma_g/\sigma_m = 8.5\ (1 \pm .42)$

$= 8.5 \pm 3.6$

Neutron Energy - 2.6 MeV

$te = 10$ min.

$Ag = 1400 \pm 60$

$Am = 150 \pm 40$

$\sigma_g/\sigma_m = 9\ (1 \pm .375)$

$= 9 \pm 3.5$

and

$\sigma_{n,\gamma}/\sigma_{n,\alpha} \approx 1.5 \pm .4$

Neutron Energy - 2.8 MeV

$te = 6$ min.

$(1-e^{-\lambda_g te}) = 1$

$(1-e^{-\lambda_m te}) = 0.610$

$Ag = 1800 \pm 60$

$Am = 140 \pm 40$

$\sigma_g/\sigma_m = 9.5 \pm 3.0$

and $\sigma_{n,\gamma}/\sigma_{n,\alpha} \approx 0.92 \pm 0.26$

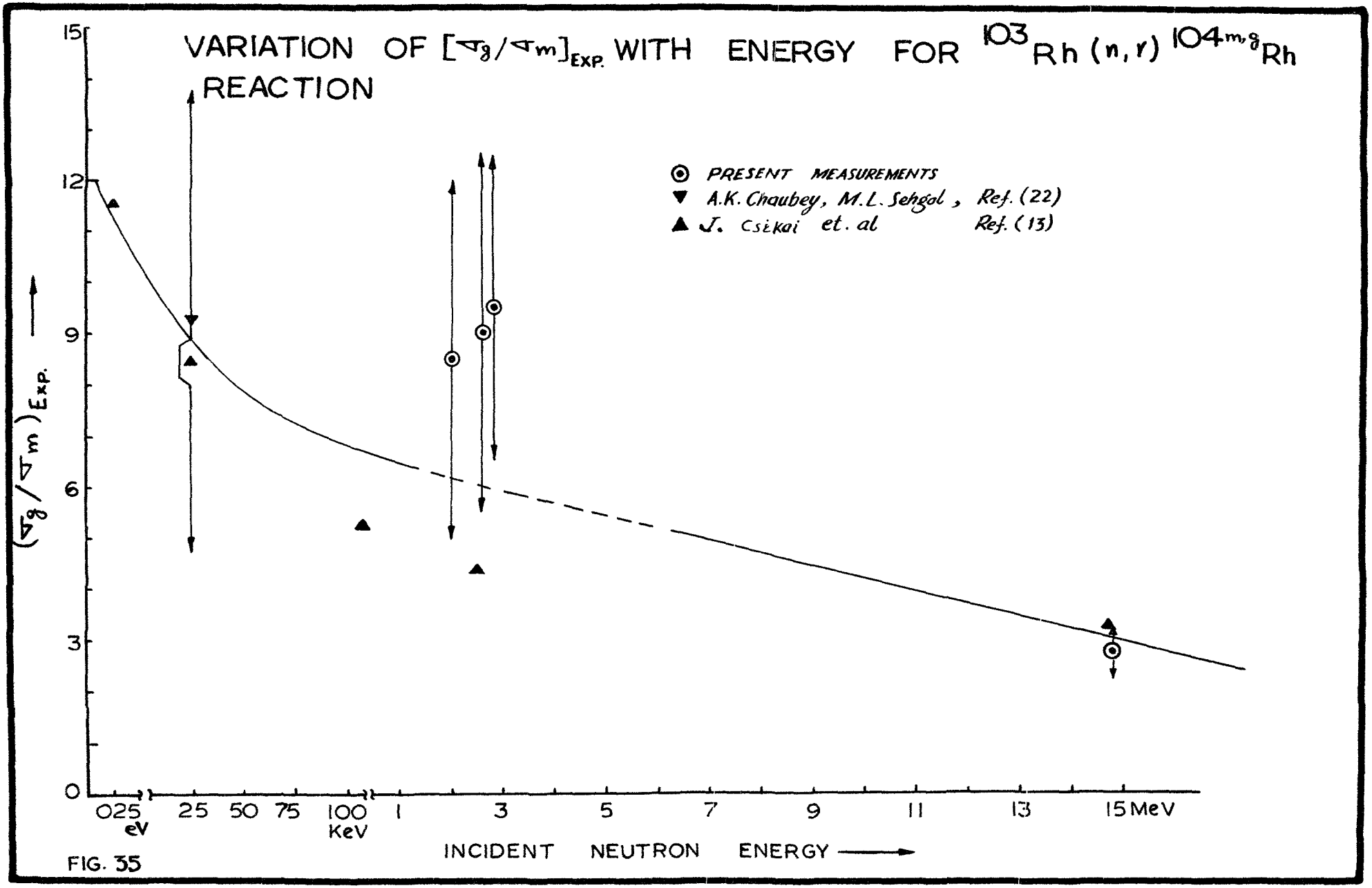
VARIATION OF $[\sigma_g/\sigma_m]_{EXP.}$ WITH ENERGY FOR $^{103}Rh(n,\gamma)^{104m,g}Rh$ REACTION
PRESENT MEASUREMENTS
A.K. Chaubey, M.L. Sehgal, Ref. (22)
J. Csikai et. al Ref. (13)
$(\sigma_g/\sigma_m)_{EXP.}$
15
12
9
6
3
0
025 eV
25
50
75
100 KeV
1
3
5
7
9
11
13
15 MeV
INCIDENT NEUTRON ENERGY

FIG. 35

The results of isomeric cross-section ratios for ^{103}Rh (n,γ) $^{104m,g}Rh$ reaction are tabulated in table IX. A graph is plotted between isomeric cross-section ratio $(\sigma_g / \sigma_m)_{Exp}$ against incident neutron energy for ^{103}Rh (n,γ) $^{104m,g}Rh$ reaction and is shown in Fig.35. From the graph it appears that our values of the ratio $(\sigma_g/\sigma_m)_{Exp}$ are larger than those reported by Csikai et al[13]. Since Csikai et al. have not mentioned the various errors involved in their measurements, it is possible that within the limits of the errors our values may be overlapping with their values. As is clear from the figure, in general the ratio $(\sigma_g/\sigma_m)_{Exp}$ decreases with energy.

The results of (n,2n) isomeric cross-section ratios are tabulated in table X. The details of measurement etc. for (n,2n) isomeric cross-sections are given in chap. V.

6.3 Details of Analysis:

The various factors upon which isomeric cross-section ratio depends are:

1) the spin of the compound nuclear state.
2) the number and the type of steps in the de-excitation of the compound state
3) the angular momenta carried away at each step
4) the probability of forming states of different spin during each step of cascade
5) the spins of the isomeric states.

TABLE - IX ; Isomeric Cross-section Ratios At Different Neutron Energies For (n,γ) Reaction & Corresponding $(\alpha_{sp})_{Exp}$

Incident Neutron Energy (MeV)	Target Nucleus Spin	Products Nucleus	Spin of the Isomers	σ_g/σ_m Experimental		Theoretical value of $\bar{\nu}$	$(\alpha_{sp})_{Exp}$
				Present	Others		
2.0	½	$104m_{Rh}$	5	8.5 ± 3.6		~6	$2.25^{+.35}_{-.20}$
		$104g_{Rh}$	1				
2.6	"	"	"	9.0 ± 3.5		~6	$2.15^{+.3}_{-.15}$
2.8	"	"	"	9.5 ± 3.0		~6	$2.125^{+.225}_{-.125}$
14.8	"	"	"	2.75 ± 0.5	3.28 [13]	~8	$2.20^{+.10}_{-.10}$

The distribution of the angular momenta in the compound nucleus formed by the capture of incident neutron of energy E_n, is given by the equation[15)]

$$P(J_c, E) \propto (2J_c+1) \sum_{S=|J-s|}^{J+s} \sum_{\ell=|J_c-S|}^{J_c+S} T_\ell (E_n) \quad \ldots\ldots \quad (3)$$

Where $P(J_c, E)$ is the relative probability of the formation of the compound state with angular momentum J_c; J and s are the spins of the target nucleus and the incident particle respectively (for neutrons spin $s = \frac{1}{2}$). $T_\ell (E)$ are the transmission coefficients at the neutron bombarding energy E_n. In the second stage of the nuclear reaction, compound nucleus de-excites through one of the various possible modes.

In the case of (n, γ) reaction, de-excitation takes place only through γ-rays cascade. The γ-rays cascade is believed to consist of mostly dipole radiations.[9-11)] So the redistribution of angular momenta after each step of γ-cascade is determined by the probability $P_{J_c \rightarrow J_c + 1}$, of going from a state of spin J_c to a state of spin $J_c + 1$. The probability $P_{J_c \rightarrow J_c + 1}$, is given by

$$P_{J_c \rightarrow J_c + 1} = \frac{\rho(J_c + 1)}{\rho(J_c + 1) + \rho(J_c) + \rho(J_c - 1)}$$

similarly

$$P_{J_c \rightarrow J_c} = \frac{\rho(J_c)}{\rho(J_c + 1) + \rho(J_c) + \rho(J_c - 1)} \quad \ldots\ldots \quad (4)$$

and

$$P_{J_c \rightarrow J_c - 1} = \frac{\rho(J_c - 1)}{\rho(J_c + 1) + \rho(J_c) + \rho(J_c - 1)}$$

Where $\rho(J)$ denotes spin dependent part of the density and to a good approximation may be expressed by [7,8]

$$\rho(J) \propto (2J+1)\ \mathrm{Exp}\left\{-(J+\tfrac{1}{2})^2/2\,\sigma^2_{sp}\right\} \qquad \ldots\ldots\ldots \quad (5)$$

It is assumed that with the emission of last γ-ray., only two states, namely the ground state and the metastable state are populated. Last γ-ray populates either the high spin state or low spin state, depending on which transition has a small spin change.

The multiplicity of the γ-rays (the average number of γ-rays emitted by a nucleus of excitation energy E_o) may be given as [16]

$$\bar{\nu} = \tfrac{1}{2}\sqrt{aE_o} \qquad \ldots\ldots\ldots \quad (6)$$

In the (n,2n) reactions the decay of the compound nucleus takes place in three steps. In the first two stages emission of two neutrons take place one after another, and then the final nucleus de-excites emitting dipole γ-radiations. With the emission of the first neutron an intermediate compound nucleus c' is formed. The redistribution of the spins in the compound nucleus "c'" may be obtained using the expression

$$P(J_c \rightarrow J_{c'},\ E) \propto \rho(J_{c'}) \sum_{S=|J_{c'}-\frac{1}{2}|}^{J_{c'}+\frac{1}{2}} \sum_{\ell=|J_c-S|}^{J_c+S} T_\ell\,(E_{n1}) \quad \ldots\ (7)$$

Where $P(J_c \rightarrow J_{c'}, E)$ is the relative probability of the transition from a state with angular momentum J_c in the compound nucleus "c" to a state with angular momentum $J_{c'}$ in intermediate compound nucleus c'. E_{n1} denotes the energy of the emitted neutrons and can be replaced by the energy corresponding to the maximum energy of the evaporation spectrum. To a good approximation this value can be taken as $2T_1$, where T_1 is the nuclear temperature of compound nucleus c' and is correlated with the excitation energy $E_{c'}$ by the relation

$$aT_1^2 = E_{c'}$$

$$= E_c - S_c - \delta_{c'} - 2T_1$$

or

$$aT_1^2 = E_n - \delta_{c'} - 2T_1 \quad \ldots\ (8)$$

where 'a' is the level density parameter and is taken to be (1/8)A. S_c is the binding energy of the last neutron in the compound nucleus C and $\delta_{c'}$ is the pairing energy of the nucleus C'. Last neutron binding energies and pairing energies were taken from ref. 17 & 18).

From equation (8) one gets

$$T_1 = \frac{1}{a}\left\{1 + \sqrt{1+a(E_n-\delta_{c'})}\right\} \quad \ldots\ (9)$$

Similarly the emission of second neutron from the compound nucleus C' takes place. The energy of the second neutron can be taken as :

$$En_2 = 2T_2$$

and $$aT_2^2 + 2T_2 = E_{c'} - S_{c'} - \delta_f \quad \ldots\ldots\ldots \quad (10)$$

where $S_{c'}$ is the binding energy of the last neutron in compound nucleus c', and δ_f is pairing energy in the final nucleus. The relative probability $P(J_{c'} \longrightarrow J_f, E)$ can be calculated in an analogous way as described in formula (7).

The relative probability of formation of a final nucleus with spin J_f is given by

$$P_{J_f} \propto \sum_{J_{c'}} \sum_{J_c} P(J_c, E)\ P(J_c \rightarrow J_{c'}, E)\ P(J_{c'} \rightarrow J_f, E) \quad \ldots\ldots (11)$$

The final nucleus decays by the emission of dipole γ-rays. The multiplicity of γ-rays and the redistribution of spins after each step of cascade can be calculated in a similar way as described in the case of (n, γ) reaction.

Theoretically σ_{sp}^2 can be related to the moment of inertia I, by the equation[19]

$$\sigma_{sp}^2 = (I/\hbar^2)T \quad \ldots\ldots\ldots \quad (12)$$

DEPENDENCE OF $[\sigma_g/\sigma_m]$ ON "a_{sp}" AND ν; $^{103}Rh(n,\gamma)^{104m,g}Rh$ REACTION

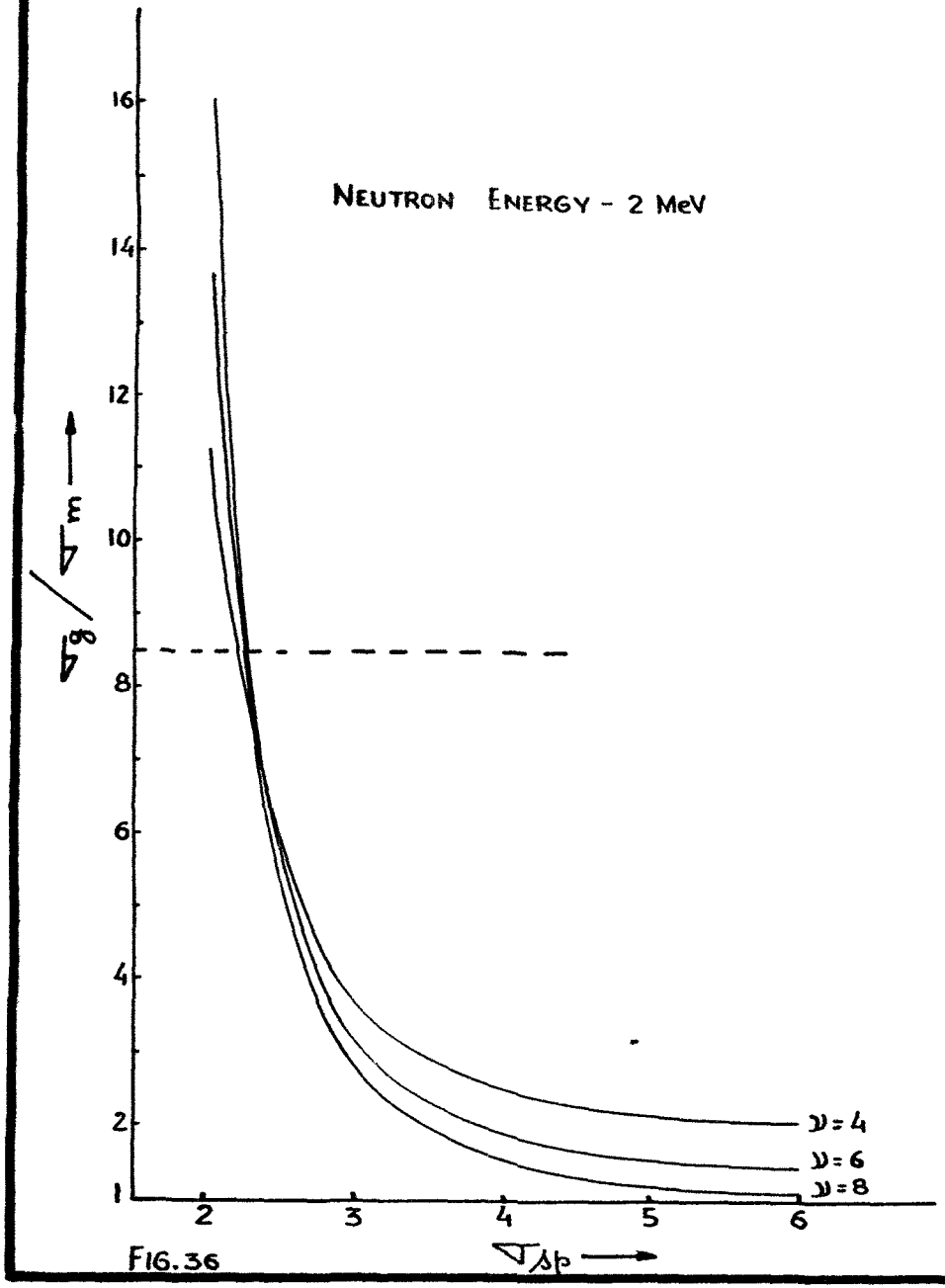

FIG. 36

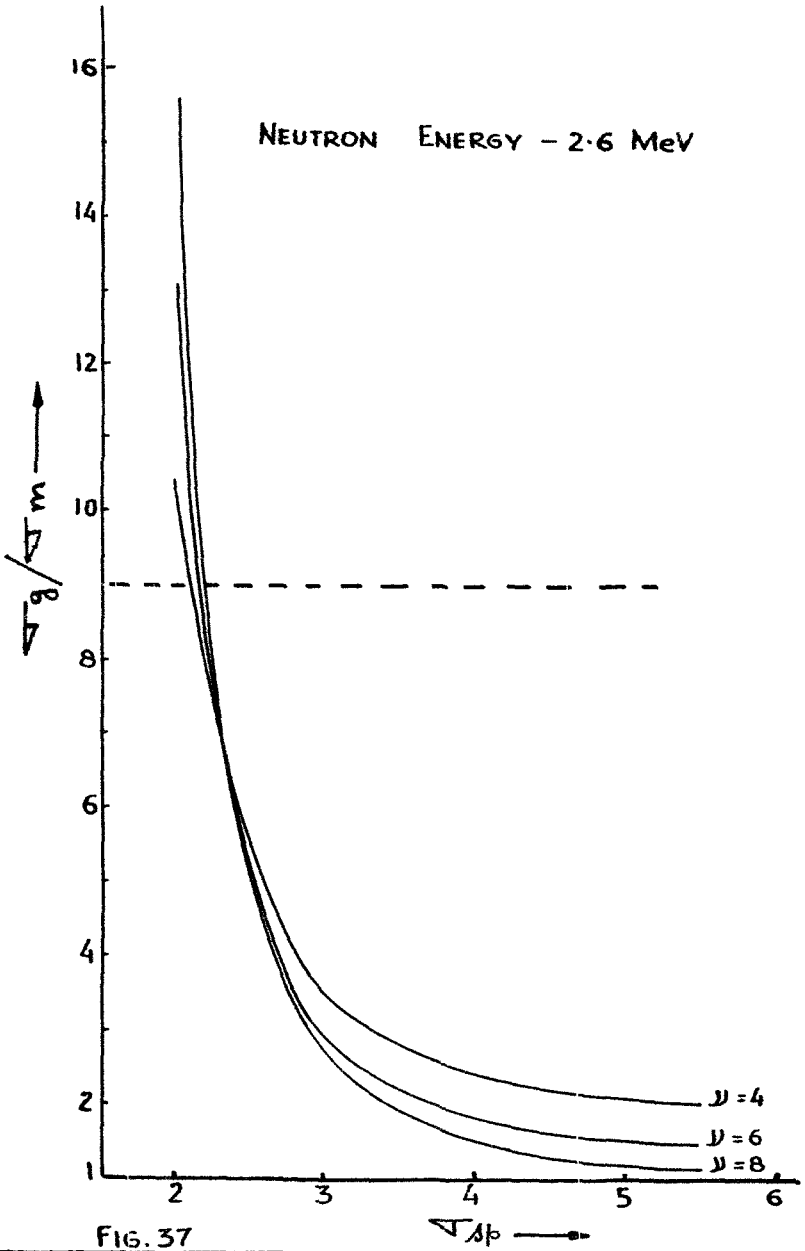

FIG. 37

DEPENDENCE OF (σ_g/σ_m) ON "α_{sp}" AND ν; $^{103}Rh(n,\gamma)^{104m,g}Rh$ REACTION

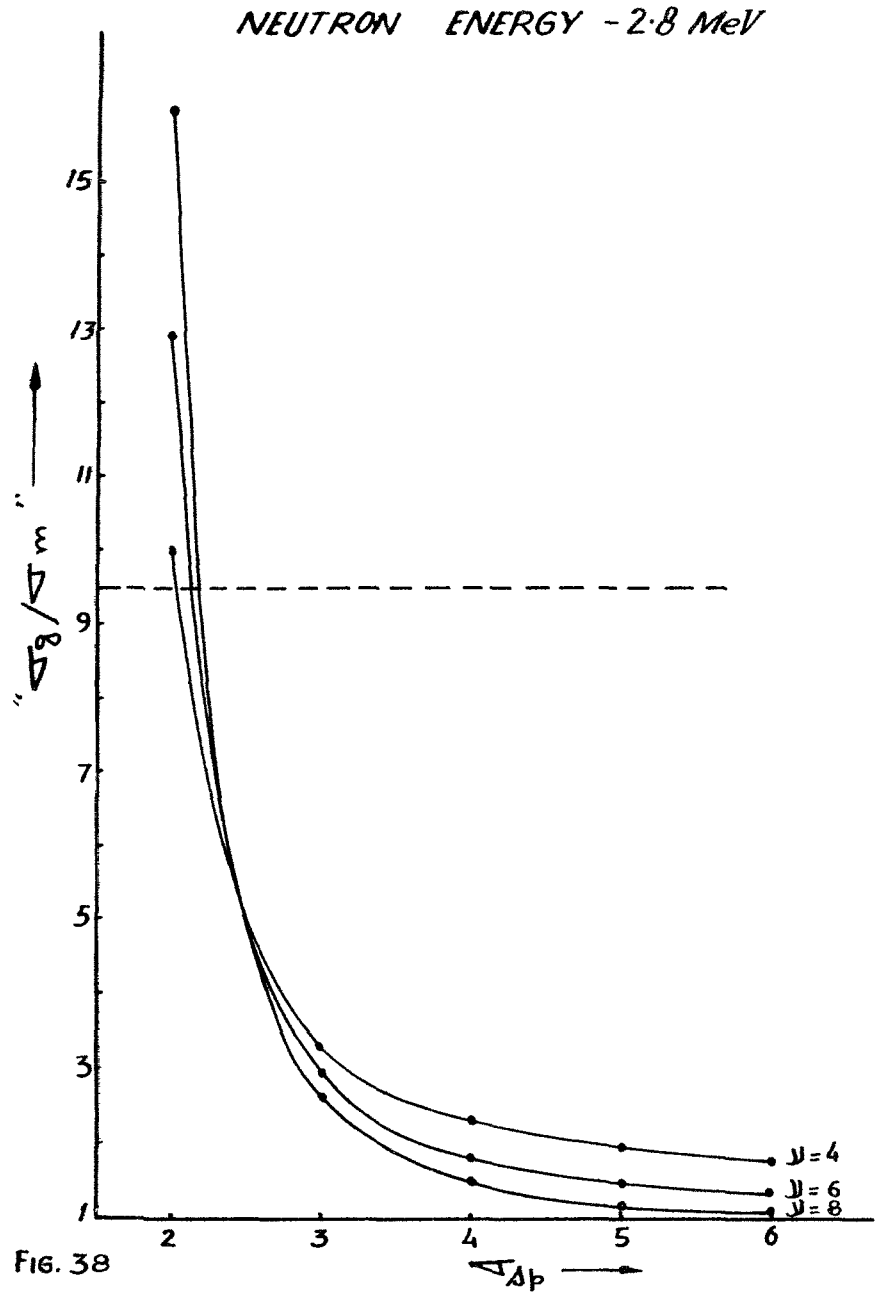

FIG. 38

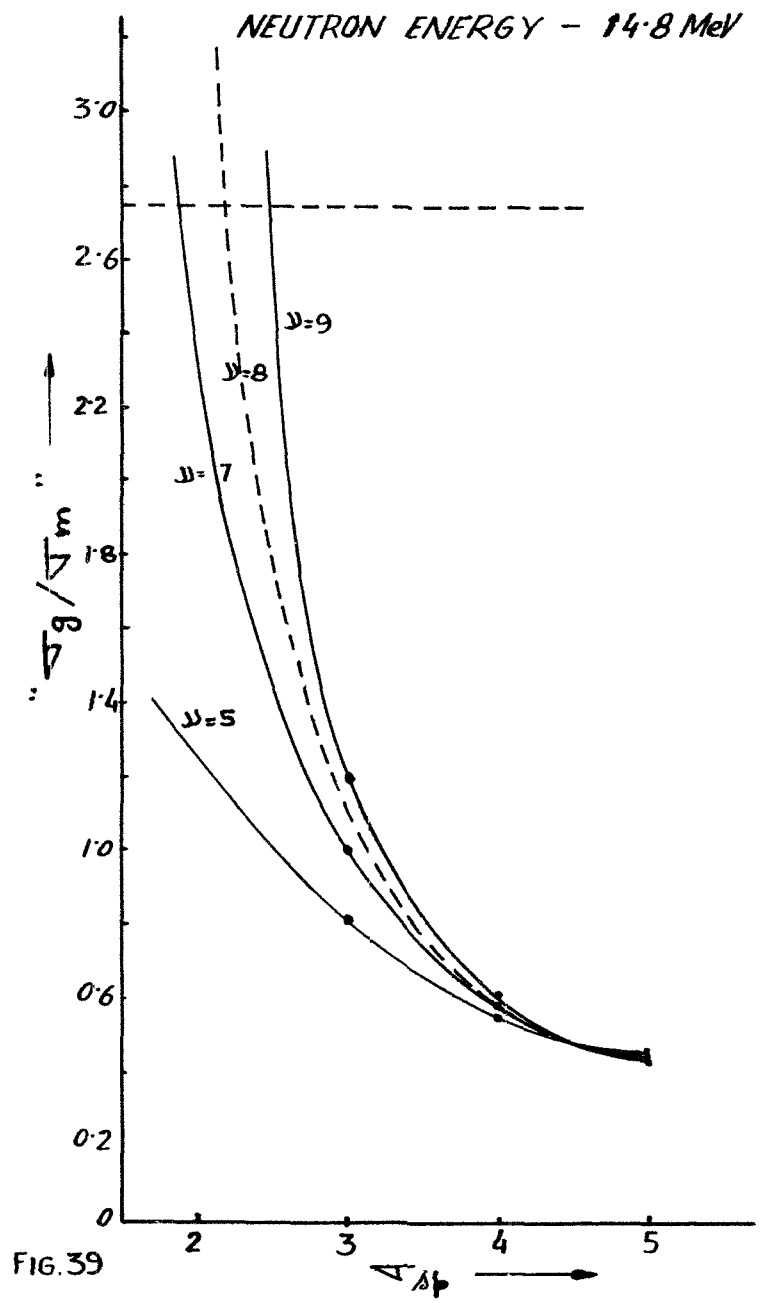

FIG. 39

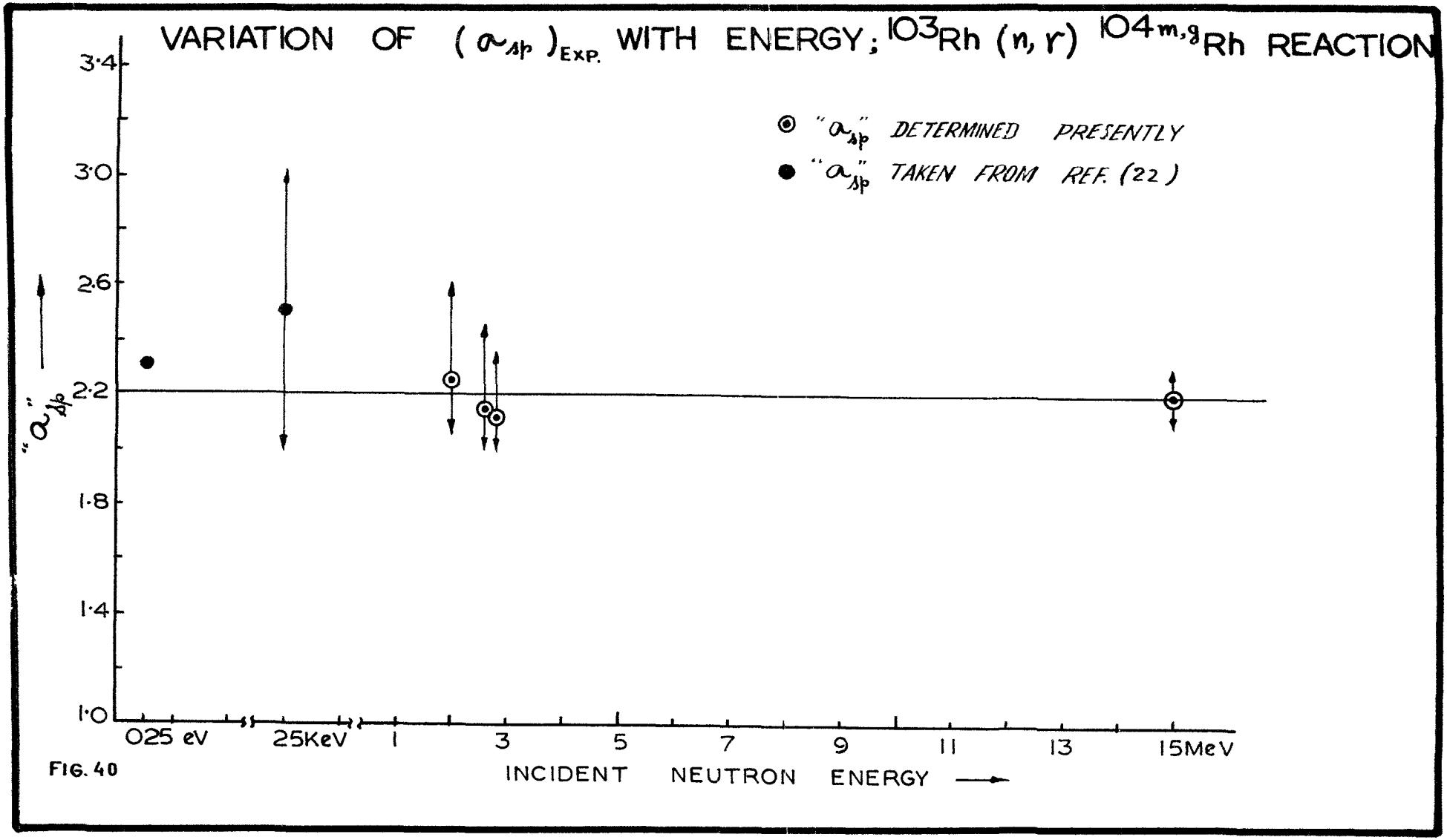
VARIATION OF $(\alpha_{sp})_{EXP.}$ WITH ENERGY; $^{103}Rh\ (n,\gamma)\ ^{104m,g}Rh$ REACTION
"α_{sp}" DETERMINED PRESENTLY
"α_{sp}" TAKEN FROM REF. (22)
"α_{sp}"
3·4
3·0
2·6
2·2
1·8
1·4
1·0
025 eV
25KeV
1
3
5
7
9
11
13
15MeV
INCIDENT NEUTRON ENERGY

FIG. 40

where T^{**} is the nuclear temperature.

The well known formula for the rigid body moment of inertia is given by

$$I_{rig} = 2/5\ m.A.R.^2 \qquad \ldots\ldots \qquad (13)$$

Where m is the nucleonic mass; A and R correspond to the atomic Wt. and radius of the nucleus. Transmission coefficient for neutrons were taken from Ref.20).

6.4 Results and Discussion:

For (n, γ) reaction values of $\bar{\nu}$ comes out to be~6 for neutron energies 2.0 MeV to 2.8 MeV and~8 for 14.8 MeV neutrons. Isomeric cross-section ratios are calculated for α_{sp}=2,3,4 and 5 and $\bar{\nu}$ =4,6,8 in the 2 MeV region. At 14.8 MeV this cross-section ratio is analysed for α_{sp} = 3,4,5 and $\bar{\nu}$ = 5,7,9. Isomeric cross-section ratios are plotted against α_{sp} for different values of $\bar{\nu}$ and are shown in Fig.36 to 39. Dotted lines show the experimentally measured values. The values of $(\alpha_{sp})_{Exp}$ were obtained by the comparison of theoretical values with the experimental results. In doing so theoretically predicted values of $\bar{\nu}$ were used. These values of $(\alpha_{sp})_{Exp}$ when

---

**Nuclear temperature (T) and thermodynamic temperature (t) are two different quantities and may be given by expressions[19]

$$\frac{1}{t} = \frac{d}{dE} \log N(E) \text{ ——— (a) and } \frac{1}{T} = \frac{d}{dE} \log \rho(E) \text{ ——— (b)}$$

where N(E) is total number of levels with excitation energies less than E. From equation (a) and (b) we get

$$\frac{1}{T} = \left(1 - \frac{dt}{dE}\right) \frac{1}{t}$$

However for appreciable excitation energies where $\rho(E)$ has essentially exponential behaviour the two temperatures are equal

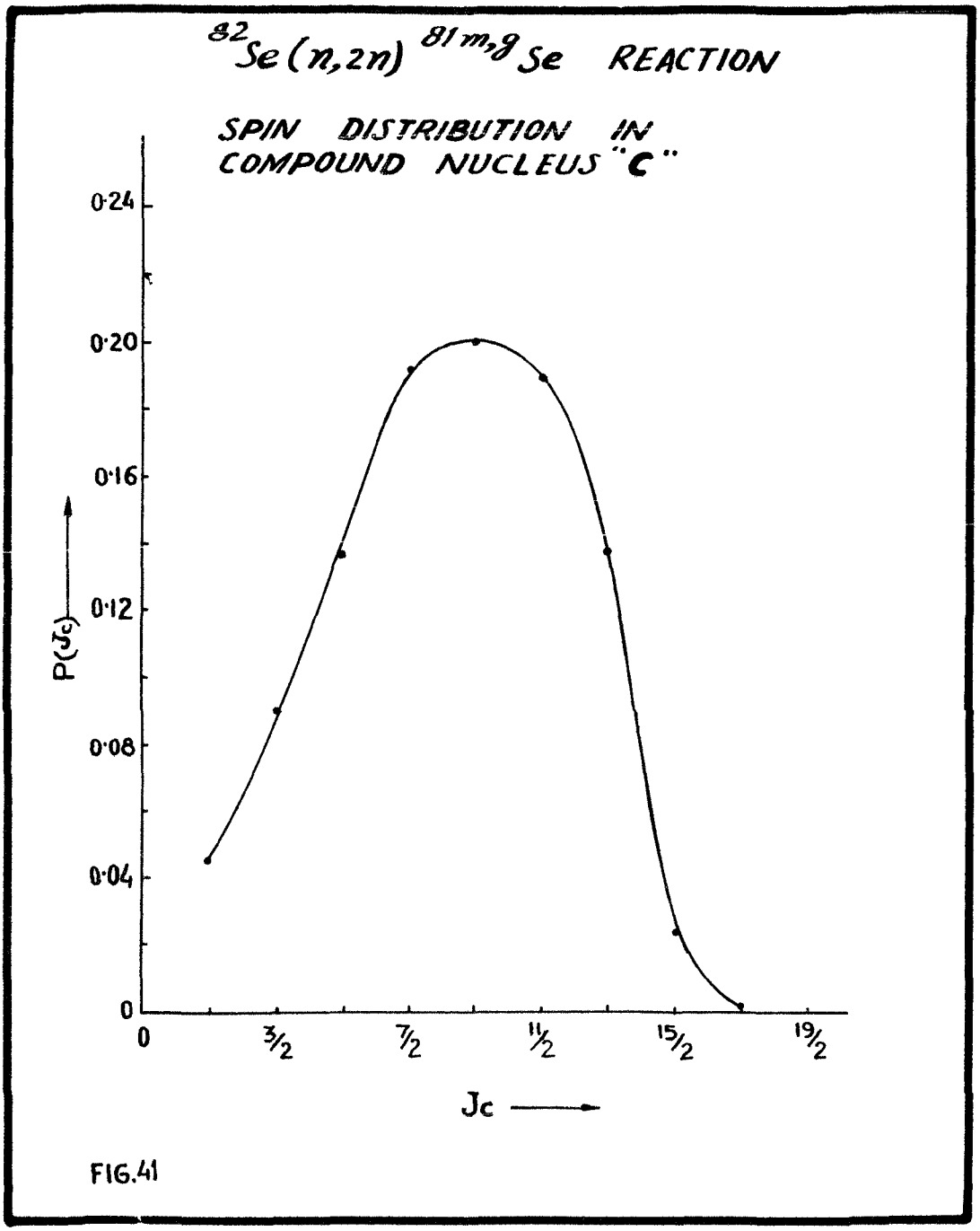
82Se (n,2n) 81m,gSe REACTION
SPIN DISTRIBUTION IN COMPOUND NUCLEUS "C"
0·24
0·20
0·16
0·12
0·08
0·04
0
P(Jc)
0
3/2
7/2
11/2
15/2
19/2
Jc

FIG.41

$^{82}Se(n,2n)^{81m,g}Se$ REACTION

SPIN DISTRIBUTION IN FINAL NUCLEUS "f"

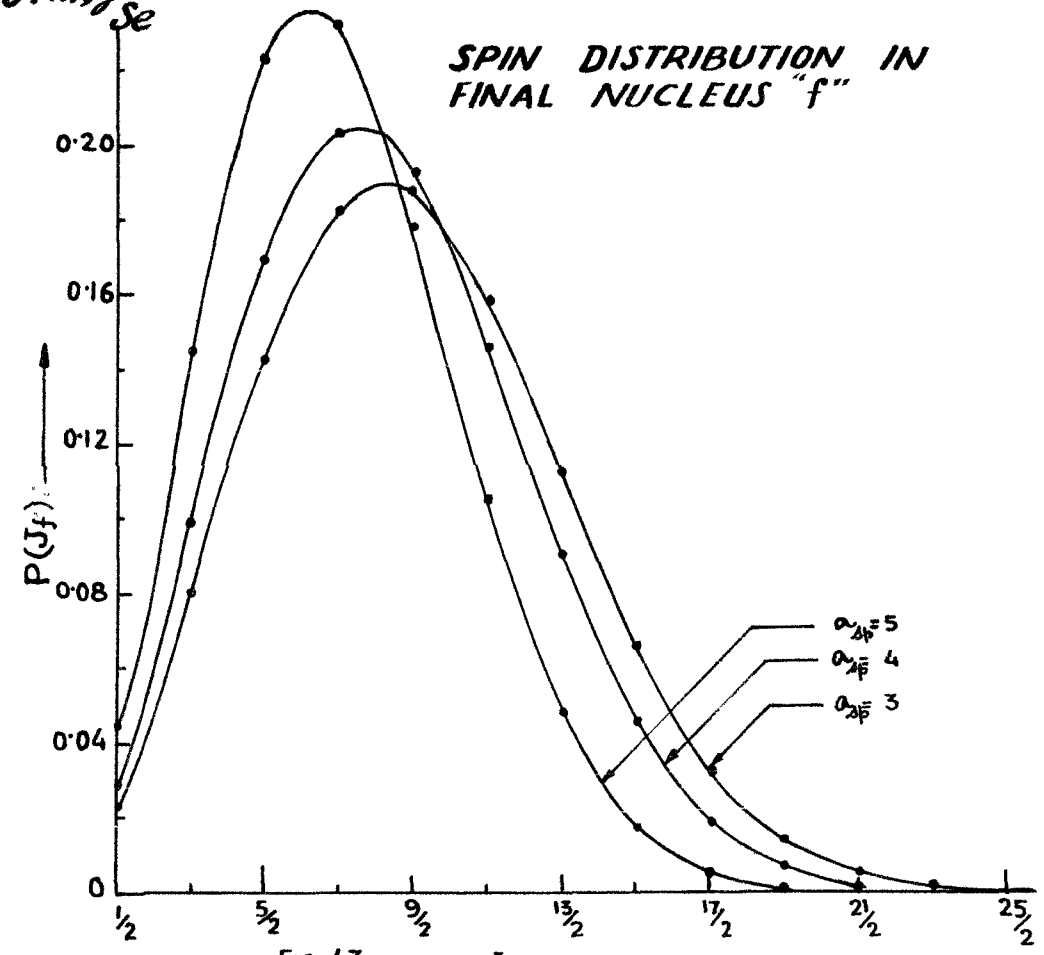

FIG. 43

SPIN DISTRIBUTION IN COMPOUND NUCLEUS "C' "

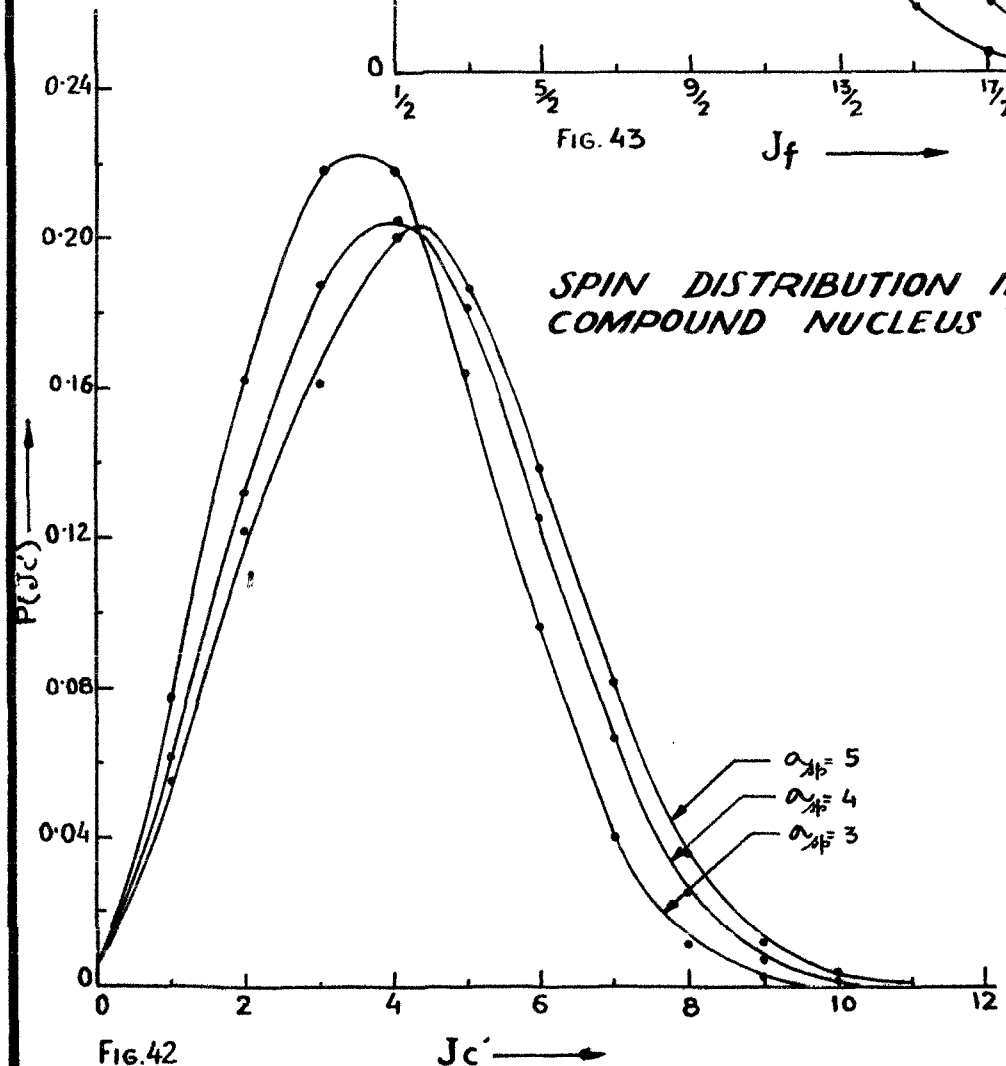

FIG. 42

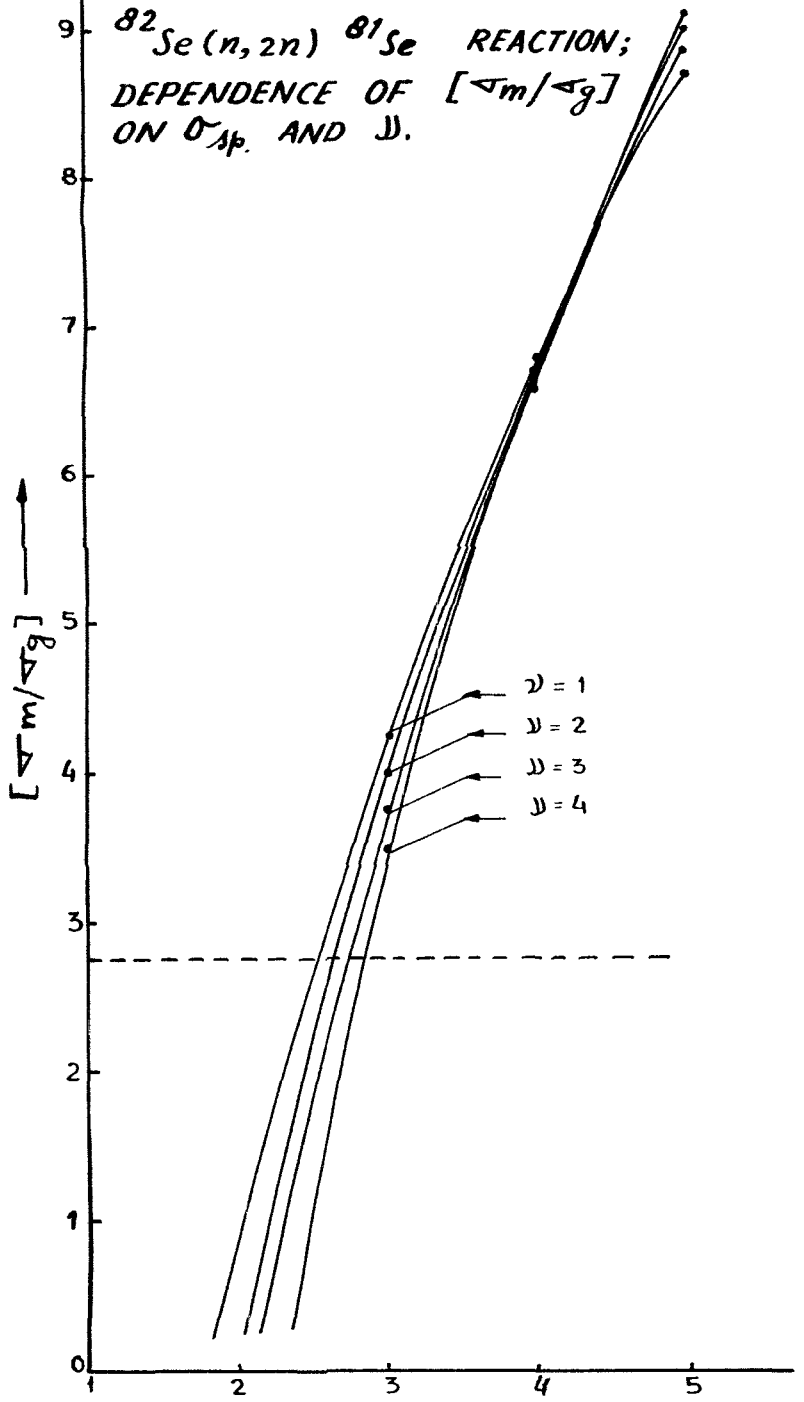
$^{82}Se(n,2n)\ ^{81}Se$ REACTION;
DEPENDENCE OF $[\sigma_m/\sigma_g]$
ON σ_{sp} AND ν.
$[\sigma_m/\sigma_g]$
σ_{sp}
$\nu = 1$
$\nu = 2$
$\nu = 3$
$\nu = 4$

Fig. 44

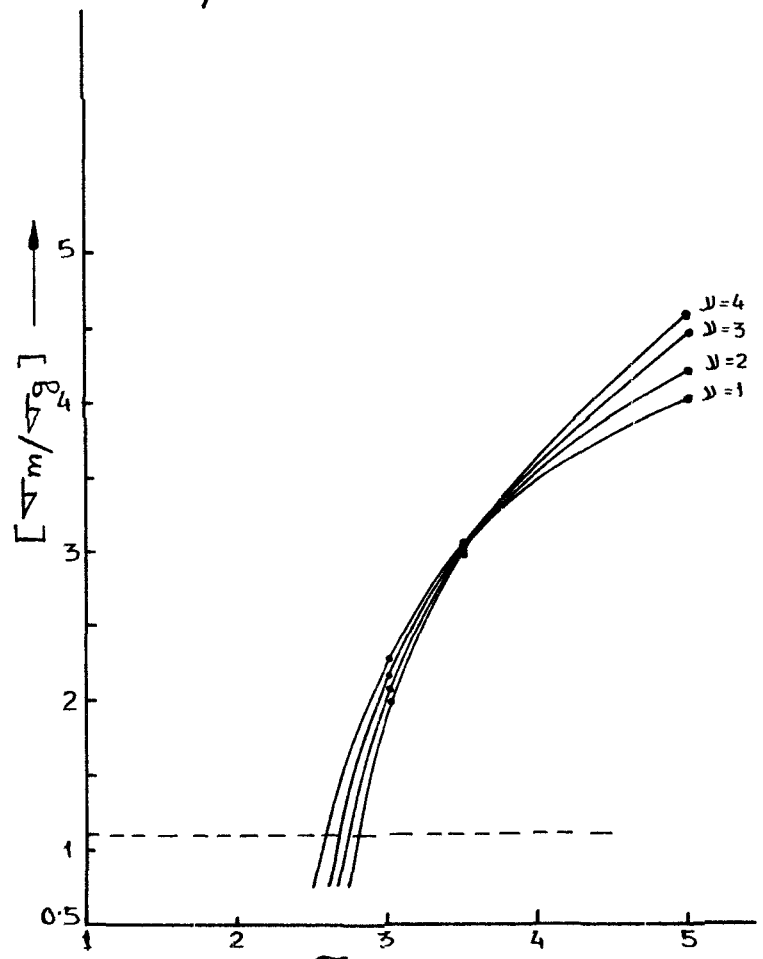
$^{92}Mo(n,2n)\ ^{91m,g}Mo$ REACTION;
DEPENDENCE OF $[\sigma_m/\sigma_g]$ ON
σ_{sp} AND ν
$[\sigma_m/\sigma_g]_4$
σ_{sp}
$\nu=4$
$\nu=3$
$\nu=2$
$\nu=1$

Fig. 45

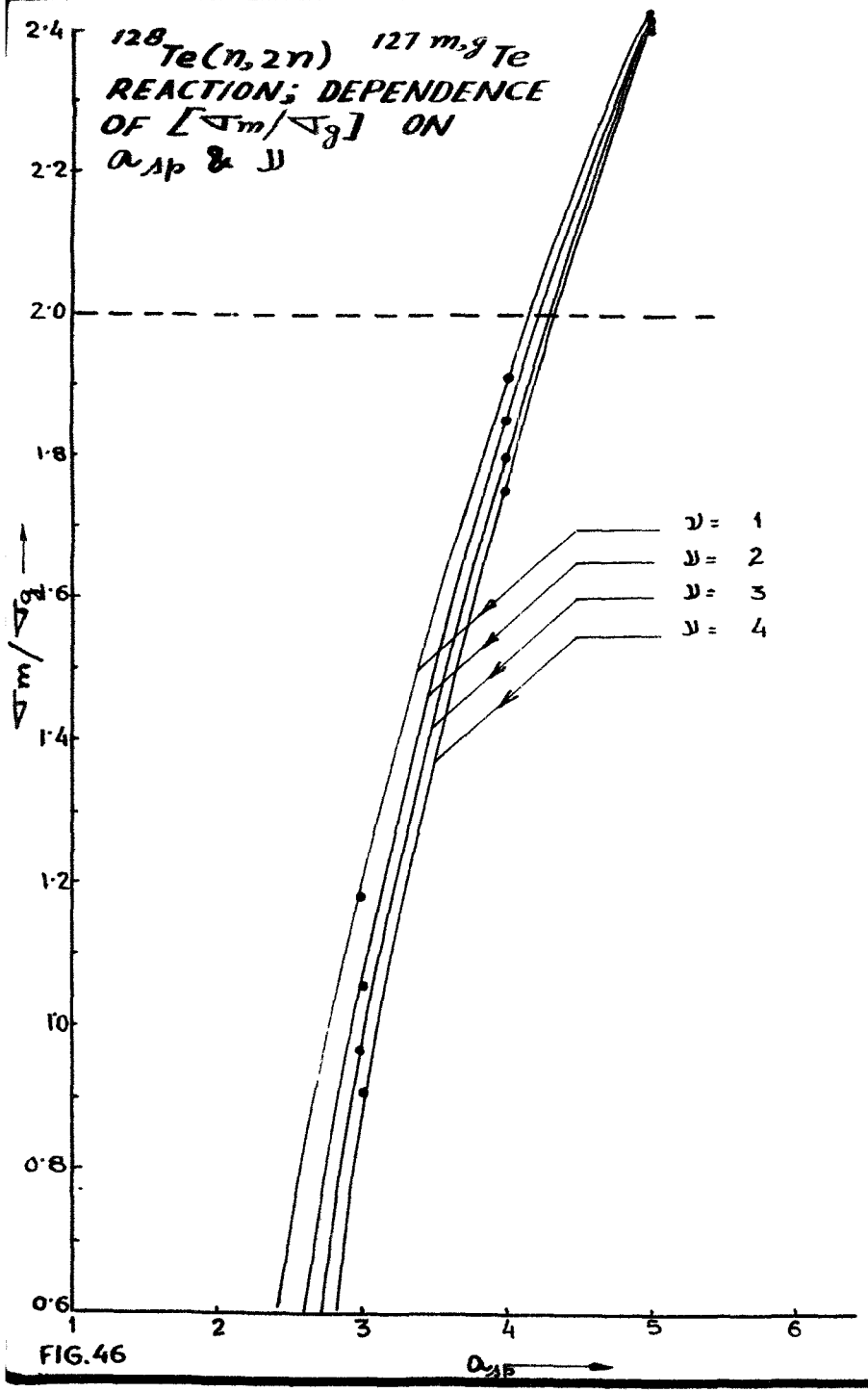
$^{128}Te(n,2n)^{127m,g}Te$ REACTION; DEPENDENCE OF $[\sigma_m/\sigma_g]$ ON α_{sp} & ν
σ_m/σ_g ⟶
α_{sp} ⟶
$\nu = 1$
$\nu = 2$
$\nu = 3$
$\nu = 4$
2·4
2·2
2·0
1·8
1·6
1·4
1·2
1·0
0·8
0·6
1
2
3
4
5
6

FIG. 46

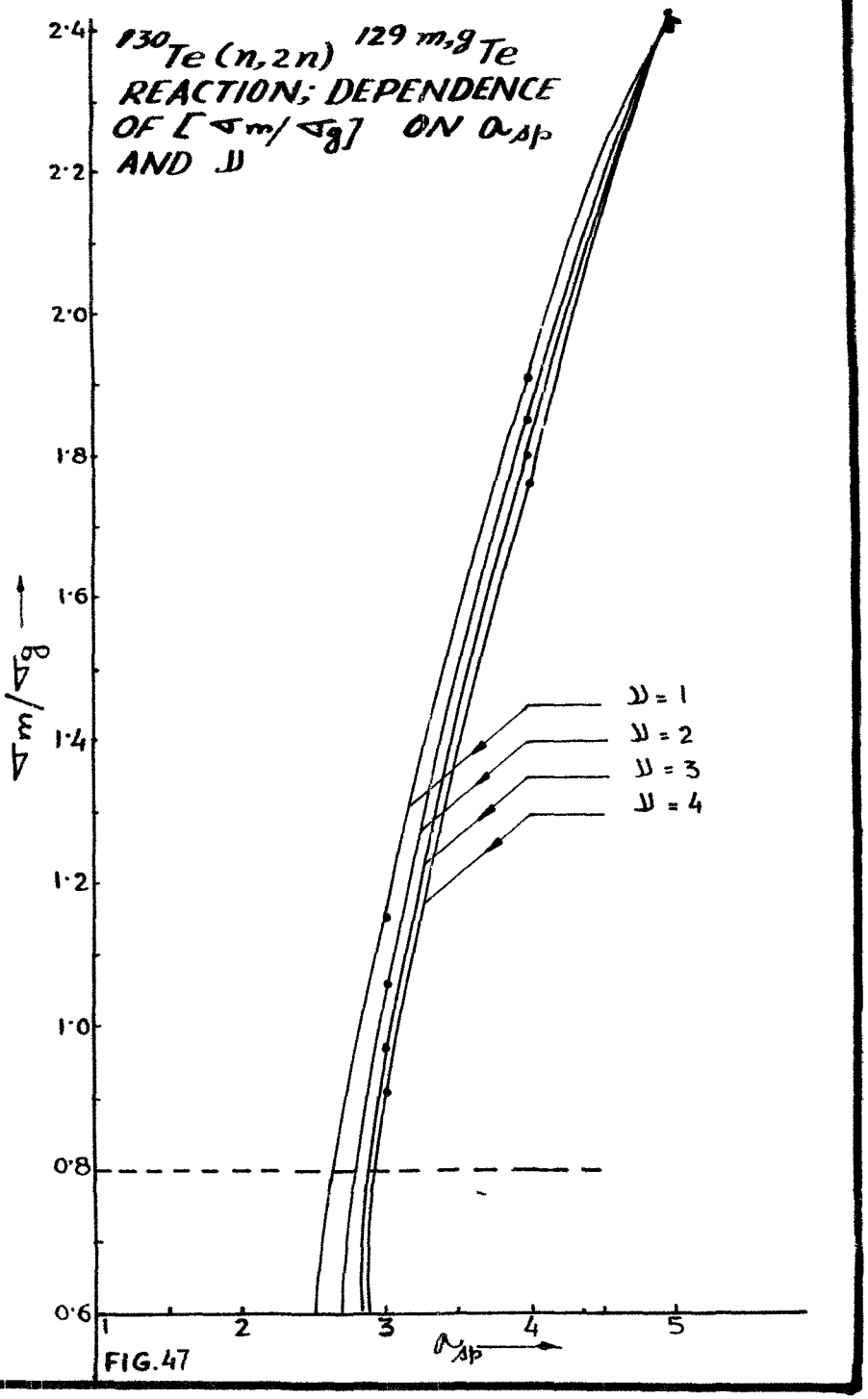
$^{130}Te(n,2n)^{129m,g}Te$ REACTION; DEPENDENCE OF $[\sigma_m/\sigma_g]$ ON α_{sp} AND ν
σ_m/σ_g ⟶
α_{sp} ⟶
$\nu = 1$
$\nu = 2$
$\nu = 3$
$\nu = 4$
2·4
2·2
2·0
1·8
1·6
1·4
1·2
1·0
0·8
0·6
1
2
3
4
5

FIG. 47

plotted against incident neutron energy (Fig.40) do not show any appreciable variation in the value of σ_{sp} with energy.

For (n,2n) reactions at 14.8 MeV, isomeric cross-section ratios were calculated for σ_{sp}= 3,4,5 and $\bar{\nu}$= 1,2,3 and 4. Figs.41 to 43 show how the spin distribution is effected by the emission of the first and second neutron for different values of σ_{sp}. The results of analysis are plotted in the form of graphs between the isomeric cross-section ratios and σ_{sp} for different values of $\bar{\nu}$(see Fig. 44 to 47). Dotted lines in these figures show experimentally measured isomeric cross-section ratios. Our $(\sigma_{sp})_{exp}$ values are generally 3 $\pm$ 0.5 and are in agreement with the values of σ_{sp} obtained by other workers[23,24,28] for (n,2n) reactions in the 14 MeV region. Values of $(\sigma_{sp})_{rig}$ have been calculated theoretically, taking moment of inertia of the nucleus corresponding to its rigid body value I_{rig}. The value $(\sigma_{sp})_{rig}$ is the mean of the two values obtained at temperatures T_1 and T_2. As can be seen from table X $(\sigma_{sp})_{exp}$ values are generally smaller than $(\sigma_{sp})_{rig}$ values. Probably it is due to generally noted fact that at lower excitation energies "Fermi gas model" does not hold good, since residual interactions are significant. Consequently moment of inertia is reduced by a certain factor from its rigid body value.[31]

TABLE - X ; Results of isomeric cross-section ratios analysis for (n,2n) reactions

Target Nucleus	Product Nucleus	Spin of the isomers	σ_m/σ_g (Experimental) Present	Others	Nucl. Temp. T_1 (MeV)	T_2	$(\alpha_{sp})_{rig}$ at temp T_1	at temp. T_2	multiplicity ν	$(\widetilde{sp})_{rig}$ (mean)	$(\widetilde{sp})_{Exp}$
^{82}Se	^{81m}Se	7/2	2.74 ± .25	4 ± 0.4 [25]	1.153	0.494	5.81	4.79	~3	4.79	2.75
	^{81g}Se	½		2.8 ± 0.14 [26]							
^{92}Mo	^{91m}Mo	½	1.07 ± .2	$.09 \pm .009$ [27]	1.098	0.100	6.24	0.69	~ 1	3.45	2.6
	^{91g}Mo	9/2		$.25 \pm .05$ [28]							
**^{128}Te	^{127m}Te	11/2	< 2		0.928	0.474	7.57	5.36	~4	6.45	4.35
	^{127g}Te	3/2									
*** ^{130}Te	^{129m}Te	11/2	0.82 ± .2		0.926	0.488	7.64	5.51	~4	6.56	2.95
	^{129g}Te	3/2									

** An upper limit for $(\sigma_m + \sigma_g)$ is taken to be the value of (n,2n) cross-section predicted by Pearlstein Ref.29)

*** σ_m taken from Ref.30)

The drawbacks of the present method of calculating the value of 'σ_{sp}' are the following :

1) In the present analysis it is assumed that the value of σ_{sp} remains constant through out the de-excitation of the compound nucleus. Theoretically it is predicted[19] that

$$\sigma_{sp}^2 \propto I.\ T \qquad \ldots\ldots \qquad (14)$$

As both I and T may depend on energy, therefore σ_{sp}^2 may also depend upon the energy. However, so far there is no evidence available which indicates the variation of σ_{sp} with excitation energy.

2) At lower excitation energies correlations between the nucleons are significant and hence a more correct expression for level density must be used. Recently few workers have studied isomeric ratios using superconductor model.[32,33]

*****

R E F E R E N C E S:

1. E. Segre and A.C. Halmholz, Revs. Mod.Phys. 21 (1949) 27
2. M. Goldhaber and R.D. Hill, Revs.Mod. Phys. 24 (1952) 179
3. E der Mateosian and M. Goldhaber, Phys. Rev.108(1957) 766
4. J.R. Huizenga and R. Vandenbosch, Phys.Rev. 120(1960) 1305
5. R. Vandenbosch and J.R. Huizenga, Phys.Rev. 120(1960) 1313
6. M.G. Mayer, Phys.Rev. 74 (1948) 235;75(1949) 1969; 76(1950) 1622
7. H.A. Bethe, Revs. Mod. Phys. 9 (1937) 84
8. C. Bloch, Phys. Rev. 93 (1954) 1094
9. A.G.W. Cameron, Can. J. Phys., 35 (1957) 666
10. V.M. Strutinski et al., Nucl. Phys. 16 (1960) 657
11. B.B. Kinsey and G.A. Bartholomew, Phys. Rev.101 (1956) 1328
12. Nuclear Data Sheet (1959-65),Academic Press,New York and London
13. J. Csikai etal., Nucl. Phys. 41 (1963) 316
14. J. BASCO et al., Nucl. Phys. 67 (1965) 443
15. J.M. Blatt and V.F. Weisskopf, Theoretical Nuclear Physics, John Wiley and Sons, New York, London
16. L.V. Groshev et al., Proceedings of the Second United Nations International Conference, Geneva (1958)
17. P.S. Seeger, Nucl. Phys. 25, (1961) 1
18. A.G.W. Cameron, Can. J. Phys., 36 (1958) 1040
19. T. Ericson, Nucl. Phys. 11 (1959) 481
20. G.S. Mani et al., Rapport, CEA 2380 (1963)

21. A.K. Chaubey, M.L. Sehgal, Phys. Rev. 152 (1966) 1055

22. A.K. Chaubey, M.L. Sehgal, Nucl. Phys.A117(1968) 545

23. B. Minetti and A. Pasquarelli, Nucl.Phys. A118 (1968) 449

24. J. Karolyi et al., Nucl. Phys. A122 (1968) 234

25. P.V. Rao and R.W. Fink, Phys. Rev. 154 (1967) 1023

26. B. Minetti and A. Pasquarelli, Nucl. Phys. A100 (1967) 186

27. J. Bacso et al., Act. Phys. Hing. 18 (1965) 295

28. R. Prasad and D.C. Sarkar, Nucl. Phys. A94 (1967) 476

29. S. Pearlstein Nucl. Data A3 (1967) 327

30. N.K. Majumdar and A. Chatterjee, Nucl.Phys. 41 (1963) 192

31. C.T. Bishop, Report ANL-6405 (1961) 116

32. H.K. Vonach et al., Nucl. Phys. 60 (1964) 70

33. A. ABBOUD et al., Nucl. Phys. A 139 (1969) 42

****

S. S. HASAN, *et al.*
11 Dicembre 1968
Il Nuovo Cimento
Serie X, Vol. 58 B, pag. 402-406

S. S. HASAN - A. K. CHAUBEY - M. L. SEHGAL

Study of the Average Level Spacing from Neutron-Capture Cross-Section.

BOLOGNA
TIPOGRAFIA COMPOSITORI
1968

Study of the Average Level Spacing from Neutron-Capture Cross-Section.

S. S. HASAN, A. K. CHAUBEY and M. L. SEHGAL

Physics Department, Aligarh Muslim University - Aligarh

(ricevuto il 10 Giugno 1968)

Summary. — Neutron-activation cross-sections have been measured for 19 cases at 24 keV, A Sb-Be photoneutron source was used for these measurements. The value of the average level spacing D has been estimated for these cases using statistical theory of nuclear reaction. These estimated values of average level spacing have been compared with the experimental values wherever they are known from low-energy resonance parameter data. An agreement between these two sets of values is found.

1. – Introduction.

The (n, γ) cross-sections at 24 keV have been measured by many workers ([1-6]). The present work was undertaken to complete the (n, γ) cross-section data at 24 keV. An intense antimony-beryllium photoneutron source along with a low-background beta-counting setup was used for the study of these cross-sections. All these cross-sections have been measured relative to that of ^{127}I(n, γ)^{128}I whose cross-section was taken equal to 0.82 b ([3]). The present measurements also include some previously measured cases. For these cases our results are in agreement with earlier reported values.

([1]) A. K. CHAUBEY and M. L. SEHGAL: *Nucl. Phys.*, **66**, 267 (1965).
([2]) A. K. CHAUBEY and M. L. SEHGAL: *Phys. Rev.*, **152**, 1055 (1966).
([3]) R. L. MACKLIN, N. H. LAZOR and W. S. LYON: *Phys. Rev.*, **107**, 504 (1957).
([4]) R. BOOTH, W. P. BALL and M. H. MACGREGOR: *Phys. Rev.*, **112**, 226 (1958).
([5]) J. F. VERVIER: *Nucl. Phys.*, **9**, 569 (1959).
([6]) V. N. KONONOV, IU. IA. STAVISSKI and V. A. TOLISTIKOV, *Journ. Nucl. Energy*, A **11**, 46 (1959).

The measured (n, γ) cross-sections were used to estimate the value of average level spacing D. Using the earlier results of CHAUBEY and SEHGAL [2], the value of the parameter $\xi = D/2\pi\Gamma_\gamma$ was calculated knowing the experimental value of the cross-section. The value of D was found in those cases where the value of Γ_γ was known [7]. These estimated values of D are compared with the experimentally observed values of D, wherever they are known [7], and a good agreement between the two values is found.

2. – Results.

The experimental procedure, errors in the measurements and formula used are the same as described earlier [1]. The Sb-Be photoneutron source was obtained from Bhabha Atomic Research Centre, Trombay, Bombay and the flux of the neutrons was greater than 10^7 neutrons/s. The elements studied

TABLE I. – *Neutron capture cross-sections at* 24 keV, *relative to* ^{127}I.

Target nucleus X	Half-life of $X+1$	Cross-section σ (mb)	Earlier reported values σ (mb)
^{23}Na	15 h	1.65 ± 0.48	1.0 ± 0.2 [a], 1.72 ± 0.34 [b]
^{27}Al	2.3 min	3.36 ± 1	1.4 ± 0.2 [a], 2.6 ± 0.22 [c]
^{37}Cl	38 min	3.12 ± 1	1.1 ± 0.2 [a], 3.71 ± 0.74 [b]
^{63}Cu	13 h	110 ± 10	116 ± 12 [a], 105 ± 21 [d]
^{75}As	26.5 h	310 ± 20	740 ± 70 [a], 650 ± 160 [d]
^{87}Rb	18 min	25 ± 5	75 ± 15 [a], 29 ± 6 [b]
^{89}Y	64 h	25 ± 5	28 ± 7 [d],
^{98}Mo	67 h	110 ± 15	209 ± 21 [a], 415 ± 98 [c]
^{120}Sn	27 h	77 ± 11	
^{122}Sn	41 min	195 ± 50	
^{124}Sn	9.5 min	220 ± 55	
^{121}Sb	2.8 d	700 ± 70	950 ± 100 [a], 810 ± 250 [d]
^{123}Sb	1.3 min	5.4 ± 1.3	
^{123}Sb	21 min	3.1 ± 1.5	
^{123}Sb	60 d	575 ± 50	456 ± 46 [a], 230 ± 100 [d]
^{148}Nd	1.9 h	165 ± 35	
^{150}Nd	12 min	125 ± 25	
^{170}Er	7.8 h	255 ± 30	298 ± 30 [a]
^{205}Tl	4.3 min	30 ± 8	

(a) See ref. [8].
(b) See ref. [8].
(c) See ref. [5].
(d) See ref. [4].

[7] *Neutron Cross-Sections*, BNL-325, second edition, supplement No. 1, 1960.

were obtained from Johnson Mathey & Co. Ltd., London and were more than 99.9% pure. The half-lives of various activities, the energies of the beta-particles emitted and their branching ratios were taken from literature [8,9]. The irradiation time of different elements was so chosen as to minimize the complexities which could have arisen due to mixture of undesired activities.

The measured cross-sections are shown in Table 1. The earlier reported values of the cross-sections are also shown in the same Table wherever they are known. In case of ^{63}Cu, ^{89}Y, ^{121}Sb, and ^{123}Sb and ^{170}Er our cross-section values are in agreement with those of BOOTH *et al.* [4] and MACKLIN *et al.* [3], respectively. In ^{27}Al cross-section value is in agreement with that of VERVIER [5]. In ^{23}Na, ^{37}Cl, and ^{87}Rb cross-section values are in agreement with those of KONONOV *et al.* [6], while in ^{98}Ye and ^{75}As our values of capture cross-sections completely disagree with other reported values.

3. – Estimation of average level spacing.

The expression for (n, γ) cross-section, using statistical theory can be given as [10]

$$(1) \qquad \sigma_E(\mathrm{n},\gamma) = \frac{\pi\lambda\!\!\!^{-2}}{2(2I+1)} \sum_{l=0}^{\infty} \left[T_l(E) \sum_{J=0}^{\infty} \frac{\varepsilon_{jl}^{J}(2J+1)}{1+\xi f_{JI}(E) \sum_{l'} \sum_{n} \varepsilon_{j_n l'}^{J} T_{l'}(E-E_n)} \right],$$

where I is the spin of the target nucleus, j is the channel spin, J is the spin of a level in the compound nucleus, $2\pi\lambda\!\!\!^{-}$ is the de Broglie wavelength of incident neutron, E_n is the energy of the n-th excited state, T_l is the transmission coefficient for the l-th partial wave, l' is the angular momentum of the emitted neutron and ε_{jl}^{J} is the statistical factor. ξ is defined as $D/2\pi\Gamma_\gamma$, where Γ_γ and D are radiation width and average level spacing respectively.

In our previous paper [2], values of ξ were calculated from eq. (1) by putting values of σ_E(n, γ) and other quantities involved in the equation, for 72 cases. A graph was then plotted between σ and $\log\xi$. It was seen that $\log\xi$ varies with σ almost exponentially. Using the graphs [2] between σ and $\log\xi$ we have estimated the value of ξ for all the nuclei for which σ is measured in the present case. From these values of ξ, D can be calculated, if one knows the value of Γ_γ [7].

---

[8] *Nuclear Data Sheets*, National Academy of Science, N.R.C., Washington D.C. (1960-1964).

[9] D. STROMINGER, J. M. HOLLANDER and G. T. SEABORG: *Rev. Mod. Phys.*, **30**, 585 (1958).

[10] B. MARGOLIS: *Phys. Rev.*, **88**, 327 (1952).

The values of average level spacing estimated are shown in Table II under column D_{es}. Average level spacing can also be obtained from low-energy resonance parameters (7). These experimentally observed values (D_{ob}) are also tabulated in Table II, wherever they are known.

TABLE II. – *A comparison of estimated and observed level spacing.*

Target nucleus	D_{es} (eV)	D_{ob} (eV)
^{63}Cu	1810^{+350}_{-300}	2300 ± 15
^{75}As	320 ± 40	174 ± 1
^{87}Rb	5190^{+1730}_{-860}	4275 ± 50
^{89}Y	5190^{+1730}_{-860}	7500 ± 150
^{98}Mo	860 ± 110	480 ± 20
^{120}Sn	720^{+190}_{-155}	425 ± 18
^{122}Sn	250^{+53}_{-33}	
^{124}Sn	190^{+51}_{-32}	62.5 ± 0.9
^{121}Sb	36^{+10}_{-6}	26 ± 0.6
^{123}Sb	49 ± 9	52.5 ± 1
^{148}Nd	290^{+70}_{-40}	
^{150}Nd	420^{+105}_{-60}	
^{170}Er	105 ± 26	
^{205}Tl	1950^{+1300}_{-325}	

In case of ^{63}Cu, ^{87}Rb, ^{89}Y, ^{121}Sb and ^{123}Sb the experimentally observed value of D is in agreement with the estimated value. In case of ^{75}As and ^{98}Mo the agreement between the two values is not good. In case of ^{120}Sn and ^{121}Sn the measured cross-sections are for ground state and isomeric state respectively. Cross-sections for the population of isomeric state of ^{121}Sn and ground state of ^{125}Sn are not known at this energy. When contribution due to these states is also taken into account this will increase the cross-section value shown in Table I

and hence will lower the value of D_{es} making a good agreement with D_{ob}. In the case of ^{122}Sn, ^{148}Nd, ^{170}Er and ^{205}Tl values of D_{ob} are not known. Therefore it is not possible to make a comparision, while in the case of ^{23}Na, ^{27}Al and ^{37}Cl, values of I'_γ are not known and hence average level spacing could not be estimated in these cases. From this comparison it is seen that if one knows capture cross-section for any case the value of D can be calculated immediately by using our graph (2) between σ *vs.* $\log \xi$.

* * *

We wish to thank Prof. R. AHMED for his kind interest in this work. Authors A.K.C. and S.S.H. are thankful to C.S.I.R. for providing financial assistance.

RIASSUNTO (*)

Si sono misurate le sezioni d'urto d'attivazione neutronica per 19 casi a 24 keV. Si è usata, per queste misure, una sorgente di fotoneutroni di Sb-Be. Si è valutato per questi casi il valore medio della distanza dei livelli D, usando la teoria statistica delle reazioni nucleari. Si sono confrontati i valori ottenuti con quelli sperimentali ogniqualvolta erano noti dai dati dei parametri delle risonanze di bassa energia. Si trova accordo fra i due gruppi di dati.

(*) *Traduzione a cura della Redazione.*

Изучение среднего расстояния между уровнями из поперечного сечения захвата нейтронов.

Резюме (*). — Были измерены поперечные сечения нейтронной активации для 19 случаев при 24 кэВ. Для этих измерений был использован фото-нейтронный источник Sb-Be. Используя статистическую теорию ядерных реакций, была оценена величина среднего расстояния D между уровнями для этих случаев. Эти оцененные величины среднего расстояния между уровнями были сравнены с экспериментальными величинами, повсюду где они известны из данных для параметров резонанса при низких энергиях. Получено согласие между этими двумя системами величин.

(*) *Переведено редакцией.*